PROCESSING AND FUNCTIONALITY IMPROVEMENTS OF LAYER-BY-LAYER ASSEMBLED MULTILAYER SUPER GAS BARRIER NANOCOATINGS

A Dissertation

by

YIXUAN SONG

Submitted to the Office of Graduate and Professional Studies of
Texas A&M University
in partial fulfillment of the requirements for the degree of

DOCTOR OF PHILOSOPHY

Chair of Committee,	Jaime Grunlan
Committee Members,	Jodie Lutkenhaus
	Svetlana Sukhishvili
	Micah Green
Head of Department,	Ibrahim Karaman

May 2018

Major Subject: Materials Science and Engineering

ABSTRACT

High oxygen barrier materials are becoming increasingly important for food packaging, pressurized systems, and flexible electronics protection. The widely used traditional aluminized plastics and inorganic gas barrier coatings (SiO_x and Al_xO_y) exhibit low transparency and/or flexibility. Layer-by-layer assembly (LbL) provides a cost-effective and environmental-friendly alternative, with lower oxygen permeability and greater transparency. This dissertation focuses on improvements of the coating process and development of new functionalities. Four studies are discussed in detail on this topic and two future research directions are also introduced.

Layer-by-layer assembled multilayer nanocoatings have been shown to provide excellent oxygen barrier to poly(ethylene terephthalate) (PET) film, which is commonly used for encapsulation and packaging. Polymer-clay (polyethylenimine (PEI)/vermiculite (VMT)) and all-polymer ((PEI)/poly(acrylic acid) (PAA)) multilayer systems are shown to be equally beneficial as barrier coatings for polyolefin substrates (e.g., polyethylene and polypropylene), which suffer from a high oxygen transmission rate. A 30 bilayer PEI/VMT nanocoating reduces the OTR of biaxially oriented polypropylene (BOPP) by more than 160X, rivaling most inorganic coatings. WVTR is simultaneously reduced by 43%.

In addition to VMT, montmorillonite (MMT) clay has been widely used to prepare gas barrier nanocoatings. In an effort to produce high oxygen barrier with fewer deposition steps, pH of the MMT aqueous suspension was reduced. In a PEI/PAA/PEI/MMT

quadlayer system, the reduced pH of MMT causes the preceding PEI layer to be more charged, which results in more clay deposited. A compromise between high polyelectrolyte diffusion (high pH) and high clay deposition (low pH) was found at pH 6, where the best oxygen barrier is obtained. A 179 μm thick PET substrate, coated with just three quadlayers (44 nm thick), exhibits an undetectable oxygen transmission rate (< 0.005 $cm^3/(m^2$ day atm)).

In another attempt to achieve better oxygen barrier of the PEI/MMT bilayer (BL) system, a "salty clay" strategy was carried out, where an "indifferent" electrolyte (NaCl) was introduced into the MMT suspension. NaCl alters the ionic strength of the clay suspension and subsequently changes the rheological behavior of clay platelets. As a result, a multilayer film with a more tortuous path and better clay coverage (and alignment) is produced. Lower OTR is achieved as a result of this structural engineering. An 8 BL PEI/MMT film, assembled with a clay suspension containing 5 mM NaCl, exhibits an order of magnitude reduction in OTR relative to its no-salt counterpart.

The ability to self-repair after damaging (e.g., cracking) and restore original properties is highly desired for polymers and composites. The PEI/PAA nanocoating has the ability to self-heal after being cracked by stretching. Cracks in the film lead to loss of oxygen barrier. High humidity is employed as an external healing stimulus to repair these cracks. The OTR of a PEI/PAA multilayer nanocoating remains below detection after 10 stretching-healing cycles, which shows this healing process to be highly robust.

DEDICATION

I would like to dedicate this dissertation to my parents, Mr. Shelu Song and Mrs. Huijun He, for giving me the best family education that a son can ever have. I also want to dedicate this dissertation to my fiancée Miss Shuang Qin, for her great support, help, and advice in my life and my career. Finally I want to dedicate this dissertation to my beloved motherland People's Republic of China, for protecting her fellow people from famine, war, and poverty.

ACKNOWLEDGEMENTS

First I want to thank my advisor and committee chair Dr. Jaime Grunlan, for providing guidance and support throughout my Ph.D. study. The past few years in the Polymer NanoComposites Lab has been the most productive and rewarding period of time in my life. I would also like to thank all of my committee members Dr. Jodie Lutkenhaus, Dr. Svetlana Sukhishvili, and Dr. Micah Green for their feedback and suggestions in my prelim exam, and also for their time.

I would like to thank all the professors and staff who helped me during my study here at Texas A&M. I want to thank Dr. Wilson Serem for his assistance on AFM and nanoindentation. Thanks also go to Mr. Richard Littleton and Dr. Hansoo Kim at the Microscopy and Imaging Center (MIC) who helped me a great deal in microtome sample preparation and TEM training. I also want to thank Dr. Yordanos Bisrat for her help with SEM and XRD.

I want to thank all the former and present members of Polymer Nanocomposites Lab for their kind help and support, including Dr. Bart Stevens, Dr. Ping Tzeng, Dr. Fangming Xiang, Dr. David Hagen, Dr. Tyler Guin, Dr. Kevin Holder, Dr. Merid Haile, Dr. Marcus Leistner, Dr. Chaowei Feng, Dr. Chaoqun Zhang, Dr. Mario Culebras, Dr. Igor Jordanov, Dr. Abbas Fahami, Dr. Chungyeon Cho, Ryan Smith, Shuang Qin, Simone Lazar, Thomas Kolibaba, Carolyn Long, Xiaodong Liu, and Dan Stevens. I want to thank my undergraduate assistants, Matthew McMahon, Kyle Falke, Joseph Gerringer, and

Alexander Ahmed for their time and effort in helping me with the work presented in this dissertation.

I want to thank the collaborators I had the privilege to work with. Thanks go to Dr. Sergei Nazarenko, Kevin Meyers, and RameshKrishnan Ramakrishnan at the University of Southern Mississippi, for their hospitality when I visited and also for their delicate help in OTR and PALS measurements. I would like to thank Dr. Benjamin Wilhite and Dr. Elva Lugo for their collaboration on the gas separation projects.

I want to thank all my friends Shuang, Marcus, Xinyu, Bosheng, Yi, and Mario for their company and friendship.

CONTRIBUTORS AND FUNDING SOURCES

Contributors

This work was supervised by a dissertation committee consisting of Professor Jaime Grunlan [advisor and committee chair], Professor Jodie Lutkenhaus, Professor Svetlana Sukhishvili, and Professor Micah Green of Department of Materials Science and Engineering.

The nanoindentation data in Chapter VI was provided by Professor Andreas Polycarpou of Department of Mechanical Engineering. The oxygen barrier results in Chapter VI were obtained by Kevin Meyers from the School of Polymers and High Performance Materials, University of Southern Mississippi. The experiments in Chapter IV were designed and performed by David Hagen of Department of Mechanical Engineering. All other work conducted for the dissertation was completed by Yixuan Song independently.

Funding Sources

The work in this dissertation was made possible in part by National Science Foundation (NSF) under grant number CBET 1403686 and DMR 0423914.

NOMENCLATURE

OTR	Oxygen Transmission Rate
WVTR	Water Vapor Transmission Rate
PEI	Polyethyleneimine
PAA	Poly(acrylic acid)
MMT	Montmorillonite
OLED	Organic Light-Emitting Diode
PE	Polyethylene
LDPE	Low Density Polyethylene
PVD	Physical Vapor Deposition
CVD	Chemical Vapor Deposition
PP	Polypropylene
BOPP	Biaxially Oriented Polypropylene
PET	Poly(ethylene terephthalate)
LbL	Layer-by-Layer
VMT	Vermiculite
BL	Bilayer
PVOH	Polyvinyl Alcohol
PU	Polyurethane
DI	Deionized
TEM	Transmission Electron Microscopy

QL	Quadlayer
QCM	Quartz Crystal Microbalance
EDL	Electrical Double Layer
AFM	Atomic Force Microscope
UV-vis	Ultraviolet–Visible
SEM	Scanning Electron Microscopy
PALS	Positron Annihilation Lifetime Spectroscopy
FEA	Finite Element Analysis
EPAs	Electroactive Polymers
DMA	Dynamic Mechanical Analysis

TABLE OF CONTENTS

Page

LIST OF FIGURES

Page

LIST OF TABLES

Page

CHAPTER I

INTRODUCTION

1.1 Background

Transparent and flexible high oxygen barrier film is of great interest for food packaging, pressurized systems, and flexible electronics protection, where low oxygen and water vapor transmission rates (WVTR and OTR) are required.[1, 2] For longer shelf-life and more reliable performance, sensitive food, LED displays, and photovoltaics require an OTR below 10^{-2} $cm^3/(m^2$ day atm) and a WVTR below 0.1 $g/(m^2$ day) provided by encapsulation techniques.[3] The barrier requirement is even higher for sensitive organic light-emitting diode (OLED) displays and organic solar cells (OTR < 10^{-5} $cm^3/(m^2$ day atm) and WVTR < 10^{-6} $g/(m^2$ day)).[1] Typical packaging polymers, including polyethylene (PE), biaxially oriented polypropylene (BOPP), and poly(ethylene terephthalate) (PET), need coatings to fulfill such barrier requirements. Although metalized plastics (aluminum coated PP or PE), with high oxygen and moisture gas barrier, have become the most widely used packaging materials (1.7 million tons used in US in 2005),[4] the vacuum assisted process and difficult recycling procedures are energy and capital intensive. Moreover, metalized plastics lack the desired transparency and flexibility for food and electronics packaging.[5] Other inorganic gas barrier coatings, including SiO_x and Al_xO_y, have been heavily investigated, but they suffer from defects (pinholes, cracks, etc.) and poor adhesion to the polymer substrate.[6, 7] Polymer-clay composites can maintain the desired mechanical strength and provide good adhesion,[8, 9] but the random orientation and poor

exfoliation of clay platelets reduce transparency and oxygen barrier.[10] For instance, in order to achieve high optical clarity, a saponite/poly(acrylic acid) polymer membrane (%T ~90 with a thickness of 10 μm) has a compromised OTR of 0.1 $cm^3/(m^2$ day atm) due to the restricted clay loading (~20 wt%).[11]

Layer-by-layer (LbL) assembly, shown schematically in Figure 1, has become one of the most studied methods to prepare multifunctional nanocoatings in the past few decades due to its simplicity and environmental friendliness.[12-14] With the ability to assemble a wide range of molecules and nanoparticles on various substrates, this technique has been shown to achieve impressive properties including gas barrier,[15-17] thermoelectricity,[18] gas separation,[19] flame resistance,[20-22] drug delivery,[23, 24] and high strength.[25, 26] This multilayer assembly process involves depositing species having complementary functionality, with electrostatic interaction being the most studied driving force.[13] Highly organized structures are created one nanolayer at a time using polymers and various nanoparticles such as dots,[27] rods,[28] tubes,[29] sheets,[30] platelets,[31] and spheres.[32] Beyond choosing components, there are many other parameters that can be altered to further tailor the thin film morphology: concentration,[33, 34] pH,[35] temperature,[36] ionic strength,[37] and component molecular weight.[38] These multilayer nanocoatings, constructed with polyelectrolytes and/or nanoplatelets (e.g., clays and graphene oxide), have proven to be flexible and transparent super oxygen gas barriers.[39-41]

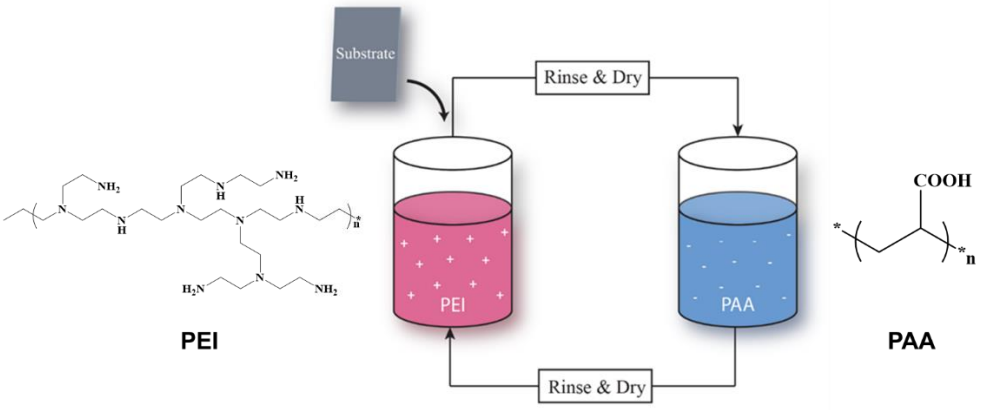

Figure 1. Schematic of the dip coating process of layer-by-layer assembled polyethylenimine (PEI)/poly(acrylic acid) (PAA) multilayer nanocoating.

1.2 Dissertation Outline

Chapter II provides an overview of the commonly used barrier materials, including inorganic aluminized plastics, metal oxide coatings, and polymer composites. A review of layer-by-layer assembly is also in this chapter, which includes the preparation process, applications, and gas barrier performance. Moreover, the stimuli responsive behavior of layer-by-layer assembly is introduced as the background for the self-healing gas barrier in Chapter V and vapor driven polymer actuator in Chapter VII.

Chapter III demonstrates that layer-by-layer assembled gas barrier nanocoatings are effective for polyolefin substrates (e.g. polyethylene and polypropylene). As the most widely used polymer substrate in packaging industry, biaxially oriented polypropylene (BOPP) suffers from a high oxygen transmission rate (OTR) and it's challenging to coat duo to its low polarity. A polyethylenimine (PEI)/vermiculite (VMT) nanocoating can improve the OTR of 17.8 μm thick BOPP by more than 160X at 100% relative humidity,

rivaling most inorganic coatings. This high barrier BOPP meets the criteria for sensitive food and some electronics packaging applications.

Chapter IV studies the influence of MMT suspension pH on the oxygen barrier of PEI/poly(acrylic acid) (PAA)/PEI/montmorillonite (MMT) quadlayer nanocoatings. Reducing the pH of MMT causes the following PEI layer highly charged, which leads to more clay deposition per layer. An optimization between high polymer diffusion (high pH) and high clay deposition (low pH) is found at pH 6, where the best oxygen barrier is achieved.

Chapter V investigates the influence of ionic strength of the MMT suspension on the structure and gas barrier of the PEI/MMT multilayer system. Sodium chloride (NaCl) is introduced into the MMT suspension as an "indifferent electrolyte". Moderate NaCl promotes the edge-to-edge bonding between MMT platelets and improves the clay alignment and coverage. As the result of this structural engineering, a 10X improvement is achieved for an 8 BL PEI/MMT nanocoating over films prepared without ionic strength alteration.

Chapter VI demonstrates the super oxygen barrier and self-healing behavior of PEI/PAA multilayer films. Although an 8 BL PEI/PAA improves the oxygen barrier of a poly(ethylene terephthalate) (PET) substrate by more than three orders of magnitude, cracks resulting from tensile stretching lead to gas barrier failure. High humidity is then employed as the healing stimulus, which completely eliminates cracks and restores the oxygen barrier. This healing process is robust, withstanding at least 10 damaging-healing cycles.

Chapter VII provides conclusions for the work from Chapter III to VI and outlines two potential future studies. This dissertation demonstrates the effectiveness of LbL nanocoatings to improve polyolefin gas barrier and investigates the influence of clay pH and ionic strength on gas barrier of polymer-clay multilayer nanocoatings. Moreover, the self-healing property of a PEI/PAA super gas barrier is demonstrated. These improvements in coating process and new functionalities make layer-by-layer assembly more powerful as a functional coating technique. To further reduce the time required to prepare a flexible and semitransparent polymer-clay gas barrier coating, a polyvinyl alcohol (PVOH)/MMT complex coating is proposed. Preliminary results show that this PVOH/MMT coating, with a thickness of ~3 μm and clay concentration of 50%, exhibits oxygen transmission rate below the detection limit of commercial instrumentation (<0.005 $cm^3/(m^2$ day atm)). The second future study involves a multilayer polymer actuator constructed with PEI/PAA and polyurethane (PU)/PAA stacking. Initial results reveal a two-way responsive behavior in water vapor and organic vapor environments. The curling degree can be precisely controlled by varying the thickness ratio of hydrophobic (PU/PAA) and hydrophilic (PEI/PAA) sections. A parallel circuit was constructed to demonstrate the environmental detection ability of this chemical vapor responsive polymer actuator.

CHAPTER II

LITERATURE REVIEW

Due to their low cost and ease of processing, plastics are commonly used to replace metal and glass for various packaging applications (i.e., food, electronics, photovoltaic modules, etc.). Unfortunately, the encapsulation performance of most polymers (Table 1) is not satisfactory for these packaging applications,[6] where lower oxygen and water vapor permeabilities are required (see Figure 2).[42] For example, the lifetime for an OLED device is reduced to hours when deposited on poly(ethylene terephthalate) (PET) and exposed directly to atmospheric conditions.[5] Two major types of encapsulation barrier materials can be found on the current packaging market: inorganic and polymer composite gas barriers. The vacuum deposited inorganic coatings (including aluminized plastic, SiO_x, Al_xO_y, etc.) provide an excellent barrier, while remaining 100-1000 times thinner than their polymeric substrates.[5, 43] It's also a cost-effective technology, with product cost as low as several hundred dollars per metric ton. Despite wide acceptance and usage (11 billion square meters of metalized plastic consumed in 2001), there have been attempts to replace inorganic gas barrier materials due to environmental and health concerns.[44] It is challenging to recycle the metalized plastics and separate aluminum from polymer, as the coating is designed to be resist delamination, so the majority of metalized plastic ends up in the landfills.[45, 46]

Table 1. Oxygen and water vapor permeabilities of polymers used for packaging applications.[6] Reprinted from Ref. 6.

Polymer	Oxygen permeability at 23°C 50% or 0% RH [cm^3 mm/(m^2 day atm)]	Water vapour permeability at 23°C 85% RH [g mm/(m^2 day)]
Poly(ethylene terephthalate) (PET)	1–5	0.5–2
Polypropylene (PP)	50–100	0.2–0.4
Polyethylene (PE)	50–200	0.5–2
Polystyrene (PS)	100–150	1–4
Poly(vinyl chloride) (PVC)	2–8	1–2
Poly(ethylene naphthalate) (PEN)	0.5	0.7
Polyamide (PA)	0.1–1 (dry)	0.5–10
Poly(vinyl alcohol) (PVAL)	0.02 (dry)	30
Ethylene vinyl alcohol (EVOH)	0.001–0.01 (dry)	1–3
Poly(vinylidene chloride) (PVDC)	0.01–0.3	0.1

Polymer composites improve the gas barrier with impermeable inorganic fillers, which force gas molecules wiggle around. The major drawback of these materials is the loss of transparency and relatively low barrier due to the randomly oriented and sometimes aggregated filler. As a relatively new barrier material, layer-by-layer assembled multilayer nanocoatings have proven to be flexible and transparent high oxygen barriers.[35, 40] Moreover this is a cost-effective and environmentally friendly technique with a wide range of ingredients, including environmentally benign and renewable materials. The coating process and barrier performance will be further discussed in Section 2.3 and the subsequent chapters.

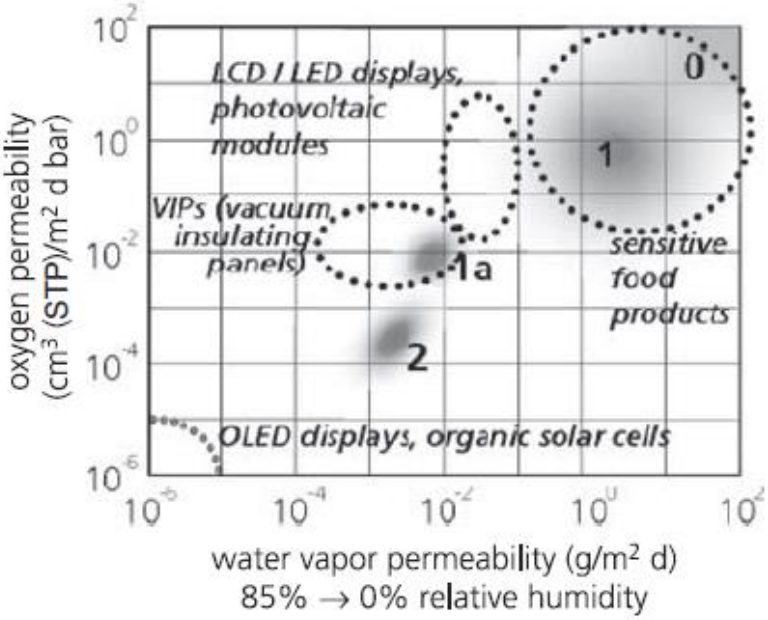

Figure 2. Barrier properties required for various packaging applications (dotted circles). The numbers represent the performance of packaging materials: (0) polymer substrates alone, (1) inorganic coatings, (2) inorganic/polymeric multilayer systems.[42] Reprinted from Ref. 42.

2.1 Inorganic Gas Barrier

Vacuum deposited inorganic layers are commonly used to improve the gas barrier of polymer films, which represent the first gas barrier coatings.[6] It was estimated that more than 15 billion square meters of these inorganic barrier coatings are consumed each year.[3] These inorganic coatings have the ability to reduce the gas permeability up to three orders of magnitude compared to uncoated substrates (PET, BOPP, etc.).[47] This section will focus on the two most common inorganic barrier coatings: metal thin film coatings and transparent oxide coatings.

2.1.1 Metal Thin Film Coating

Vacuum deposited thin films were first demonstrated by Grove in the 1850s and widely used for gas barrier materials since the 1970s. [48, 49] These coatings are usually deposited through physical vapor deposition (PVD) with deposition rates of 1-10 nm per second. Pure elements or alloy sources are vaporized in a plasma environment and condensed on the substrate surface.[50] A wide range of materials can be deposited using this method, including Au, Ag, Al, Cu, C, and Cu-Au alloy. The most commonly used techniques for PVD are vacuum and sputter depositions. Vacuum deposition is a thermal vaporization process, where a high vacuum condition is employed to eliminate the collision between gas molecules. Tungsten wire coils or high energy electron beam are used to evaporate the source materials, as shown in Figure 3.[51] In the non-thermal sputter deposition process, target surface atoms are ejected by high energy gaseous ions accelerated by plasma. Additionally, arc vapor deposition and ion plating techniques have also been used for PVD.[52]

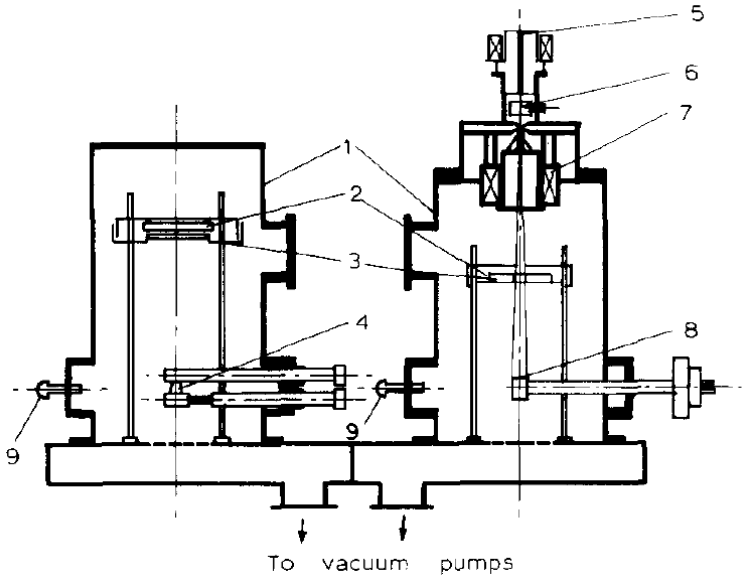

Figure 3. Diagram of a vacuum evaporation system: 1 vacuum chamber, 2 heater, 3 substrate, 4 electron gun, 5 gas valve, 6 ion source, 7 magnetic coil, 8 target, 9 vacuum gauge.[51] Reprinted from Ref. 51.

Aluminum is often used as a source material to deposit flexible permeation barrier coatings, which markedly reduce the OTR and WVTR.[53] Table 2 summarizes the typical barrier improvements of PET and OPP after metallization. One should expect virtually zero oxygen and water vapor transmission based on the bulk diffusivity of aluminum, but these high gas permeabilities from the published data indicate the presence of microscopic defects.[5] The number of defects is usually determined by the adsorbents on substrate surface, which have a geometrical shadowing effect and lead to pinholes, poor surface coverage and weak adhesion.[54, 55] Non-planar surfaces, including sharp steps and angles may cause the same problem. The influence of adsorbents and geometrical shadowing can be alleviated by improving vacuum conditions and reducing thermal and mechanical stress.[53]

Table 2. Metalized PET and OPP barrier.[53] Reprinted from Ref. 53.

Film	Thickness (μm)	OTR (cm^3 m^{-2} d^{-1})	WVTR (g m^{-2} d^{-1})
PET film	25	31–93	16–20
PET film, metallized	25	0.16–1.7	<1.0
OPP film	25	1550–2500	3.9–6.2
OPP film, metallized	25	19–160	<0.6

Recyclability is another concern for the widely used metalized plastic, which has already occupied a great amount of landfill and negatively impacted the environment. Several attempts have been reported to reclaim and rejuvenate plastic. For example, Paula *et. al.* added recycled LDPE or virgin LDPE to aluminized LDPE after an agglutination process.[45] Unfortunately, the low mechanical strength and high water absorption of the final product suggests the need for further improvement. Another example of metalized plastic recycling used a cryogenic process that can liberate almost all the metal from polymer.[46] Despite good progress on the technical aspects, the major challenge of metalized plastic recycling still lies in public awareness.

2.1.2 Transparent Oxide Coating

A small fraction of inorganic gas barrier coating (about 1 billion square meters per year) uses transparent oxides (SiO_x, Al_xO_y, etc.).[56] These inorganic oxide coatings are usually applied through PVD of SiO or plasma assisted chemical vapor deposition

(PACVD) of organosilane and oxygen.[6] Figure 4 shows a roll-to-roll CVD coater for the SiO_x coating.[57] After chamber evacuation, the organosiliane (e.g., tetramethoxysilane) and oxygen gas mixture flow through the chamber and are polymerized by plasma, resulting in a thin SiO_x coating on the substrate surface.

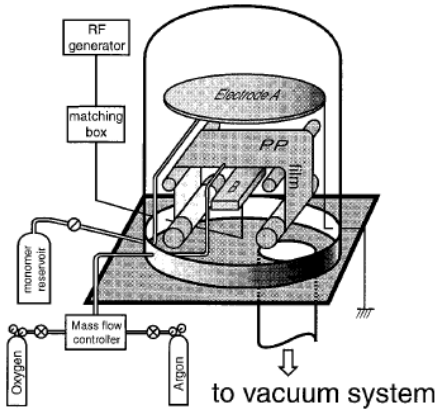

Figure 4. Schematic of a roll-to-roll CVD deposition apparatus. The organosiliane is kept in the monomer reservoir.[57] Reprinted from Ref. 57.

Similar to metalized plastic films, inorganic oxide coatings also exhibit excellent barrier performance if no significant defects exist.[6, 47, 58] For example, a 100 nm thick SiO_x coating exhibits oxygen permeability of 1.4×10^{-17} cm^3 cm/(cm^2 s cmHg) and improves the oxygen barrier of PET by more than two orders of magnitude.[60] Even so, pinholes and poor adhesion are common, especially when a significant mismatch (mechanical properties, surface chemistries, etc.) exists between coating and substrate.[59] Figure 5 shows an optical microscope image of a poorly coated SiO_x layer on PET, the pinholes in the image could lead to complete loss of gas barrier.[60] These inorganic oxide

coatings also suffer from extensive cracking upon stretching. For example Figure 6 shows the cracked surface of a 100 nm SiO_x coated PP after only 1.6% strain.[43]

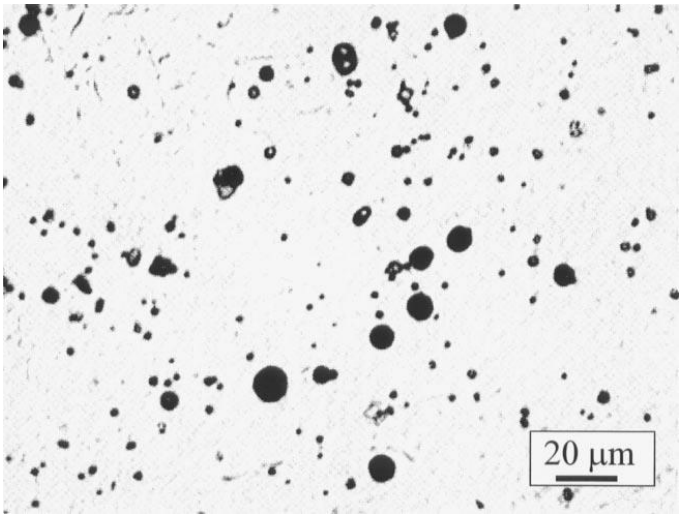

Figure 5. Optical microscope image of the surface of a SiO_x coated PET.[60] Reprinted from Ref. 60.

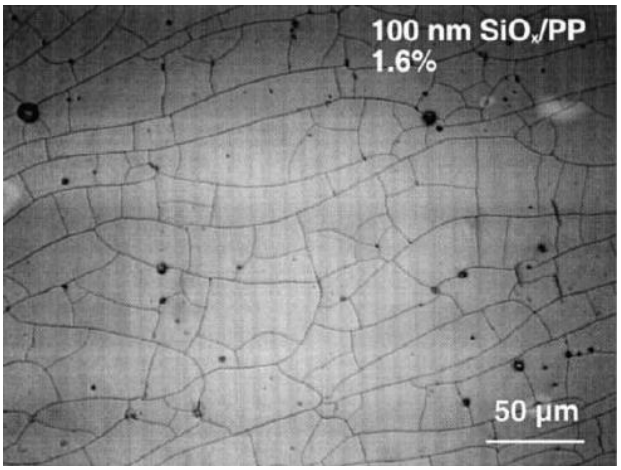

Figure 6. SEM surface image of 100 nm SiO_x coated on PP after 1.6% equibiaxial loading.[43] Reprinted from Ref. 43.

2.2 Organic/Inorganic Gas Barrier

2.2.1 Polymer Composite Gas Barrier

Polymer composites show improved mechanical, barrier, electrical, thermal stability and flame resistance properties over neat polymers.[61, 62] A variety of nanoparticles can be incorporated into polymeric matrix, including TiO_2,[63] Ag,[64] clay,[65] carbon nanomaterials (graphene, carbon nanotubes).[66] Since one of the earlies studies of DNA adsorption on montmorillonite (MMT),[67] and the first commercial example of clay-nylon composite in the automotive industry,[68] polymer nanocomposites have been widely studied and used for a various applications (catalysis, drug delivery, antibacterial, packaging, etc).[6, 69-71] Four primary techniques have been used to prepare the polymer composites: blending, sol-gel processing, in situ polymerization, and in situ growth of nanoparticles.[61, 62] Polymer solution/melt blending is the most straightforward method, which usually involves annealing through shear stress (see Figure 7).[72, 73] Moreover, ordinary compounding devices including extruders and mixers could be used, which is why almost all the thermoplastic polymers (e.g., poly(ethylene terephthalate) (PET), ethylene vinylacetate (EVA), polyolefins, polyurethanes, etc.) have been studied to form composites using this method.[74-77] The major challenge in the preparation of blended polymer composites is to achieve homogenous dispersion of particles, because the inorganic fillers tend to aggregate. For example, a nylon and clay nanocomposite prepared through melt blending exhibits significant phase separation and clay aggregation when clay concentration is above 5 wt%.[78] Other techniques for polymer composites help to solve the particle dispersion problem by synthesizing inorganic particles or polymers in

situ. For instance, Ag nanoparticles were nucleated and grew in a polyvinyl alcohol (PVA)/polyvinylpyrrolidone (PVP) polymer matrix after silver nitride reduction.[79] The particles were homogenously dispersed without any surface modification. Even so, blending remains the most versatile and universal technique for polymer composites preparation. Special processing and long fabrication time make the other techniques unfavorable.

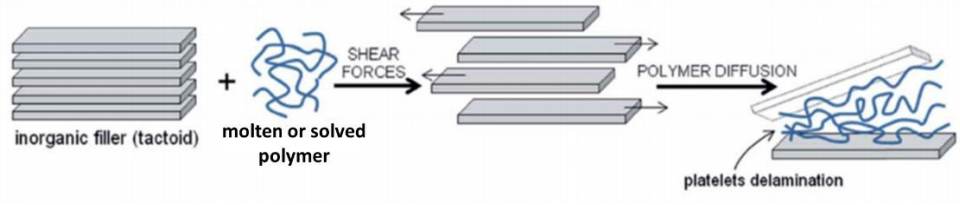

Figure 7. Illustration of melt/solution blending. Shear stress (stirring, sonication, etc.) is used to exfoliate and intercalate the clay particles.[73] Reprinted from Ref. 73.

The motivation for polymer composite gas barrier is to eliminate the use of vacuum and the preservation of desired thin film mechanical properties.[80, 81] The most studied polymer composite barriers consist of inorganic platelet-shaped fillers (mica, clay, etc.), which are impermeable to most gases.[82] The barrier improvement can be explained by the tortuous path model, in which gas molecules wiggle around the platelets and follow a random pathway, as show in Figure 8.[9] Three factors were identified to play a major role in the polymer nanocomposite permeability: clay volume fraction, orientation and aspect ratio.[9] High clay loading, better clay exfoliation and alignment lead to better oxygen barrier. Several theoretical models have been proposed to quantify the gas transport in

polymer composites. Nielsen first described the tortuosity factor (τ) as the ratio of distance traveled by the gas molecules through polymers with (d) and without (d') clay fillers, which could be further defined by aspect ratio and volume fraction of clay ($\emptyset_s$): [83]

$$\tau = \frac{d\prime}{d} = 1 + \frac{L}{2W}\emptyset_s \tag{2.1}$$

The permeability of polymer-clay composites is then expressed as:

$$\frac{P_c}{P_p} = \frac{1-\emptyset_s}{\tau} \tag{2.2}$$

where P_c and P_p are the permeabilities of polymer composites and neat (i.e., unfilled) polymers, respectively. Numerous improvements were made based on this simple model, including the Cusller equation, which is more suitable to composites with high clay loading:[83]

$$\frac{P_p}{Pc} = 1 + \mu\alpha^2\left(\frac{{\emptyset_s}^2}{1-{\emptyset_s}^2}\right) \tag{2.3}$$

where μ is a geometric factor and α is half of the aspect ratio (L/2W) of the filler. These models about parallel nanoplatelets were based on the assumption that clay does not affect the polymer permeability, which was later proven to be invalid.[84] More models were proposed based on the random position of plates,[85] and platelets with random orientation.[86]

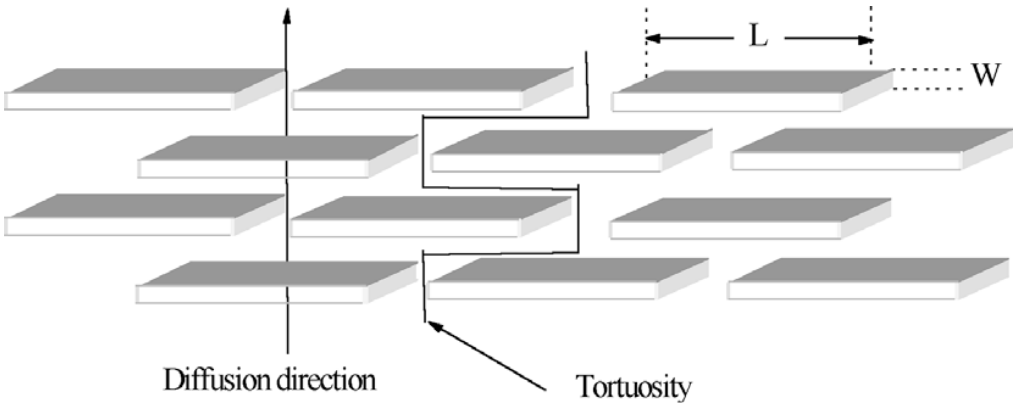

Figure 8. Proposed model of the tortuous paths in an exfoliated polymer-clay composite, where L and W represent the width and thickness of the nanoparticles, respectively. The direction of gas diffusion is indicated by the arrow.[9] Reprinted from Ref. 9.

Incorporating clay particles significantly improves the gas barrier of polymer matrices if high exfoliation and alignment are achieved, which is especially difficult when high clay loading or high transparency is required.[87] For example, Triantafyllidis *et. al.* prepared a 100 μm thick epoxy/MMT composite film using epoxy resin and amine curing agent.[10] Although exhibiting a good gas barrier (permeability<0.1 cc mL/(m^2 day)) at ~80 wt% clay loading, this polymer composite film has a hazy appearance due to clay aggregation. In another study, a poly(acrylic acid) sodium salt/saponite paste was prepared with a homogenizer, followed by casting and heating. The composite has reasonable transparency (~80%) and oxygen barrier (0.074 cm^3/(m^2 day atm) at 80 wt% clay concentration.[11] This combination of high barrier and transparency is possibly related to the good clay alignment formed during the drying process (see Figure 9). Except for the lack of transparency, another drawback of traditional polymer nanocomposites is the barrier deterioration at high humidity, which is related to the hydrophobicity of clay platelets and the matrix polymer.[88, 89]

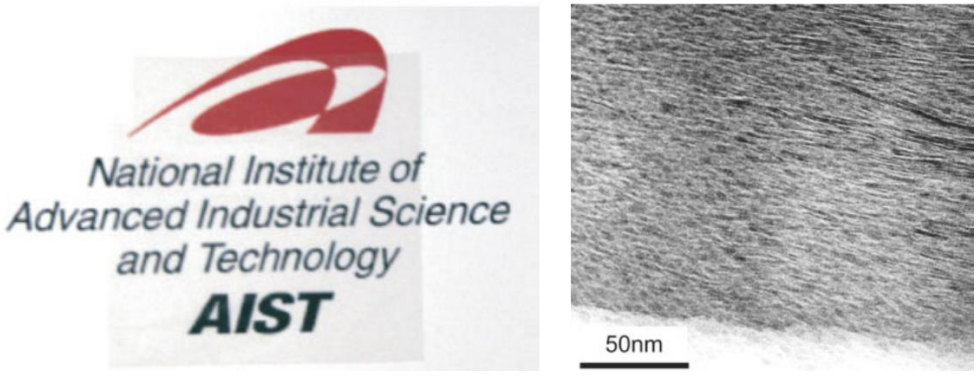

Figure 9. Optical clarity (left) and TEM cross-sectional image (right) of poly(acrylic acid) sodium salt/saponite film with 80 wt% clay loading.[11] Reprinted from Ref. 11.

2.2.2 Multilayer Organic/Inorganic Gas Barrier

Organic/inorganic multilayer thin films have been commonly used in semiconductor packaging and solar cell encapsulation due to their high water vapor barrier performance.[90-93] The substrates are usually first coated with a polymer (e.g., silicone or polyimide) for good adhesion, followed by a metal or inorganic oxide thin film coating. The multilayer film structure is built by repeating this organic/inorganic pair (dyad) through CVD and free radical polymerization.[5] This multilayer structure improves the barrier performance of the single layer inorganic coatings by preventing the propagation of permeation pathways, as shown in Figure 10, which are the result of the defects (i.e., cracks and pinholes).[94] A ~200 nm multilayer coating comprised of two SiN_x layers (~10 nm) and one poly(glycidyl methacrylate) layer (200 nm) exhibits a WVTR < 5×10^{-7} g/(m^2 day) after 190 days.[94] It's worth mentioning that a completely inorganic Al_2O_3/ZrO_2

multilayer film has also been prepared.[95] A 5 dyad stack of this coating, with a thickness of only 50 nm, exhibits a WVTR below detection while remaining transparent. Despite having high water vapor barrier, these films require very complicated coating and recycling process.

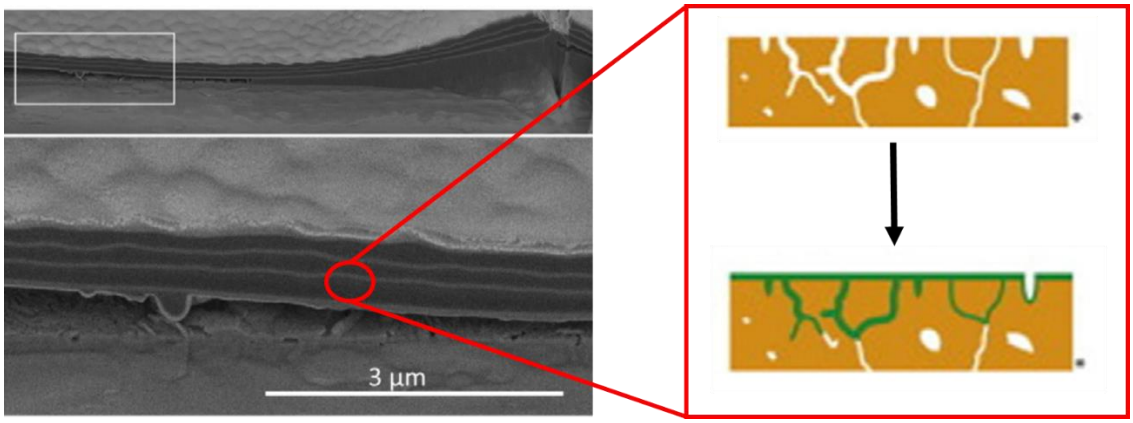

Figure 10. SEM cross-sectional image of a SiN_x/poly(glycidyl methacrylate) multilayer coating (left). Illustration of the defect decoupling through polymer interlayers (right).[94] Reprinted from Ref. 94.

2.3 Layer-by-Layer Assembly

2.3.1 Introduction to Layer-by-Layer Assembly

The history of layer-by-layer (LbL) assembly can be traced back to 1966 when Iler demonstrated the first multilayer assembly of colloidal particles.[96] It was not until the early 1990s, when Decher *et. al.* firstly demonstrated LbL assemblies of "fuzzy supramolecular objects",[97, 98] that LbL began to attract significant attention. The concept of this template-assisted assembly technique is shown in Figure 11, where a charged surface is needed to deposit the first polyion layer, which inverses the surface zeta potential. This surface

charge inversion provides the driving force for the adsorption of the oppositely charged polyion.[14] While electrostatic attractions (i.e., ionic bonding) are the most common driving force for deposition, other interactions (e.g., hydrogen boding) can also be used to deposit these multifunctional films. Moreover, it should be noted that the substrate does not necessarily need to be charged, the multilayer film growth is independent of substrate geometry (planar, porous, particulate, tubular, and etc.) and surface chemistry beyond certain number of deposition cycles.[13]

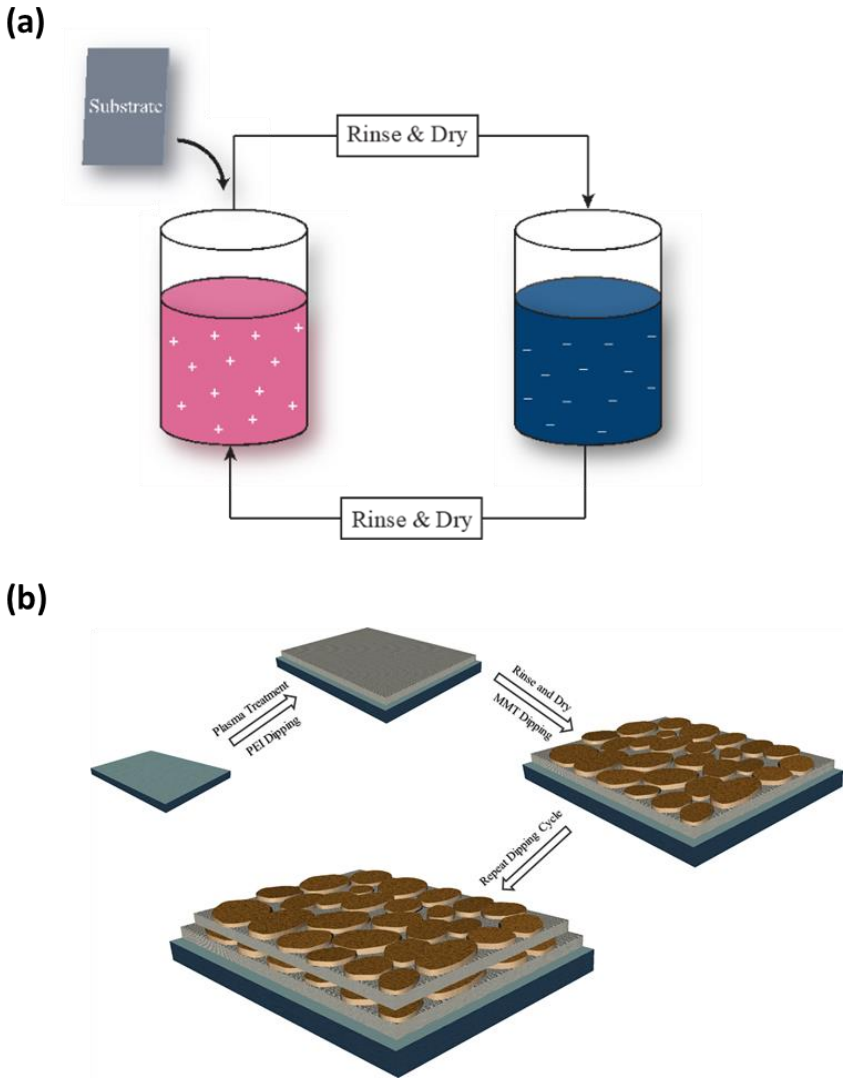

Figure 11. (a) Schematic of layer-by-layer assembly. (b) Structure of multilayer film comprised of cationic polyethylenimine and anionic montmorillonite clay.

A wide range of materials can be incorporated in the layer-by-layer assemblies including polyelectrolytes,[99] nanoparticles,[100] dyes,[101] graphene oxide,[102] peptides,[103] clay minerals,[104] carbon nanotubes,[105] proteins,[106] viruses,[107] DNA,[108] etc. In addition to the

most widely used electrostatic interactions,[109] hydrogen bonding,[110] hydrophobic interactions,[111] host-guest interactions,[112] covalent bonding,[113] etc.[114, 115] have been employed as the driving force to assemble these multilayer films. The influence of solution pH, ionic strength, temperature, and polymer molecular weight on the multilayer film growth have also been investigated.[13] Various means of layer deposition, including dipping,[116] spinning,[117] and electrodeposition[118] have been reported. Recent progress with spray-based deposition, [119, 120] and pilot scale continuous immersion,[121, 122] suggests that the LbL technique is amenable to large scale production. It is due to this versatility of materials, driving forces, and coating procedures that layer-by-layer assembly has become one of the most studied multilayer fabrication techniques. These multilayer films can exhibit properties such as superhydrophilicity,[123] anti-reflection,[124] drug delivery,[125] tissue engineering,[126] thermoelectricity,[127] gas separation,[128] flame resistance,[129] and high strength.[130]

2.3.2 Gas Barrier of Layer-by-Layer Assembly

It can be concluded from Section 2.2 that highly-ordered and defect free layered structures are critical for transparent high gas barriers. The layer-by-layer technique is an ideal candidate for accomplishing this due to its excellent control over thin film structure. Ever since Kotov *et. al.* reported the first LbL gas barrier membrane assembled with MMT and poly(diallyldimethylammonium) chloride in 1998,[131] LbL assemblies of polyelectrolytes and clays have been used to impart transparency, flexibility and super gas barrier to various substrates.[15-17, 19, 41, 132, 133] The nanobrick wall coatings assembled with

PEI and MMT almost perfectly realize the Nielsen's tortuosity model.[83] The highly ordered polymer/clay multilayer structure can be seen in the TEM cross-sectional image in Figure 12(a). The oxygen permeability of a 10 BL PEI/MMT multilayer nanocoating (~80 nm thick) assembled with a pH 4 clay suspension is as low as 2.9×10^{-20} cm^3 cm/(cm^2 s Pa).[15] Larger clay spacing was realized in a PEI/PAA/PEI/MMT quadlayer film, which creates a longer diffusion path between the clay layers (Figure 12(b)). 5 QL of this multilayer film on poly(ethylene terephthalate) (PET) substrate, with a thickness of only 51 nm, exhibits an OTR below the detection limit of commercial instrumentation (<0.005 cm^3/(m^2 day atm)).[40] This coating is flexible and highly transparent (visible light transmission > 95%). More barrier improvements have been made through pH and ionic strength manipulation of the MMT suspension, which will be discussed in detail in Chapters IV and V. In addition to polyester substrate, layer-by-layer assembled gas barrier coatings were proven to be applicable to polyolefin films, the coating systems and barrier improvement could be found in Chapter III.[134]

Despite the excellent oxygen barrier, these multilayer nanocoatings are not exempt from barrier loss at high humidity. The use of Nafion as a hydrophobic component has been reported, and water vapor permeability was reduced by 75%.[135] Song *et. al.* attempted to fill the vacancies between MMT platelets in a PVOH/MMT multilayer film with Au_2O_3, which resulted in good water vapor barrier (WVTR = 3.2×10^{-3} g/(m^2 day)).[136] The water transport mechanism in the multilayer film is still unclear, and the production of a cost-effective LbL water vapor barrier remains challenging for applications like flexible electronics protection. Although it's difficult to maintain high barrier at humid

environment, high humidity can be used as the healing stimulus and repair the damage to these LbL gas barrier coatings (see Chapter VI).

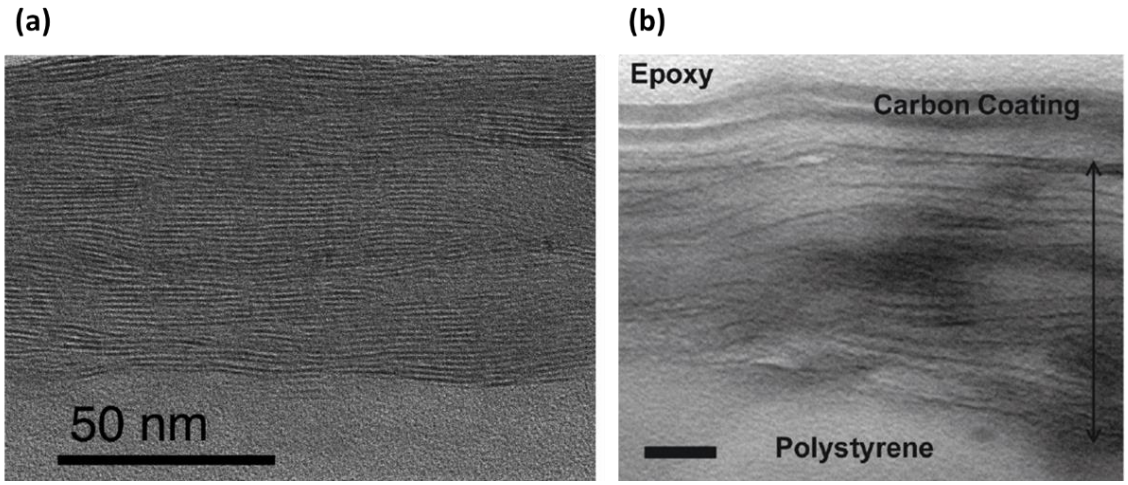

Figure 12. TEM cross-sectional images of (a) 10 BL PEI/MMT[15] and (b) 5 QL PEI/ PAA/PEI/MMT films. The scale bar is 20 nm in (b).[40] Reprinted from Ref. 15 and 40.

2.3.3 Stimuli Responsive Behavior of Multilayer Films

Responsive polymers (or smart polymers) are a group of materials that can change shape in response to external stimuli, or convert chemical signals to thermal and mechanical signals (and vice versa).[137] Temperature, pH, pressure, chemicals, and electric field are the most commonly used stimuli for these polymers.[138] Although a relatively new type of material, stimuli responsive polymers have already been used for shape memory,[139] biomedical applications,[140, 141] and sensors.[142] Due to the precise control over the thin film properties (i.e., components, thickness, interaction between layers,

hydrophobicity/hydrophilicity, etc.), multilayer films prepared with layer-by-layer assembly have shown great potential as stimuli responsive polymers.[143] Most of the work in this area is focused on microscopic shape change for drug/protein releasing/targeting and self-healing, which relies on the physicochemical property changes in response to pH, ionic strength, light, humidity, etc.[144]

A sacrificial core technique (Figure 13) is commonly employed to prepare drug delivery and biosensing LbL assemblies. In this process, a negatively charged core with loaded targeting material is used as a template to deposit oppositely charged polyelectrolytes, the hollowed micro or nanoshells are formed after core removal in suitable solutions.[145, 146] A variety of core ($CaCO_3$, polystyrene, Au nanoparticles, etc.) and loading (proteins, DNAs, dyes, etc.) materials have been reported.[145] By carefully choosing the + and thickness of these multilayer capsules, magnetic field,[147] ultrasound,[148] light,[143] pH,[149] and ionic strength[150] can be used to control the release. For example, Antipov *et. al.* assembled the multilayer microcapsules on melamine formaldehyde and $CdCO_3$ particles with sodium poly(styrene sulfonate) (PSS) and poly(allylamine hydrochloride) (PAH).[149] The "on" (permeable to small molecules (albumin or dextrans)) and "off" (impermeable to small molecules) status of microcapsule were found to be switchable at pH 8.

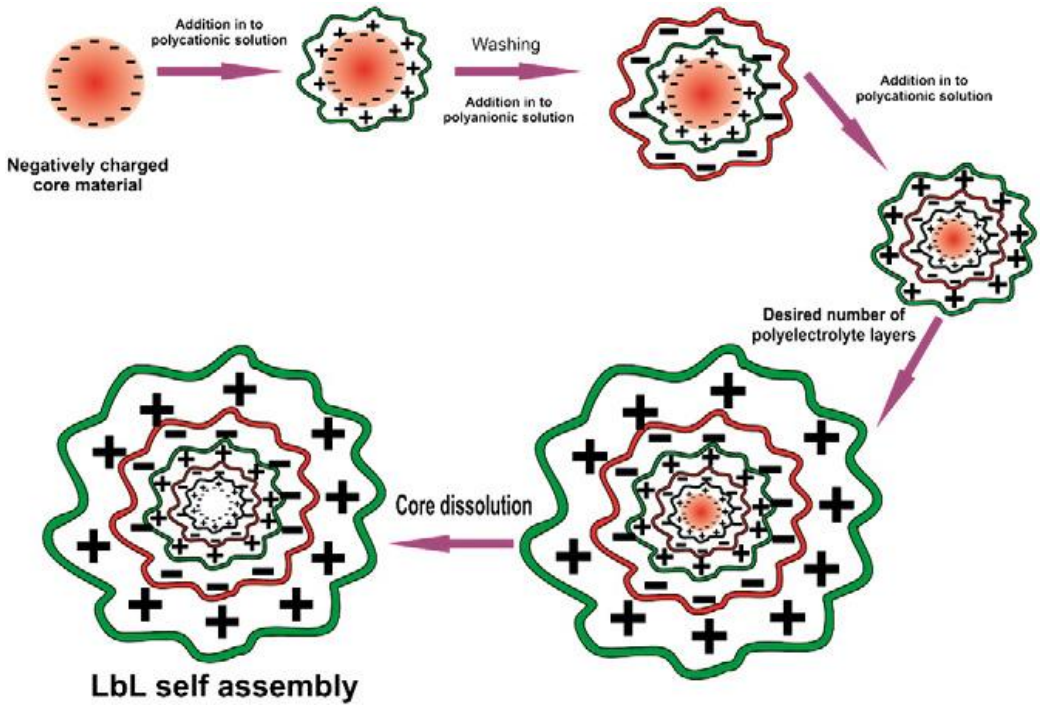

Figure 13. Schematic of core sacrificing technique for LbL assembled drug delivery microcapsules.[145] Reprinted from Ref. 145.

The ability to self-repair (or self-heal) after being damaged (e.g., cracked) and restore desirable properties (e.g., mechanical strength, gas barrier, or conductivity) is an important trait for polymers and composites.[151] Rapid and efficient self-healing behavior was observed in an ionically-bonded complex of polyacrylic acid (PAA) and poly(allylamine hydrochloride) (PAH) using sodium chloride as a promoter.[152] The porous and loosely packed structure made this complex less robust than more dense layer-by-layer (LbL) polyelectrolyte assemblies. The self-healing behavior of LbL-assembled films has been extensively explored (Table 3).[153, 154] Self-healing of antifouling,[155] antibacterial,[156] superhydrophobic,[157] conductive[158] and flame-retardant[159] LbL films have also been reported.

Table 3. Compositions, healing stimuli and applications of layer-by-layer assembled responsive films.[157] Reprinted from Ref. 157.

Composition of multilayers		Additional component	Stimuli	Application area
PAH-SPEEK	PAA	POTS	Humidity	Super hydrophobic surfaces
PAH-SPEEK	PAA	POTS, PFOS	Humidity	
bPEI	PAA	Triclosan	Water	Antibacterial coating
bPEI	PAA	–	Water	–
PEI	PSS	8-Hydroxyquinoline	pH, ionic strength	Corrosion protection
PEI	PSS	–	pH, ionic strength	Corrosion protection
PEI, PDADMAC	PSS, PAA	8-Hydroxyquinoline	pH, ionic strength	Corrosion protection
–	PSS	8-Hydroxy-quinoline, benzotriazole	pH, ionic strengh	Corrosion protection; antibacterial coating
PDADMAC	*p*-NIPAm-AAc		Water	Antifouling biocoating
BMAADq micelles	–	–	pH	Antibacterial, self-recovery, self-cleaning
PVPON	PAA	–	Water/ethanol	–
PEI	PVDMA	*n*-decylamine	pH	superhydrophobic surfaces

The most commonly observed self-healing behavior in assembled films depends on water or solvent-induced mobility of polymer chains.[160] In the swollen state, the increased free volume in the film allows the diffusion and rearrangement of polyelectrolyte chains, which results in the healing and restoration of the original properties. For instance, an electrically conductive multilayer composite was prepared by depositing silver nanowires in a PEI/PAA film. Conductivity was recovered simply by dipping the composites in water.[158] There are also reports about LbL composite capsules used for self-healing. Healing agents were carried in the multilayer capsules and released during cracking.[161] In addition to the multilayer drug delivery and self-healing materials, there have been reports about stimuli responsive multilayer assemblies used as actuator and shape memory materials.[162] [163] A two-way vapor responsive multilayer polymer actuator will be discussed here in Chapter VII, which is the first demonstration of its kind.

CHAPTER III

SUPER OXYGEN AND IMPROVED WATER VAPOR BARRIER OF POLYPROPYLENE FILM WITH MULTILAYER NANOCOATINGS*

3.1 Introduction

Biaxially oriented polypropylene (BOPP) film is produced when polypropylene is stretched in two perpendicular directions when held between its glass transition and melting temperatures.[164] This orientation improves mechanical and optical properties relative to cast polypropylene film, which makes BOPP the most widely used film in packaging.[165] Oriented polypropylene has a good water vapor barrier but a relatively poor oxygen barrier due to its nonpolar polymer backbone. In this study, polymer-only (PEI/PAA) and polymer-clay (PEI/VMT) bilayers were independently deposited on BOPP film to improve its oxygen and moisture barrier at various relative humidities. Both systems were able to lower the OTR by more than an order of magnitude, making BOPP more suitable for a variety of food and electronics packaging applications. [42, 166]

---

*Reprinted with permission from Song, Y.; Tzeng, P.; Grunlan, J. C. Super Oxygen and Improved Water Vapor Barrier of Polypropylene Film with Polyelectrolyte Multilayer Nanocoatings. *Macromol. Rapid Commun.* **2016,** 37, 963. Copyright 2016 John Wiley and Sons.

3.2 Experimental Section

Branched polyethylenimine (Mw=25,000 g/mol, ρ=1.10 g/cm3) and poly(acrylic acid) (M_w=100,000 g/mol, ρ=1.20 g/cm^3) were purchased from Sigma-Aldrich (Milwaukee, WI) and used as received. 0.1 wt% PEI and 0.2 wt% PAA aqueous solutions were prepared with 18.2 MΩ deionized (DI) water and rolled for 24 h to achieve homogeneity. Natural vermiculite (VMT) clay dispersion (Microlite 963++) was supplied by Specialty Vermiculite Corp. (Cambridge, MA). A 1 wt% VMT aqueous suspension was prepared by diluting the 7.5 wt% slurry with DI water and rolling for 24 h. The supernatant was then collected after sedimentation for another 24 h, resulting in a 1 wt% VMT suspension.

Biaxially oriented polypropylene film, with a thickness of 17.8 μm (0.7 mil), was purchased from Xiamen Foreign Trade Co. (Xiamen, China) and used as the substrate for OTR testing. 179 μm thick (7 mil) poly(ethylene terephthalate) (PET) film was purchased from Tekra (New Berlin, WI) and used as the substrate for transmission electron microscopy (TEM). Prior to deposition, the BOPP and PET substrates were cleaned by rinsing with deionized water, methanol, and DI water again, followed by drying with filtered air. Corona treatment was applied using a BD-20C Corona Treater (Electro-Technic Products, Inc., Chicago, IL) to impart negative charge to film surface in an effort to improve adhesion. Single-side-polished silicon wafers, purchased from University Wafer (South Boston, MA), were used as the substrate to monitor film growth. Silicon wafers were rinsed with acetone and DI water followed by plasma treatment for 5 min just before use.

Layer-by-layer coating was carried out with a programmable home-built robotic dipping system.[167] Prior to deposition, the pH of cationic PEI solution and anionic PAA solution were altered to 10 and 4, using 1 M HCl and NaOH, respectively. The pH of the VMT suspension was left unaltered at 9.2. As illustrated in Figure 14, each substrate was dipped into the cationic PEI solution for 5 min, followed by rinsing and drying, and then dipped into an anionic PAA or VMT solution for another 5 min to complete the initial bilayer (BL). All subsequent deposition cycles were completed with 1 min dips in both cationic and anionic solutions, with rinsing and drying in between. The assembled films are denoted as $(PEI/PAA)_x$ or $(PEI/VMT)_x$, where x is the number of bilayers deposited.

Multilayer film thickness was measured by a P6 profilometer (KLA-Tencor, Milpitas, CA). Several parallel scratches were made on the coated silicon wafer to allow thickness to be measured by the step height difference created by the scratch. Each reported thickness was the average of 9 step height measurements. Adhesion of the multilayer assembly to the polypropylene substrate was evaluated by a simple tape test (Paul N. Gardner Co., Inc., Pompano Beach, FL). A 22 mm wide pressure-sensitive tape was placed on the film and then removed by pulling off rapidly at an angle of 180°. TEM samples were prepared by embedding a small piece of coated PET in Epofix resin (EMS, Hatfield, PA), curing overnight and then cutting cross-sections using an Ultra 45° diamond knife (Diatome, Hatfield, PA). Samples were imaged on copper grids using a Tecnai G2 F20 (FEI, Hillsboro, OR), operated at 200 kV. In accordance with ASTM Standards D-3985 and F-1249, OTR and WVTR tests were performed by MOCON (Minneapolis, MN).

An Oxtran 2/21 instrument, operated at 23 °C and various relative humidities, measured OTR. A Permatran-W3/33 instrument, operated at 23 °C and 100% RH, measured WVTR.

3.3 Results and Discussion

Two distinct growth regimes are observed for the polyethylenimine/poly(acrylic acid) system, shown in Figure 14(b). In the first few bilayers, thickness increases exponentially as more BL are deposited, which is believed to be caused by an "in-and-out" diffusion process with the underlying layers.[168] In the second regime, a relatively large linear growth rate is realized due to saturated polyelectrolyte interdiffusion, which can be altered by deposition conditions such as solution pH and dipping time.[120, 169, 170] This type of superlinear growth is commonly observed in weak polyelectrolyte assemblies.[171-173] PEI and PAA polymer chains are initially in low charged states in the deposition solutions, but their functional groups become highly charged when exposed to the oppositely charged solution due to the pH change. This strong electrostatic interaction results in a highly complexed polymer film capable of slowing gas diffusion.[39, 128]

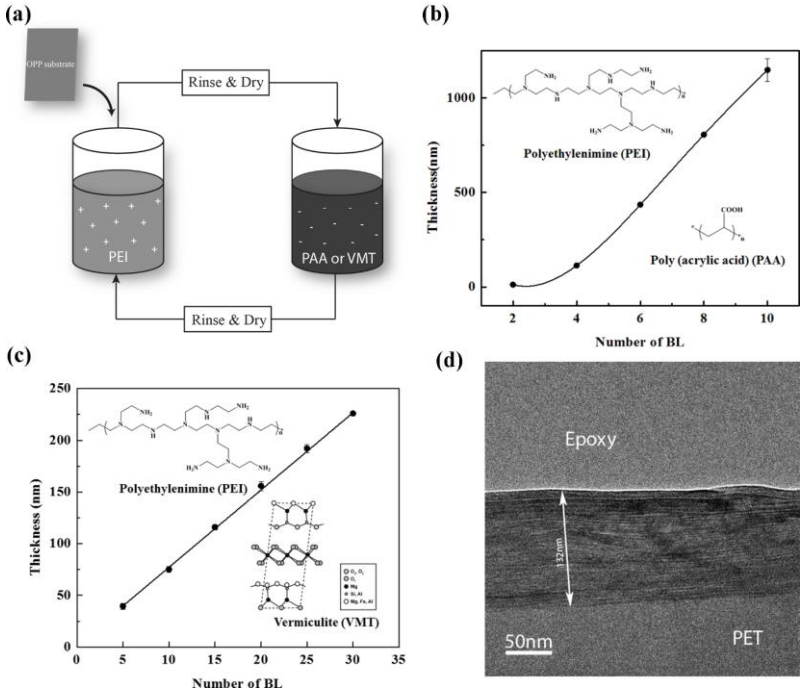

Figure 14. (a) Schematic of the layer-by-layer (LbL) coating process. Thickness as a function of bilayers deposited on a silicon wafer for (b) PEI/PAA and (c) PEI/VMT. (d) TEM image of the cross-section of a 20 BL PEI/VMT film deposited on PET.

PEI/VMT forms a more densely packed film structure, with VMT platelets lying perpendicular to the substrate, resulting in a more stratified "nanobrick wall" structure. Clay platelets prevent PEI diffusion through the multilayers, which results in the very linear film growth shown in Figure 14(c). Being completely free of aggregation, these highly aligned clay platelets create an extremely tortuous path for permeating molecules.[174] Figure 14(d) shows a TEM cross-section of a 20 BL PEI/VMT film. The exceptional platelet exfoliation and alignment is apparent in this image. There are fewer than 40 platelet edges observed here, suggesting that the vermiculite is depositing as individual nanoplatelets or doublets. It is this unique combination of alignment and platelet separation that provides high barrier in these thin films.

Oxygen transmission rate of biaxially oriented polypropylene, coated with polymer and clay-based assemblies, was tested at 23°C and 0, 50% or 100% RH, as shown in Table 4. Under dry conditions, OTR decreased as more bilayers were deposited on BOPP due to the longer and more tortuous diffusion path for oxygen molecules. A 30 BL PEI/VMT film (226 nm thick) provided an oxygen barrier almost 40 times better than the uncoated substrate (17.8 μm thick). When the relative humidity increased to 50%, the oxygen barrier of both PEI/PAA and PEI/VMT improved. It is well known that hydrophilic polymer barrier improves at intermediate humidity, which is the result of water molecules filling the free volume within the multilayer thin films. [175-178] Although the PEI/PAA nanocoating has a relatively small free volume relative to typical polymers,[179] it exhibits a greater reduction in OTR (49%) than the more densely packed PEI/VMT films (5%) . PEI/PAA loses some of its barrier at 100% RH, but PEI/VMT surprisingly improved. When the relative humidity is high, moisture absorbed by the hydrophilic sites of PEI and PAA plasticizes the polymer multilayer film, resulting in enlarged free volume and faster gas diffusion. [39, 180, 181]

Table 4. Oxygen barrier and barrier improvement factor of multilayer-coated BOPP.

LbL Systems	Relative humidity (%)	OTR ($cm^3/(m^2$ day atm))	Permeability (10^{-16} cm^3 $cm/(cm^2$ s Pa))		BIF[b)]
			Coating[a)]	Total	
uncoated BOPP	0	2278.5	N/A	462.75	N/A
PEI/PAA 8 BL	0	124.0	2.412	27.46	16.8
PEI/PAA 10 BL	0	114.9	3.169	26.34	17.6
PEI/PAA 12 BL	0	83.4	3.176	20	23.1
PEI/VMT 10 BL	0	255.8	0.495	52.38	8.8
PEI/VMT 20 BL	0	105.9	0.395	21.88	21.2
PEI/VMT 30 BL	0	57.2	0.303	11.91	38.8
uncoated BOPP	50	2511.0	N/A	509.97	N/A
PEI/PAA 12 BL	50	42.8	1.597	10.26	49.7
PEI/VMT 30 BL	50	54.1	0.285	11.26	45.3
uncoated BOPP	100	2495.5	N/A	506.83	N/A
PEI/PAA 12 BL	100	189.1	7.507	45.34	11.2
PEI/VMT 30 BL	100	15.0	0.078	3.13	161.9

[a)]The permeability of coated films were decoupled from the total permeability using a previously described method.[7] [b)]BIF=P_S/P_T, where P_S and P_T are the permeability of bare and coated BOPP, respectively.

$(PEI/VMT)_{30}$ preserves the oxygen barrier at high relative humidity due to its relative reluctance to swell. This is evidenced by an unchanged thickness of PEI/VMT film after a 12-hour exposure to ~97% humidity, while the PEI/PAA film thickness increased ~8% on average. Relative to the dry state, OTR of the clay-based assembly decreased by ~70% at 100% RH, improving the oxygen barrier of the thick BOPP film by more than 160 times. Oxygen transmission rate, permeability and barrier improvement factor (BIF) of all LbL-coated BOPP is summarized in Table 4. BIF is a standard parameter for quantifying the coating influence. This high humidity oxygen barrier, with a thickness below 250 nm, rivals most other coatings previously applied to BOPP (including inorganic oxides).[42, 182-184] Additionally, no coating was removed from the

substrate after tape testing, revealing the good adhesion of these multilayer thin films, which is a major problem for inorganic coatings.[57]

Water vapor transmission rate (WVTR) of coated and uncoated BOPP films was tested at 100% RH, as shown in Table 5 and Figure 15. Similar to OTR, thicker nanocoatings provide a longer and more tortuous diffusion path for water molecules, which reduces the WVTR. A 15% reduction in WVTR was achieved with $(PEI/PAA)_{12}$, while $(PEI/VMT)_{30}$ lowered the transmission rate by 43%. Overall, moisture barrier only improved modestly relative to oxygen due to the hydrophilic nature of these multilayer nanocoatings. It is worth mentioning that the water vapor permeability of 12 BL PEI/PAA is higher than bare BOPP (BIF < 1), likely due to the multilayer acting as a water reservoir, which also contributes to the increased OTR at 100% RH.

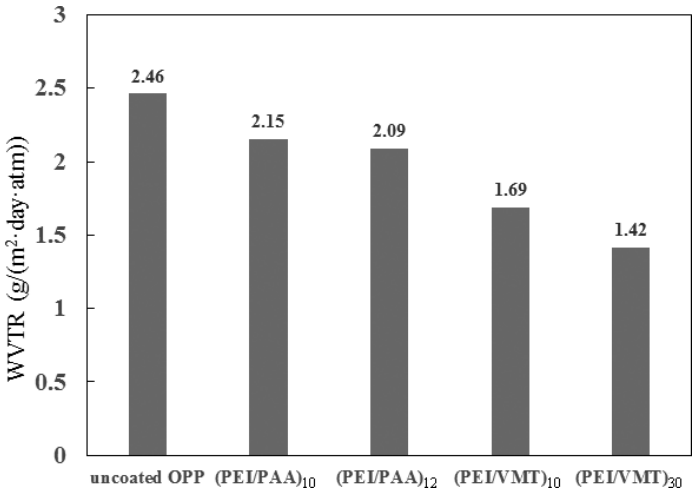

Figure 15. Water vapor transmission rate of coated and uncoated biaxially oriented polypropylene.

Table 5. Moisture barrier of multilayer thin films on biaxially oriented polypropylene.

LbL Systems	Thickness (nm)	WVTR ($g/(m^2\ day)$)	Permeability (10^{-16} g cm/(cm^2 s Pa))		BIF[b)]
			Coating	Total	
uncoated BOPP	N/A	2.465	N/A	0.5	N/A
PEI/PAA 10 BL	1147	2.155	0.449	0.494	1.013
PEI/PAA 12 BL	1606	2.093	0.509	0.502	0.998
PEI/VMT 10 BL	75	1.690	0.009	0.346	1.446
PEI/VMT 30 BL	226	1.418	0.017	0.295	1.695

3.4 Conclusions

All-polymer and polymer-clay nanocoatings were deposited layer-by-layer onto 17.8 μm thick biaxially oriented polypropylene in an effort to improve oxygen and water vapor barrier. A 30-bilayer coating of polyethylenimine and vermiculite clay (226 nm thick), reduced the oxygen transmission rate of BOPP nearly 50X and the water vapor transmission rate more than 40%. The oxygen barrier actually improves at 100% RH due to this coating's resistance to swelling. A 12-bilayer polyethylenimine and poly(acrylic acid) coating (1.6 μm thick) reduced OTR nearly as much as PEI/VMT, but this improvement diminished by a factor of two at 100% RH. More work could be done to make PEI/PAA more hydrophobic through crosslinking,[185] or incorporating water-impermeable (or scavenging) layers.[136, 186-188] These multilayer coated BOPP films, with OTR less that 100 $cm^3/(m^2\ day\ atm)$ and WVTR less than 2 $g/(m^2\ day)$, are suitable for sensitive food and even some electronics packaging.

CHAPTER IV

BALANCING POLYELECTROLYTE DIFFUSION AND CLAY DEPOSITION FOR HIGH GAS BARRIER*

4.1 Introduction

It was previously shown that reducing the pH of the clay suspension, in a polyethylenimine (PEI)-montmorillonite (MMT) clay bilayer system, increases the amount of clay deposited and improves the oxygen barrier performance.[15] The charge of montmorillonite clay platelets in water is not highly dependent upon pH, but the charge of the previously deposited layer of PEI is very sensitive. As pH is reduced below 10, PEI progressively has a higher charge density, which attracts more clay platelets to be deposited. A pH 4 suspension of MMT resulted in an optimum clay deposition that showed excellent order and approximately twice as much clay deposited per bilayer than a pH 10 suspension. It has also been shown that including additional polymer layers (e.g. PEI/MMT followed by PEI/PAA) between clay layers can decrease the permeability of the thin film by increasing the spacing between clay layers, which provides more volume in which gas molecules can reside.[40, 87] The present work combines the concepts of decreasing clay pH and increasing spacing. This optimum pH is not necessarily the same as that previously found for the PEI/MMT bilayer system (i.e. pH 4),[15] which was the

---

*Reprinted with permission from Hagen, D. A.; Song, Y.; Saucier, L.; Milhorn, A.; Stevens, B.; Grunlan, J. C. Balancing Polyelectrolyte Diffusion and Clay Deposition for High Gas Barrier. *Green Materials* **2016**, 4(3), 1. Copyright 2016 ICE Publishing.

result of maximized clay deposition. In the PEI/PAA/PEI/MMT quadlayer (QL) system, additional polymer deposition between layers can be achieved through diffusion (at high pH), which has also been shown to improve oxygen barrier properties.[40] The polymer-clay nanocomposite thin films explored here are capable of reducing the amount of material used to impart barrier due to their minimal permeability.

4.2 Experimental Section

Branched polyethylenimine (PEI) (M_w = 25,000 g/mol, ρ = 1.10 g/cm^3) and poly(acrylic acid) (PAA) (M_w = 100,000 g/mol, ρ=1.20 g/cm^3) were purchased from Sigma-Aldrich (Milwaukee, WI). PEI was used as a 0.1 wt% aqueous solution and PAA was used as a 0.2 wt% solution in deionized (DI) water. Natural sodium montmorillonite clay (MMT, trade name Cloisite NA+) provided by BYK Additives Inc. (Gonzales, TX), was dispersed as a 1 wt% suspension in DI water by rolling (to gently agitate) these solutions in bottles overnight. MMT platelets have a reported density of 2.86 g/cm^3, diameter ranging from 10-1000 nm, and individual platelet thickness of 1 nm.[189]

Poly(ethylene terephthalate) film, with a thickness of 179 μm (trade name ST505, produced by Dupont-Teijin), was purchased from Tekra (New Berlin, WI) and used as the substrate for oxygen transmission rate (OTR) testing and transmission electron microscopy (TEM). This PET film has an OTR of approximately 8.6 cm^3/(m^2·day·atm) under dry conditions. Polished silicon wafers were purchased from University Wafer (South Boston, MA) and were used as substrates for ellipsometry. The same cleaning procedure is followed for PET and silicon wafer substrates as in Chapter 3.2.

Each substrate was dipped into the 0.1 wt% PEI solution, previously adjusted to pH 10.0 using 1 M HCl, for one minute. After each dip, the substrate was rinsed with DI water and dried with filtered air. The substrate was then dipped into the anionic PAA solution, previously adjusted to pH 4.0 using 1 M NaOH. This procedure was followed by another dip into PEI and a dip into the anionic MMT suspension. The pH of MMT suspension was altered to 3, 4, 5, 6, or 8 with 1M HCl (or pH 10 with 1 M NaOH), which completed a single quadlayer dipping cycle. After the final rinsing and air drying steps, the films deposited on PET were dried in an oven at 70°C for 15 min.

Thickness measurements were taken as a function of quadlayers deposited using a P6 profilometer (KLA-Tencor, Milpitas, CA). Reported thickness is the average of four measurements from each of three different silicon wafers. The coatings were scratched with a razor blade to expose the silicon wafer surface. Mass deposition onto Ti/Au plated quartz crystals was measured using a Research Quartz Crystal Microbalance (QCM) (Maxtek Inc., Cypress, CA). Oxygen transmission rate (OTR) testing and transmission electron microscopy (TEM) imaging were performed using the sample method described in Chapter 3.2.

4.3 Results and Discussion

Exponential growth is commonly observed in weak polyelectrolyte multilayer films,[39, 171] which is believed to be caused by an "in-and-out" diffusion of polymers.[168] When clay layers are included, they act as a barrier to diffusion, but do not completely suppress the exponential growth of PEI/PAA/PEI/MMT quadlayers.[109] This combination

of aligned and impermeable clay platelets, embedded within a highly interdiffused network of PEI and PAA, exhibits much low oxygen permeability (<5 $\times 10^{-22}$ $cm^3 \cdot cm/(cm^2 \cdot s \cdot Pa)$) than that of PEI/MMT or PEI/PAA bilayer systems.[35, 39, 87] As the pH of MMT is decreased (below 10), additional clay is deposited that further suppresses exponential growth by restricting the diffusion of polymer chains into the multilayer film. This creates a tradeoff between two methods of reducing oxygen transmission, shown schematically in Figure 16. Deposition at lower pH generates better packed layers, but greater clay spacing (and overall film thickness) is achieved with higher pH clay deposition.

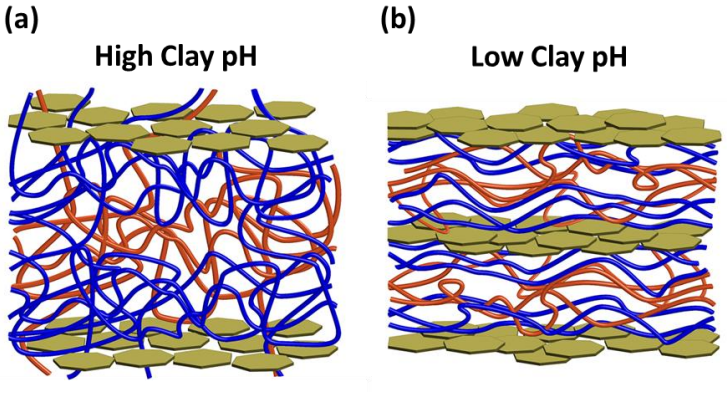

Figure 16. Schematic of PEI (blue)/ PAA (red)/PEI/MMT quadlayers deposited at (a) high and (b) low clay suspension pH.

Growth of PEI/PAA/PEI/MMT decreases with clay pH from 10 to 4, as shown in Figure 17(b). Reduced film thickness with lower clay pH is presumably due to greater inhibition of polymer interdiffusion between layers. At pH 3, QL thickness is slightly greater than that at pH 4 because this is where there is no polymer diffusion through the clay layer, as indicated by the linear growth trend. The slightly thicker growth at pH 3 is

believed to be due to modest additional clay in each layer. The mass deposited with varying clay pH does not exactly follow the thickness trend due to the competing effects of clay deposition and polymer diffusion. While having the thickest deposition, the pH 10 QL has relatively little mass deposited. The overall mass increases as clay pH decreases, with a maximum at pH 6. Below pH 6, the restricted polymer diffusion results in less overall mass deposited at pH 4 and 3, as shown in Figure 17(a).

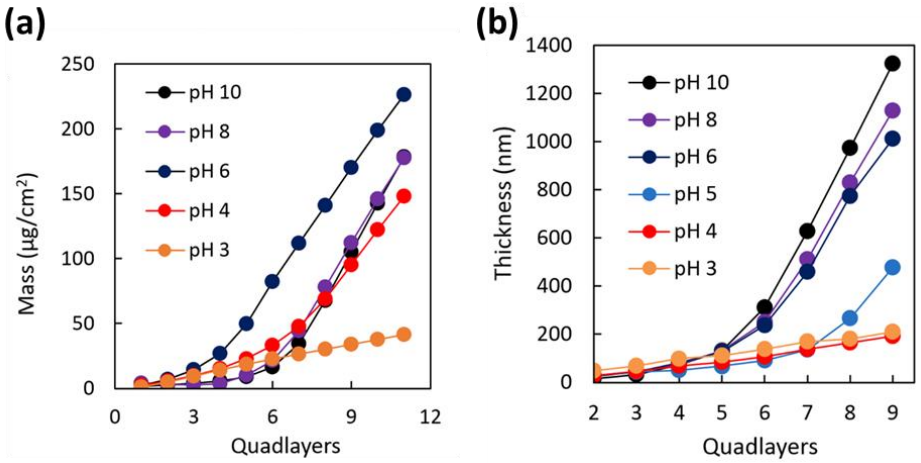

Figure 17. (a) Mass and (b) thickness as a function of PEI/PAA/PEI/MMT QL deposited, with the MMT deposited at varying pH. PEI and PAA were maintained at pH 10 and 4, respectively.

TEM cross-sectional images confirm that a 5 QL film, prepared with pH 4 MMT, has a more compact structure than the QL constructed with MMT at pH 6 (Figure 18(a) and (b), respectively). The excellent alignment of the clay platelets maintains high transparency and creates high oxygen barrier. The alignment and two-dimensional packing of the platelets causes oxygen molecules to diffuse laterally through the polymer layers, increasing the diffusion path.[83, 190] Layer-by-layer assembly makes this ordering possible. This level of order is not attainable in traditional composites, prepared by melt

or solution processing, so there is much less barrier improvement and more opacity.[191-194] It is clear that clay spacing at pH 4 is much smaller than pH 6, which is due to the inhibition of polyelectrolyte interdiffusion at lower pH. Figure 18 also shows that there are multiple clay platelets deposited every cycle, which could be a result of incomplete exfoliation of stacks.[195]

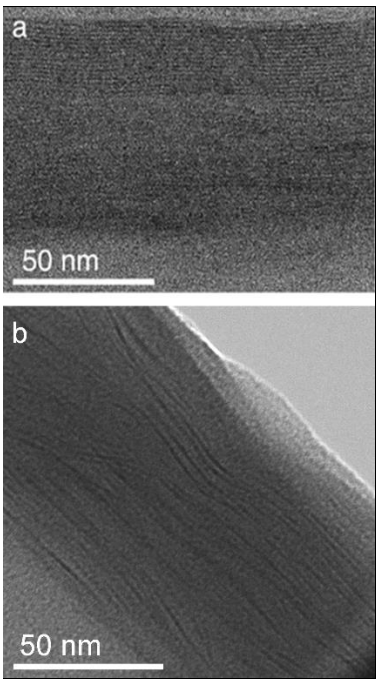

Figure 18. TEM of 5 QL PEI/PAA/PEI/MMT, with MMT deposited at (a) pH 4 and (b) 6.

Figure 19 shows that the minimum oxygen transmission rate as a function of clay deposition pH (between 4 and 10) occurs at pH 5 and 6. The pH 5 system achieves the lower limit of OTR detection (0.005 $cm^3/(m^2 \cdot day \cdot atm)$) at only 3 QL, while pH 6 registered below this level. It is at pH 6 that mass deposition is greatest (Figure 17(a)) due to the best balance between additional clay deposition and some remaining exponential film growth. The system with MMT at pH 3 shows relatively little improvement in barrier

due to the high level of disorder of the clay nanoplateletes, which was observed in a previous study.[15] This exceptionally high barrier, achieved with only 3 QL (44 nm thick), has a permeability less than 5 $\times 10^{-22}$ $cm^3 \cdot cm/(cm^2 \cdot s \cdot Pa)$. This value is ~400× lower than a 3 QL system constructed with unaltered MMT (pH~9.8).[40] Furthermore, this permeability is more than two orders of magnitude lower than SiO_x and aluminized plastic film,[196, 197] which are among the best known barriers for packaging.

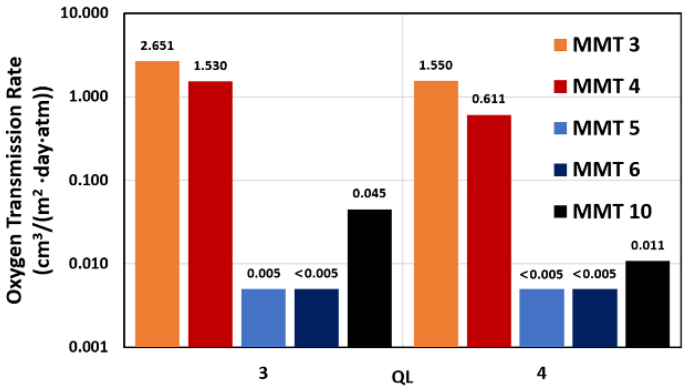

Figure 19. Oxygen transmission rate of PEI/PAA/PEI/MMT QL films on PET substrate, with MMT deposited at varying pH.

4.4 Conclusions

The pH of the montmorillonite clay suspension was altered in a repeating PEI/PAA/PEI/MMT quadlayer assembly in an effort to tailor amount of clay deposition and multilayer growth. Deposition of clay at pH 6 produced the best oxygen barrier performance, where comparatively thick growth was balanced with the largest mass deposited of any of the other systems. At only 44 nm thick, a 3 QL film on PET was below the OTR detection limit (< 0.005 $cm^3/(m^2 \cdot day \cdot atm)$) of the commercial testing equipment. This thickness and transmission rate correspond to an oxygen permeability

that is orders of magnitude below SiO_x and metalized film. Achieving such a transparent super gas barrier thin film, with just 12 total layers deposited from water, should make this an appealing system for food, pharmaceutical and electronics packaging. These results could also be applied to improve the deposition of other charged particles (rods, platelets, etc.) in LbL assemblies to improve a variety of other properties.

CHAPTER V

EDGE CHARGE NEUTRALIZATION OF CLAY FOR IMPROVED OXYGEN GAS BARRIER IN MULTILAYER NANOBRICK WALL THIN FILMS*

5.1 Introduction

It has been previously shown that lowering the pH of a montmorillonite (MMT) clay suspension leads to greater platelet adsorption onto the underlying polyelectrolyte layer due to higher charge density.[15] In the present study, attention has been paid to the surface charge distribution and associated electrical double layer (EDL) structure of MMT platelets. During the formation of anionic montmorillonite clay, platelets form permanent negative charges on the surface due to isomorphic substitution of Al^{+}, Si^{+} and Mg^{+}.[198] Platelet edges are occupied by octahedral Al-OH and tetrahedral Si-OH sites. Ionization or protonation of variable charging of MMT edges.[199] The platelet edges of MMT are neutral from pH 6 to 8 (between the pKa of Al-OH and Si-OH).[200, 201] In an unaltered aqueous MMT suspension (pH~9.8), an EDL is formed, comprised of negatively charged platelets surfaces/edges and their balancing cation layers. As platelets randomly approach each other driven by Brownian motion, the surrounding cations repel and stabilize the clay. Below a suspension these amphoteric sites is highly dependent on the pH of the MMT suspension, resulting in pH of 6, the edges become positively charged and facilitate

---

*Reprinted with permission from Song, Y.; Hagen, D. A.; Qin, S.; Holder, K. M.; Falke, K.; Grunlan, J. C. Edge Charge Neutralization of Clay for Improved Oxygen Gas Barrier in Multilayer Nanobrick Wall Thin Films. *ACS Appl. Mater. Interfaces* **2016**, 8, 34784.

the potential to form edge-to-face (E-F) bonding.[15] This "house of cards" structure, comprised of numerous E-F bonds, is detrimental to gas barrier due to misalignment of platelets.[201-203]

In this study, the pH of an unaltered montmorillonite (MMT) clay suspension was reduced to 6.5, where the amphoteric edges have a neutral net charge. Indifferent electrolytes such as NaCl alter the rheological behavior of the MMT suspension by changing the platelets electrical double layer structure. In salt-free clay suspension, the neutrally charged edges are embedded inside the counter ion cloud of the predominant surface EDL, so a second MMT platelet cannot see the edges and is repelled when approaching (Figure 20(a)). With low NaCl concentration, the EDL of the MMT surface is slightly compressed, which leads to the exposure of neutral edge sites, allowing van der Waals forces to attract the edges to one another (Figure 20(b)).[202, 204, 205] This edge-to-edge (E-E) bonding results in better clay coverage in each deposited layer that creates a more tortuous path for diffusing gas molecules. Lower OTR was achieved in a polyethylenimine (PEI)/MMT multilayer film as a result of this structural engineering. An 8 bilayer (BL) PEI/MMT film, assembled with a clay suspension containing 5 mM NaCl, exhibits an order of magnitude reduction in OTR relative to its salt-free counterpart. At higher NaCl concentration, Na^+ diffuse into the regions inside the MMT platelets where exchangeable cations force H^+ to diffuse out, which leads to a local pH drop and makes the edge sites positively charged (Figure 20(c)). This kind of EDL structure leads to E-F bonding and damages the formation of highly ordered multilayer films,[206, 207] resulting in decreased

film thickness, optical clarity and oxygen barrier. This edge-charge neutralization approach provides a new opportunity to quickly prepare high barrier nanocoatings.

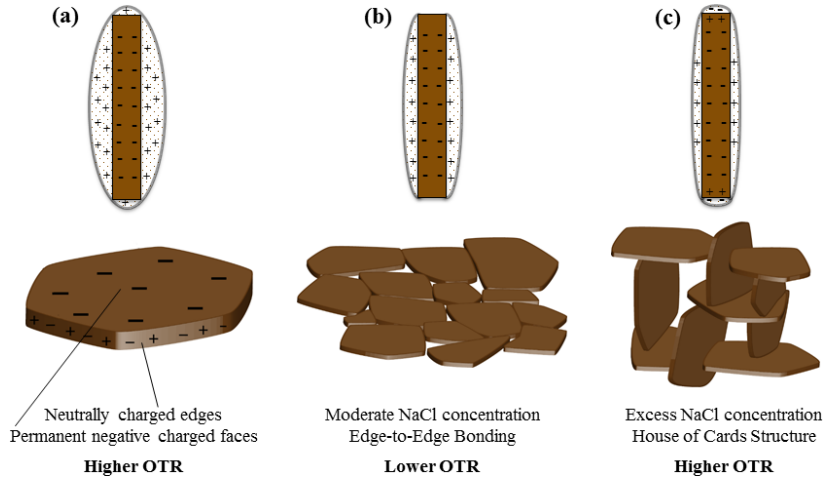

Figure 20. Schematic of clay electrical double layer structure (upper row) and clay association (lower row) at pH 6.5 with (a) no NaCl, (b) low and (c) high NaCl concentration.

5.2 Experimental Section

Natural montmorillonite clay (MMT) (Cloisite NA+) was purchased from BYK Additives Inc. (Gonzales. TX) and used as a 1 wt % suspension in deionized (DI) water after rolling overnight to achieve homogeneity. MMT platelets have an average thickness of 1 nm and diameter ranging from 100 to 1000 nm.[189] Sodium chloride (NaCl), purchased from Sigma-Aldrich (Milwaukee, WI), was added to the MMT suspension after drying at 150 °C overnight. The pH of the clay suspensions was altered to 6.5 using 1 M HCl. Branched polyethylenimine (M_w 25,000 g/mol, ρ=1.10 g/cm^3) was purchased from Sigma-Aldrich and used as a 0.1 wt % aqueous solution. The pH of PEI was altered to 10 using 1 M HCl. The molecular structures of PEI and MMT can be seen from Figure 21.

Same poly(ethylene terephthalate) (PET) film and silicon wafer were used as substrates for oxygen transmission rate (OTR) testing, transmission electron microscope (TEM) and atomic force microscopy (AFM) imaging, and film thickness measurement. 1 mm quartz slides (75mm ×25mm) were purchased from Chemglass (Vineland, NJ) and used as substrates to measure visible light transmission. Silicon wafers and quartz slides were rinsed with acetone and DI water, followed by 5 min plasma treatment, just before use.

Substrates were alternately immersed in the cationic PEI solution and anionic MMT suspension with a home-built robotic dipping system.[167] Each substrate was dipped into the PEI solution for 5 min followed by rinsing with DI water for 30 sec and drying with filtered air for another 30 sec, then dipped into the MMT suspension for another 5 min to deposit the initial bilayer (BL) to obtain the best possible surface coverage in the initial bilayer. The rest of the deposition cycles used 1 min dipping in both cationic PEI and anionic MMT solutions, with 30 sec rinsing and 30 sec drying in between. The dipping cycles were repeated to achieve the desired number of bilayers. Multilayer assemblies are denoted as $(PEI/MMT_x)_y$, where x is the mM concentration of NaCl in the clay suspension and y is the number of bilayers deposited.

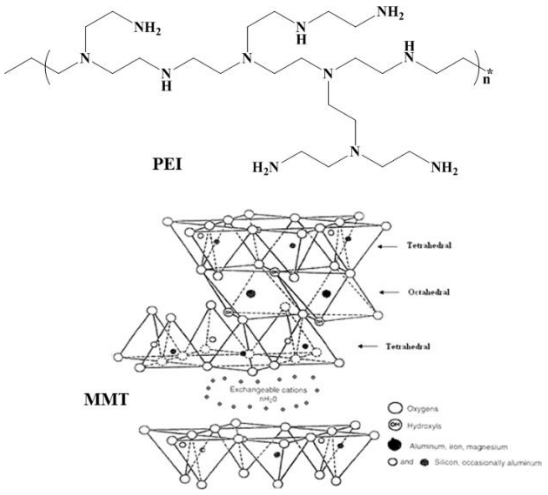

Figure 21. Molecular structures of PEI and MMT.

Film thickness was measured by an α-SE ellipsometer (J.A Woollam Co., Inc., Lincoln, NE) as a function of the number of bilayers deposited on the silicon substrate. Light absorbance between 350 and 750 nm was measured using a USB2000 ultraviolet-visible light (UV-vis) spectrometer (Ocean Optics, Dunedin, FL). The reported transmission was the average of three measurements. Atomic force microscope (AFM) imaging was performed with a Dimension Icon AFM (Bruker, Billerica, MA), using tapping mode with an HQ:NSC35/Al BS probe (Mikromasch, Lady's Island, SC). Root-mean-square roughness (Rq) was obtained from a 10×10 μm area height image. Transmission electron microscopy (TEM) images and oxygen transmission rate (OTR) data were obtained using the previously described methods.

5.3 Results and discussion

Like most polymer/clay multilayer films, PEI/MMT grows linearly as a function of bilayers deposited,[174, 208] as shown in Figure 22(a). Altering the ionic strength of the MMT suspension alters the arrangement of MMT platelets in suspension and inside the multilayer film, which influences the thickness and morphology of the LbL assembly. The influence of NaCl concentration on multilayer film thickness is shown in the inset of Figure 22(a). The thickest 25 BL film is achieved with 20 mM NaCl, a 31% increase compared to the salt-free film. This increased thickness at low NaCl concentration can be ascribed to two factors. First, besides the edge-to-edge network created by van der Waals attractions, the increased NaCl concentration helps to compress the electrical double layer of MMT, resulting in a decreased surface electron potential. Neighboring clay platelets therefore have smaller repulsion force when approaching, forming one central cation layer instead of two. As a result, more face-to-face (F-F) bonds and more aligned platelets are deposited on the underlying cationic PEI layer per each deposition cycle. Additionally, NaCl facilitates longer range of excess charge distribution of the PEI chains, which produces greater thickness of each layer (Figure 22(c)).[206, 209] The extrinsic charge compensation of PEI chains increases with NaCl concentration that forces apart the ion pairs between PEI and MMT until they cannot hold the multilayer assembly together.[210] This is the cause for the loss of thickness at very high NaCl concentration (≥100 mmol) and ultimately leads to complete dissolution of the multilayer film.[206, 207]

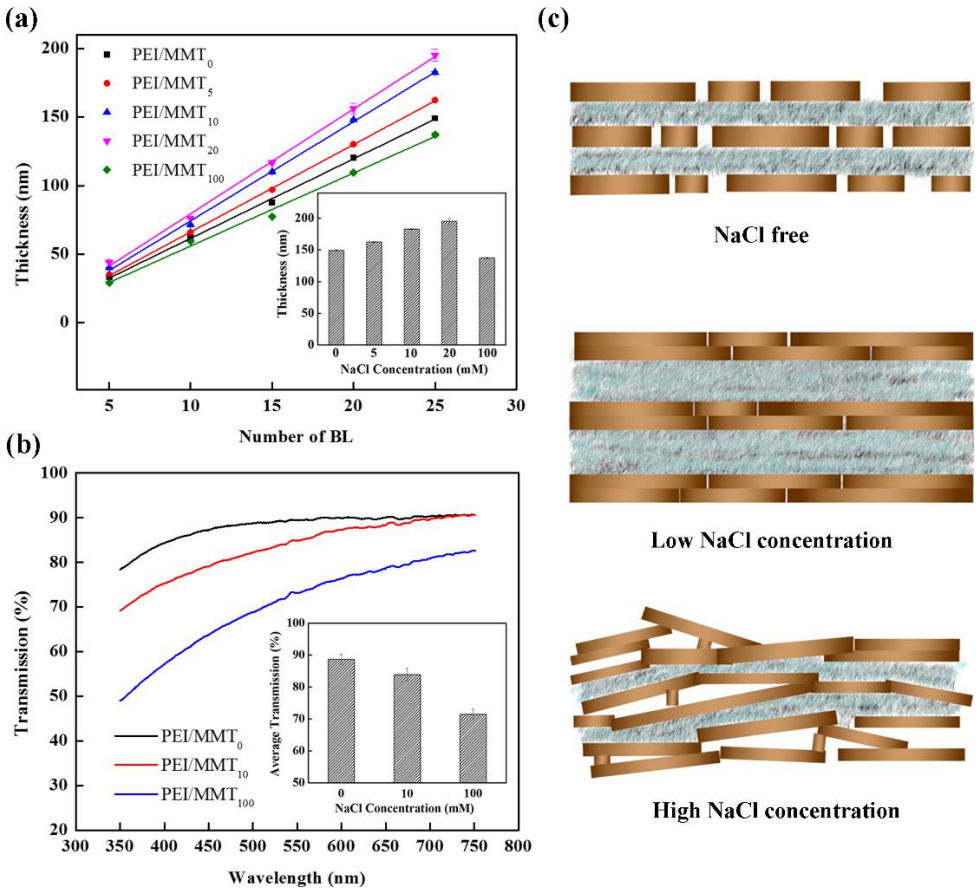

Figure 22. (a) Thickness of PEI/MMT films as a function of bilayers deposited at various NaCl concentrations. The inset shows the thickness of a 25 BL film as a function of salt concentration. (b) Visible light transmission of 30 BL PEI/MMT films, with an inset showing the average visible light transmission as a function of NaCl concentration. (c) Illustration of PEI/MMT multilayer film structure assembled with varying NaCl concentration in MMT suspension.

Due to the highly oriented and exfoliated MMT platelets inside the multilayer film, this thin nanocomposite has excellent visible light transparency. In the absence of NaCl, a 30 BL PEI/MMT film has an average light transmission of 88.7% (390-750 nm), as shown in Figure 22(b). The slightly decreased transmission of the film prepared with 10 mM NaCl (83.9%) is due to its increased thickness, according to the Lambert-Beer law.

With a similar thickness, $(PEI/MMT_{100})_{30}$ has a much lower transmission rate (71.5%) than the no-salt film. It is likely that the increased NaCl concentration further suppressed the EDL, resulting in smaller MMT platelets forming edge-to-face bonding with larger ones in the multilayer films (Figure 22(c)). This type of association leads to deteriorated alignment of platelets and a hazy appearance.

Atomic force microscopy (AFM) was used to visualize the surface morphology and roughness of PEI/MMT multilayer films assembled in the presence of varying NaCl concentration. As shown in Figure 23, the surface of the $(PEI/MMT_0)_{25}$ film (Figure 23(a), (d)) is covered with aligned platelets and small MMT platelets fill in the space between larger ones. In the $(PEI/MMT_{10})_{25}$ film (Figure 23(b), (e)), edge-to-edge bonding and suppressed repulsive force between platelets, realized by NaCl charge screening, allows for more large MMT platelets to more closely pack on top of the PEI layer. The electrical double layers are further suppressed as the NaCl concentration increases to 100 mM, which still favors large MMT platelet adsorption, but the increased screening effect begins to favor E-F interaction between small platelets edges and large platelets faces. As a result, misalignment of MMT platelets start to appear as a rougher surface in the $(PEI/MMT_{100})_{25}$ film (Figure 23(c)). Moreover similar surface roughness value (R_q) were obtained for $(PEI/MMT_0)_{25}$ and $(PEI/MMT_{10})_{25}$ (~30 nm), while the R_q is nearly double for $(PEI/MMT_{100})_{25}$ (~55nm).

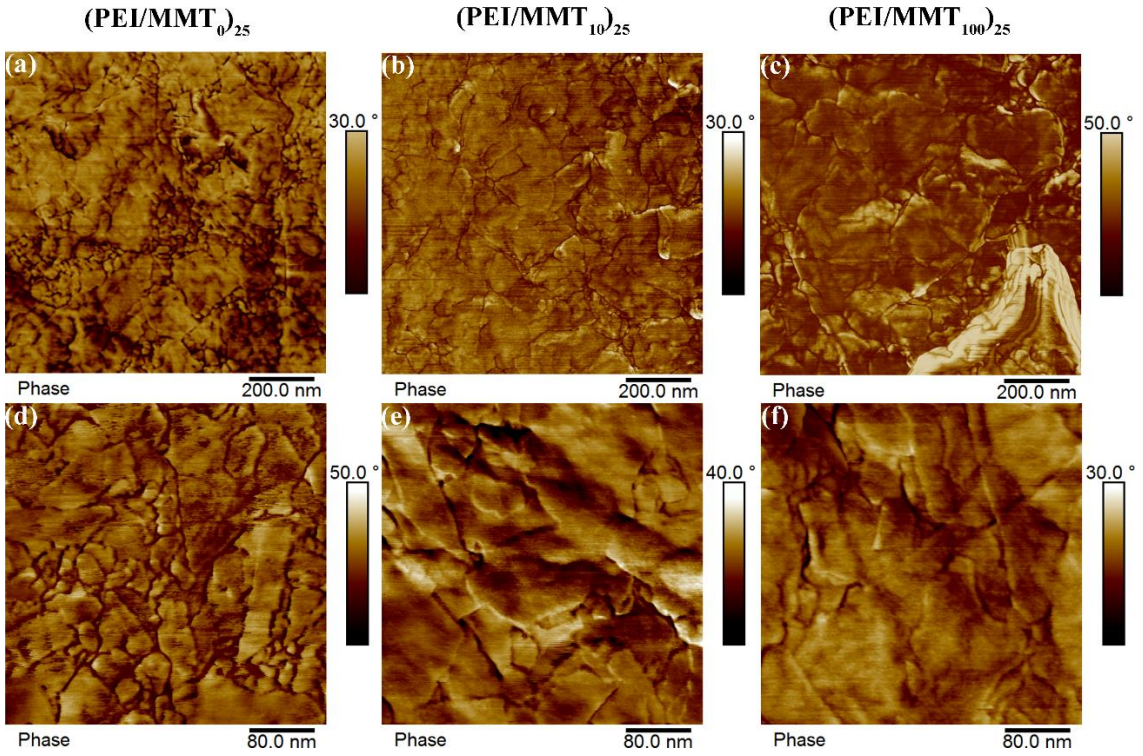

Figure 23. Atomic force microscope phase images of $(PEI/MMT_0)_{25}$ (a,d), $(PEI/MMT_{10})_{25}$ (b,e) and $(PEI/MMT_{100})_{25}$ (c,f) surfaces.

TEM cross-sectional images show the highly ordered clay layers achieved by LbL deposition (Figure 24). MMT platelets appear as dark lines due to their high electron density from Mg, Al and Si atoms. There are more than 40 clay layers seen across the thickness of these 20 BL multilayer films, suggesting that clay platelets are deposited as doublets and triplets in each cycle. It is this high alignment and good platelet separation that provides high optical clarity and gas barrier in these polymer-clay multilayer thin films.[174] The film assembled without NaCl (Figure 24(a)) has a well-ordered structure, but a smaller thickness than the film deposited with 10 mM NaCl (Figure 24(b)), where almost perfect alignment of clay platelets is observed. Misalignment and gaps between platelets

can be observed in the film assembled with 100 mM NaCl (Figure 24(c)), which contributes to decreased optical clarity and increased oxygen transmission rate.

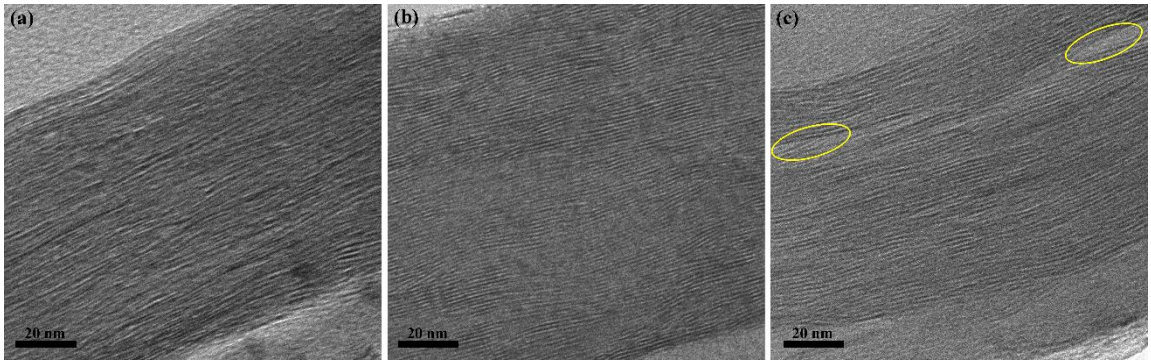

Figure 24. Transmission electron microscope cross-sectional images of (a) $(PEI/MMT_0)_{20}$, (b) $(PEI/MMT_{10})_{20}$ and (c) $(PEI/MMT_{100})_{20}$. Examples of gaps and misalignment are highlighted with yellow circles in (c).

Figure 25 shows the oxygen barrier of multilayer films assembled with varying NaCl concentration in MMT suspensions. Moderate NaCl concentration in the MMT deposition solution helps to reduce the oxygen transmission rate of PEI/MMT multilayer films by optimizing clay platelet coverage. At lower NaCl concentration (5 or 10 mM), an 8 BL PEI/MMT film exhibits almost an order of magnitude improvement in oxygen barrier relative to the same film assembled without NaCl. This improvement is a result of E-E bonding facilitated by van der Waals forces and a thicker polymer layer in the "nanobrick wall" structure, which is evidenced by greater overall film thickness (Figure 22(a)), better clay coverage (Figure 23) and better clay alignment (Figure 24). As NaCl becomes more concentrated in the MMT suspension, partial disassociation makes the PEI layers thinner and E-F bonding leads to misalignment of MMT platelets. These structural

changes result in a shorter diffusion path and more adjacent gaps in the MMT layers for permeating gas molecules, which leads to the increased OTR. To the best of our knowledge, this 'salty clay' strategy produces the lowest oxygen barrier ever reported for any polymer-clay bilayer system, even systems with larger aspect ratio clay.[134, 174] With the help of 5 mM NaCl, an 8 BL multilayer coating (~55 nm) on both sides of a 179 μm thick PET substrate managed to decrease the oxygen permeability by an order of magnitude (Figure 25). This improved gas barrier coating has lower permeability than the value reported for vacuum deposited SiO_x or Al_xO_y coatings. [15,196]

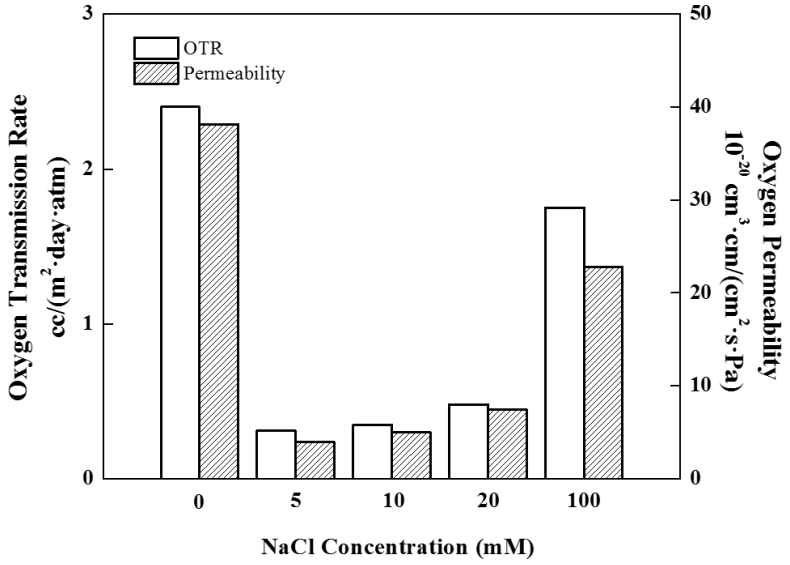

Figure 25. Oxygen transmission rate and permeability of 8 BL PEI/MMT multilayer films assembled with varying NaCl concentration. The permeability was calculated independent of the substrate using a previously described method.[7]

5.4 Conclusions

An indifferent electrolyte (NaCl) was introduced into MMT suspension in the effort to improve the oxygen barrier of PEI/MMT multilayer coatings through charge screening. With a moderate amount of NaCl (5-10 mM), the multilayer film had greater thickness due to an edge-to-edge bonding network, smaller repulsion between platelets and longer range of excess charge distribution of the polyethylenimine. These factors allow more large MMT platelets and thicker PEI to be deposited per deposition cycle. The mild charge screening effect gives the MMT platelets better surface coverage and alignment, which ultimately results in lower oxygen transmission rate and permeability. It is believed that this 'salty clay' strategy is applicable to most types of clay nanoplatelets (e.g., vermiculite and laponite). As NaCl concentration increased, aggressive charge screening starts to work against the formation of a highly ordered film by weakening the interaction between PEI and MMT. Furthermore, edge-to-face association of MMT platelets appears at high salt concentration. As a result, thinner films with misaligned MMT platelets are assembled, which leads to deteriorated oxygen barrier. This structural engineering of the PEI/MMT multilayer films, through optimizing the charge screening of NaCl, produced an order of magnitude reduction in oxygen permeability. An 8-bilayer PEI/MMT nanocoating (~50 nm thick), produced with 5 mM NaCl, exhibits oxygen permeability of 4×10^{-20} cm^3 cm/(cm^2 s pa), which is lower than vapor deposited inorganic oxides. This study demonstrates the best polymer/clay bilayer gas barrier multilayer film ever reported and provides a straightforward and cost-effective method for producing transparent and flexible packing materials.

CHAPTER VI

FAST SELF-HEALING OF POLYELECTROLYTE MULTILAYER NANOCOATING AND RESTORATION OF SUPER OXYGEN BARRIER*

6.1 Introduction

Due to their soft nature (relatively large free volume and low glass transition temperature) and ease of modification/functionalization, polymers and their nanocomposites have become the most studied category of self-healing materials.[211] Self-healing polymers fall into two categories based on their healing mechanism: extrinsic and intrinsic.[212] External healing agents (monomers and catalysts) that are encapsulated into microcapsules, hollowed microfibers or microvascular network, act as the source of healing in extrinsic materials. Cracks are healed after the healing agents are released and polymerize at the damaged site.[213-215] Although being straightforward and effective, this one-time healing process limits the potential application of these materials. In contrast, intrinsic self-healing materials are based on reversible chemical bonding (covalent, ionic, etc.).[216] The most commonly employed covalent bonding reactions are Diels-Alder and cycloaddition.[217, 218] These reactions can only be triggered by energy-intensive external stimuli, such as long time UV light or high temperature exposure.[219, 220] There is

---

*Reprinted with permission from Song, Y.; Meyers, K. P.; Gerringer, J.; Ramakrishnan, R. K.; Humood, M.; Qin, S.; Polycarpou, A. A.; Nazarenko, S.; Grunlan, J. C. Fast Self-Healing of Polyelectrolyte Multilayer Nanocoating and Restoration of Super Oxygen Barrier. *Macromol. Rapid Commun.* **2017**, 38, 1700064.

considerable interest in polymeric systems that can self-heal unassisted or when self-healing is triggered by low energy external stimuli such as changing pH or exposure to high humidity.

Non-covalent bonding, including ionic bonding,[152] hydrogen bonding,[221] supramolecular interactions,[222] metal-ligand coordination[223] and π-π interactions[224] significantly broaden the scope of self-healing materials, making highly reversible and ambient healing possible. Fast and efficient healing originates from high mobility polymer chains, which is determined by free volume and interaction strength. Stimuli such as heat and UV light provide external energy to activate the polymer chain diffusion, which also increases the free volume and initiates the healing process.[225] The amount of free volume of a polymeric system is related to its glass transition temperature and modulus, which are closely linked to performance properties like mechanical strength and gas permeability.[226] Low T_g polymers, with large free volume and mobile chains, are more likely to have self-healing ability. Unfortunately, polymers with high T_g and small free volume are usually more useful due to their higher mechanical strength, thermal stability and barrier properties. The real challenge lies in developing polymers that are both self-healing and mechanically robust, which could potentially be used in various structural and packaging applications.

Ionically-bonded systems could be healed after reshuffling and relaxation of ionically-clustered regions, which could solve the above mentioned challenge.[225] The free volume and chain mobility of ionically-bonded polymers are strongly influenced by ionic strength,[206] pH[227] and water fraction,[228-230] which could be used as stimuli to trigger

healing. Reported here for the first time is a repeatable self-healing, and restoration of compromised gas barrier, in a stretched multilayer polyelectrolyte nanocoating upon exposure them to high humidity. This polyelectrolyte multilayer nanocoating, fabricated by alternate deposition of polyethyleneimine (PEI) and polyacrylic acid (PAA) (Figure 26), has an exceptionally high elastic modulus and ultra-high oxygen barrier.[26, 39] As expected, the gas barrier vanishes after cracking due to strain, but it is completely restored after high humidity exposure (i.e., self-healing efficiency of 100%). This simple self-healing nanocoating is potentially useful for protection of food, pharmaceuticals and electronics.

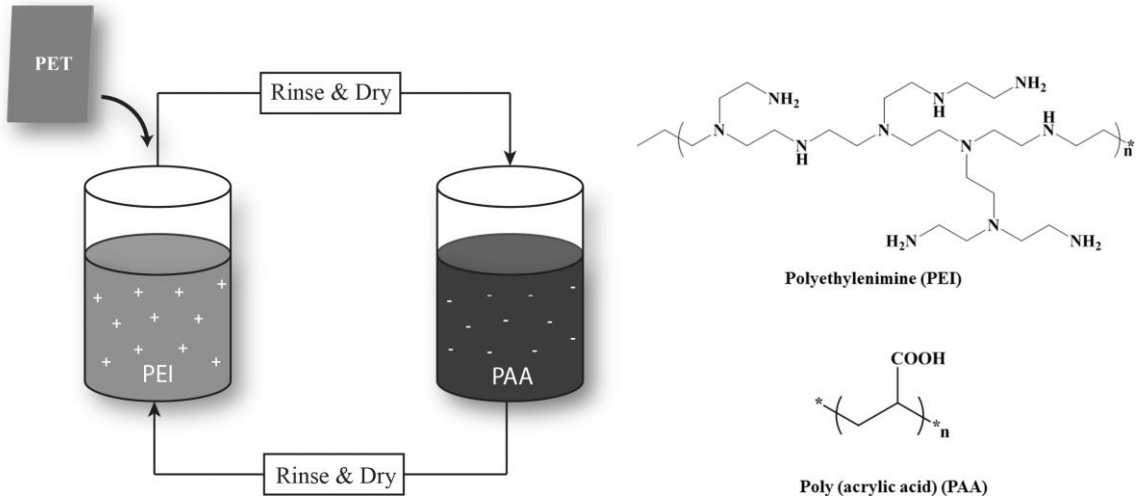

Figure 26. Schematic of layer-by-layer (LbL) assembly process. Molecular structures of polyethylenimine (PEI) and polyacrylic acid (PAA) are shown.

6.2 Experimental Section

Branched polyethylenimine (PEI) (M_w 25,000 g/mol, ρ=1.10 g/cm^3) and polyacrylic acid (PAA) (M_w=100,000 g/mol, ρ=1.20 g/cm^3) were purchased from Sigma-Aldrich (Milwaukee, WI). 0.1 wt% PEI and 0.2 wt% PAA solutions were made by diluting with deionized (DI) water and rolling overnight to achieve homogeneity. The pH of PEI and PAA solutions were adjusted to 10 and 4 using 1 M HCl and 1 M NaOH, respectively. 179 μm thick poly(ethylene terephthalate) (PET) film (tradename ST505 by Dupont-Teijin) was purchased from Tekra (New Berlin, WI) and used as the substrate for scanning electron microscope (SEM) imaging and oxygen transmission rate (OTR) testing.

PET, silicon wafers, and quartz slides substrates were cleaned and properly treated using the previously descibed method. The alternating deposition of cationic PEI and anionic PAA was carried out by a home-built robotic dipping system under ambient conditions (Figure 26).[167] Cleaned and/or treated substrates were dipped into the PEI solution for 5 min followed by rinsing with DI water and drying with filtered air. These substrates were then dipped into the PAA solution for 5 min to finish the initial bilayer (BL). The remaining deposition cycles were performed with 1 min dipping in both PEI and PAA solutions. Rinsing and drying steps were incorporated between each dipping procedure.

In-situ multilayer film thickness in air and water was measured at room temperature by an α-SE spectroscopic ellipsometer (J.A. Woollam Co., Inc., Lincoln, NE), which is equipped with a 500 μL LiquidCell (J.A. Woollam Co., Inc., Lincoln, NE). Prior to measurement, calibration of the window effect was done on a silicon wafer with a 25nm

SiO_2 layer. Multilayer film thickness was first measured in the dry state, followed by introducing DI water into the liquid cell with a syringe. The high purity H_2O ambient model was chosen to generate film thickness. Each reported thickness value is the average of at least three measurements. Film thickness in water was obtained after a 20 min immersion in the liquid cell. Coated PET was stretched 5% at a 10 inch/min strain rate using a MTS 810 tensile tester (MTS, Eden Prairie, MN), followed by holding the stress for 2 min before releasing. Nanocoating surface morphology was imaged with a JEOL JSM-7500F field emission scanning electron microscope (SEM) (JEOL Ltd, Tokyo, Japan). Each film was sputter coated with 5 nm of platinum/palladium to eliminate charging and obtain high resolution images.

Oxygen transmission rate (OTR) of the multilayer thin films was measured by a MOCON (Minneapolis, MN) Oxtran 2/21 instrument at 23 °C, 0% RH and 1 atm partial oxygen pressure difference. A continuous-flow method (in accordance with ASTM D3985-81 and ASTM F1249-01) was employed to measure the oxygen flux through the polymeric films, using nitrogen as the carrier gas. Each reported OTR value is the average of at least three tests on several different instrument modules.

Reduced elastic modulus (E_r) of the multilayer films was measured by a Hysitron Ti Premier indenter (Minneapolis, MN), using a diamond Berkovich tip with a radius of 150 nm. Elastic modulus in water was measured with a Berkovich fluid cell. Multilayer films were left in water overnight in a concave meniscus to reach full swelling before testing. Nanoindentation measurements were performed using a previously described method.[26] More than 30 indents were performed on each sample. The depth of each indent

was kept within 5-15% of the multilayer film thickness (35-105 nm) to avoid any substrate influence. Atomic force microscope images for surface roughness and 2 mN indentation residual profile were obtained using the same Berkovich tip.

A USB2000 ultraviolet-visible light (UV-vis) spectrometer (Ocean Optics, Dunedin, FL) was used to measure light absorbance between 390 and 750 nm. The plotted spectra and light transmission were the average of three measurements. Average free volume of the multilayer films at various humidity levels were measured by positron annihilation lifetime spectroscopy (PALS) on a fast-fast coincidence system.[231] Samples with a thickness of 1 mm and diameter of 1 cm were prepared by stacking free-standing 100 BL PEI/PAA multilayer films. Stacked films were vacuum dried overnight at room temperature, followed by pre-conditioning at environments with different humidities prior to PALS testing. The required humidity level was maintained by controlling the amount of wet and dry N_2 gas going into the test chamber. Seven spectra were collected for each relative humidity. The free volume was calculated using a previously described method.[232, 233]

6.3 Results and Discussion

Nanocoating thickness was measured in different environments as a function of the number of bilayers (BL) deposited (Figure 27). A swelling ratio of 52% was observed for an 8BL PEI/PAA nanocoating when immersed in water, which agrees well with a previous study.[234] The film shrinks to its original thickness (~700 nm for 8BL) after drying at 70 °C for 30 min. It has been reported that this reversible swelling-drying cycle can be

repeated at least 10 times without damaging the multilayer nanocoating.[162] This 8BL PEI/PAA nanocoating reduces the oxygen transmission rate (OTR) of 179 μm PET to the undetectable limit of commercial instrumentation (<0.005 cc/(m^2 day)).[39] This low OTR originates from the strong ionic interaction between the polyelectrolyte chains, which results in small free volume in the nanocoating. It has been reported that this PEI/PAA multilayer film has a modulus near 20 GPa in the dry state and a glass transition temperature near 100 °C,[26, 39, 128] but its gas barrier is compromised at high humidity.[39] It is believed that water molecules swell and plasticize the thin film, resulting in enlarged free volume that eases oxygen diffusion.

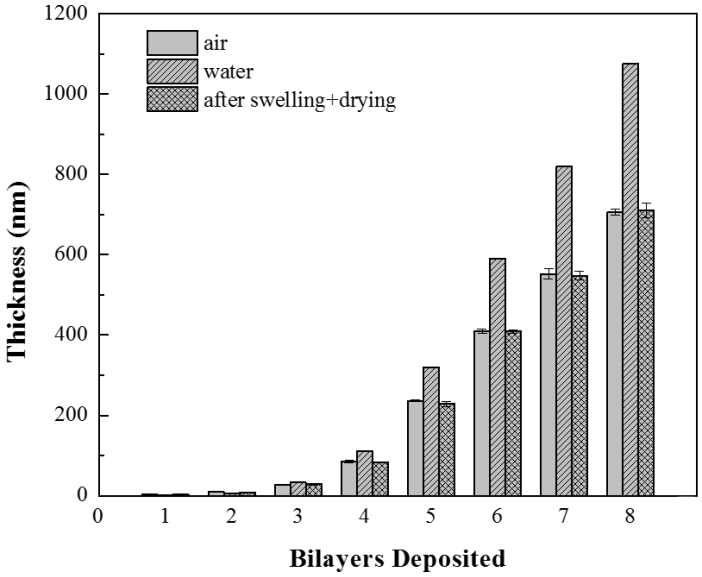

Figure 27. PEI/PAA thickness as a function of the number of bilayers deposited. Measurements were made in air, water and air after swelling and drying. The films were dried at 70 °C for 30 min after swelling.

Relative to conventional thin gas barrier layers including metal (e.g., Al), vapor deposited SiO_x and Al_xO_y,[6, 7] PEI/PAA multilayer nanocoatings exhibit high oxygen

barrier and maintain higher flexibility. It can be concluded from prior studies that gas barrier and film stretchability are mutually exclusive,[132, 235]especially in the case of glassy ionically-bonded multilayer films. As deposited, an 8BL polyethylenimine-polyacrylic acid film has a dense and uniform surface morphology (Figure 28(a)). After only 5% extension, micro-cracks appear on the coating surface (Figure 28(b)). These cracks extend all the way from the coating surface to film-substrate interface. In order to initiate self-healing, this stretched multilayer film was placed in a 97% relative humidity (RH) environment. High humidity plasticizes the nanocoating and heals the cracks (Figure 28(c)). It has been found that the cracks heal in as little as 10 min when placed in a 97% RH environment (Figure 29(c))**.** Moreover, the root-mean-square surface roughness decreases dramatically when exposed to high humidity (Figure 30), which improves the nanocoating transparency. A hazy 20 BL PEI/PAA multilayer film, with an average visible light transmission of 32.5%, becomes completely transparent (%T>98%) after high humidity exposure (Figure 31).

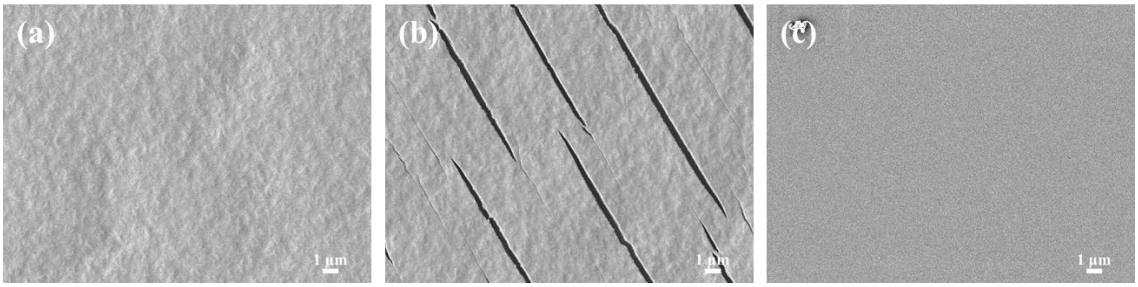

Figure 28. Scanning electron microscope (SEM) surface images of 8BL PEI/PAA a) before and b) after 5% strain (using a 10 inch/min strain rate) and c) after 5% stretching and 24h high humidity healing.

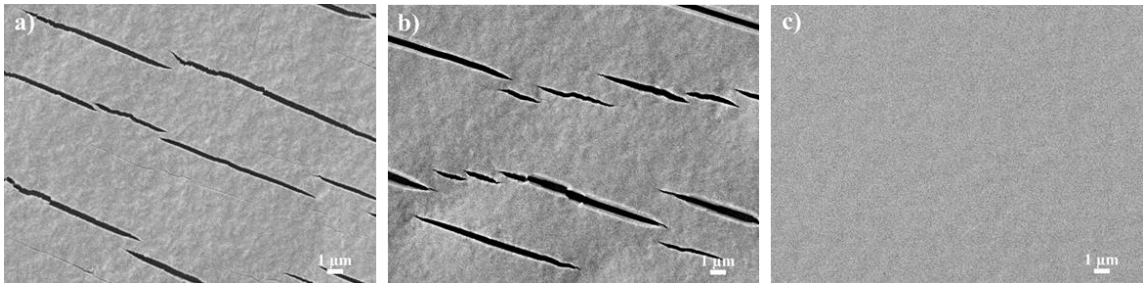

Figure 29. Scanning electron microscope (SEM) images of stretched 8BL PEI/PAA films after sitting under (a) ambient conditions (23 °C and ~45% RH) overnight or (b) 97% RH for 5 min and (c) 10 min.

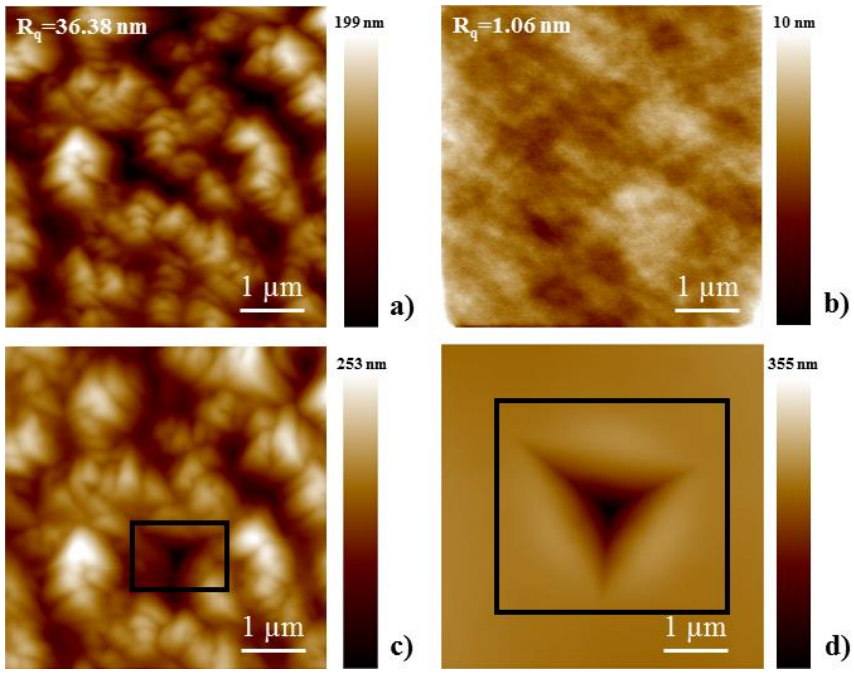

Figure 30. Atomic force microscope (AFM) images and surface roughness (inset) of 8BL PEI/PAA nanocoatings in (a) air and (b) water. Residual profiles of a 2mN indentation on 8BL PEI/PAA in (c) air and (d) water.

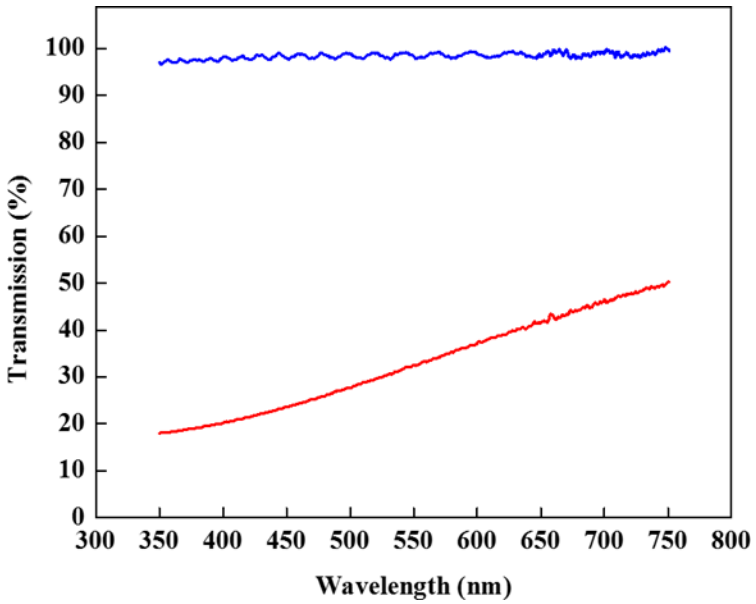

Figure 31. Visible light transmission of a 20 BL PEI/PAA multilayer film before (red) and after (blue) high humidity exposure. The average visible light transmissions are 32.5% and 98.5% (390-750 nm), respectively.

Micro-crack self-healing occurs only at high humidity. At low humidity (below 50% RH), water molecules are absorbed by the hydrophilic PEI/PAA film, which fills in free volume. This process does not cause significant swelling or increased film thickness, but results in improved gas barrier.[134, 236] Moreover, the elastic modulus and hardness of these multilayer films at 50% RH exhibits little change from those exposed to 22% RH,[237] which suggests the ionically-bonded structure remains intact. As the humidity level is gradually increased above 50%, segregated water clusters near the hydrophilic sites tend to grow and then merge, resulting in a percolating water phase network. As a result, the multilayer film is plasticized by water and the free volume increases, leading to an abrupt change in film thickness and modulus. [236, 238] Similar thickness, modulus, free volume and

oxygen permeability trends were observed for various polyelectrolyte multilayer films and polyamide, sulfonated tetrafluoroethylene (Nafion) and ethylene-vinyl alcohol (EVOH) single-polymer membranes.[176, 180, 239-241] The increased free volume and plasticization, resulting from swelling, lowers the activation energy of polyelectrolyte diffusion and imparts mobility to PEI and PAA chains. On the other hand, due to the high dielectric constant of water, strong ionic bonding in the PEI/PAA film is interrupted by the percolating water phase, allowing bonds to re-shuffle. As a result, the normally high modulus multilayer coating is softened. Diffusion and rearrangement of polyelectrolyte chains accelerate through swift ionic cluster shuffling and thermal motion, which heals cracks in the film. Although the healing time for microscope imaging and oxygen barrier testing was set to 24h in this work, healing can occur within 10 min (Figure 29). Faster self-healing is triggered by high humidity and it is possible that higher temperature or other factors could further speed up this healing. As shown in Figure S3a, a stretched multilayer film remains cracked after exposure to ambient conditions (23°C, ~50% RH) for 24h. It is believed that self-healing requires the significant free volume and elastic modules change that occurs upon high humidity exposure.

Free volume of the polyethylenimine/polyacrylic acid assembly was measured as a function of relative humidity using positron annihilation lifetime spectroscopy (PALS) (Figure 32(a)). An average hole size was ~50 $Å^3$ measured in a dry environment. This average hole size first decreases as the relative humidity increases, which can be attributed to water molecules filling the free volume. This anti-swelling effect at low relative humidity is commonly observed for glassy hydrophilic polymers.[63-64] As the humidity

continues to increase, the water phase network plasticizes and subsequently increases the free volume in the multilayer film. Nanoindentation was used to measure the thin film reduced elastic modulus (E_r), which correlates to the elastic modulus of sample (E) and indenter (E_i) by the equation $\frac{1}{E_r} = \frac{1-\upsilon^2}{E} + \frac{1-\upsilon_i^2}{E_i}$ (ν and ν_i are the Poisson's ratios of the sample and indenter, respectively).[242] The elastic modulus of the tip is usually much higher than the indented sample (E_i is 1140 GPa for a diamond tip), therefore the measured reduced modulus of polymer sample is similar to its elastic modulus. The well-known Oliver-Pharr method was used to measure hardness and calculate reduced modulus from the unloading profile of indentation.[243] An 8 bilayer PEI/PAA film, with a thickness near 700 nm, has a reduced elastic modulus of ~15 GPa (Figure 32(b)) in a dry environment. This high modulus is a result of low free volume that imparts both high gas barrier and brittleness. Measurements were also performed in water to simulate the mechanical behavior in a high humidity environment. The nearly 5X reduction in modulus is due to plasticization by water molecules (Figure 32(b)). Water-softening of the 8BL film is also evidenced by the residue profile left by a 2mN indentation (Figure 30). With the same indentation force, plastic deformation occurs more easily in water, leaving a deeper and wider indent on the film surface. The film's modulus returned to its original after drying (Figure 32(b)), demonstrating that the strong ionic bonding is restored after water (or humidity). The smaller error bars for modulus in water and after drying are the result of reduced surface roughness.

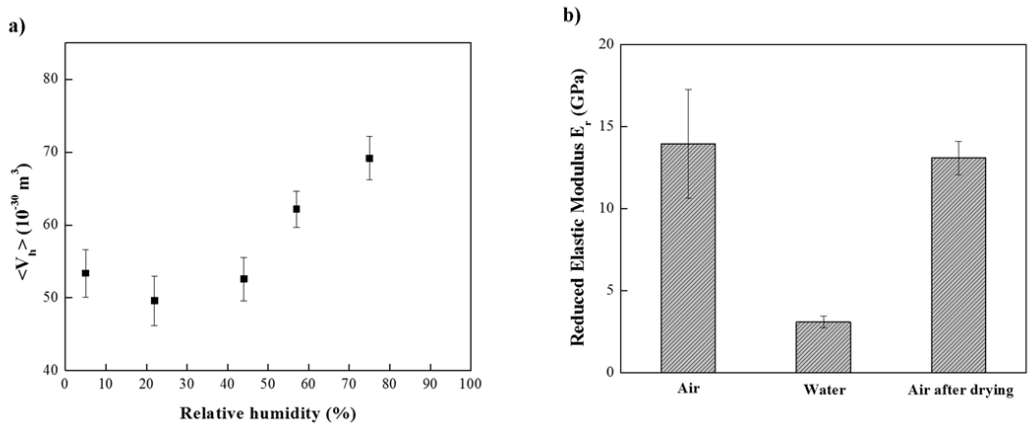

Figure 32. (a) Average free volume hole size <V_h> for the PEI/PAA assembly as a function of relative humidity. (b) Reduced elastic modulus of an 8 BL nanocoating in air, water and air after drying.

Oxygen transmission rate (OTR) of 8-bilayer PEI/PAA multilayer nanocoatings were tested before and after stretching and after 24h high humidity healing. The stretched films were immediately loaded into a MOCON Oxtran O_2 permeation module to avoid any healing in ambient conditions. After 97% RH healing, the multilayer films were dried for at least 12h prior to OTR testing. As shown in Figure 33, the 179 μm PET substrate has an OTR near 8.6 $cm^3/(m^2$ day atm), with no significant change in appearance or OTR occurring after a 5% stain. More than three orders of magnitude oxygen barrier improvement (i.e., >1000X reduction in OTR) was achieved with an 8 BL PEI/PAA nanocoating on both sides of the PET substrate, which is below the detection limit of the testing instrument. The calculated permeability of the nanocoating is below 8×10^{-21} cm^3 $cm/(cm^2$ Pa s). This super barrier completely disappears following a 5% strain due the formation of micro-cracks (Figure 28). The OTR was again undetectable after humidity healing, suggesting a healing efficiency of 100% (i.e., a full recovery of the dense and

defect-free multilayer film). The OTR of this 8BL nanocoating remained below the detection limit (<0.005 $cm^3/(m^2$ day atm)) after 10 of these stretching-healing cycles, demonstrating that this healing process is highly reversible and robust.

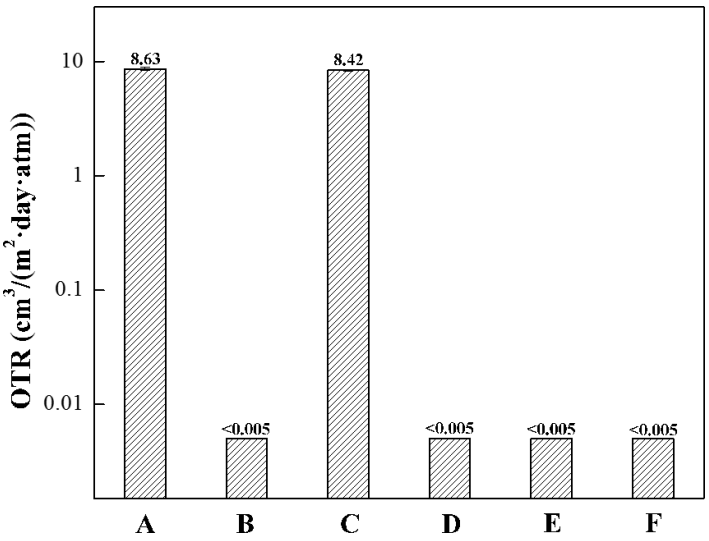

Figure 33. Oxygen transmission rates (OTR) of (a)179 μm thick PET, (b) PET with an 8 BL PEI/PAA nanocoating, (c) 8 BL PEI/PAA after 5% tensile strain, (d) 8 BL PEI/PAA after strain and 24h humidity healing, (e) 8 BL PEI/PAA after 5 and (f) 10 stretching-healing cycles.

6.4 Conclusion

In conclusion, a rigid super oxygen gas barrier nanocoating was shown to exhibit repeatable, humidity-induced room temperature self-healing. High humidity swells hydrophilic PEI/PAA multilayer thin films which leads to reduced modulus and increased chain mobility. Strain-induced cracks within the multilayer coating are ultimately sealed as a result of the plasticization brought on by humidity. The super oxygen barrier of an 8BL PEI/PAA film was completely restored (OTR<0.005 $cm^3/(m^2$ day atm)) after this

healing process, which occurs in as little as 10 minutes at 97% RH. This healing ability could prove useful in various film forming applications, such as packaging trays for food, where the desired barrier could be restored after crack formation from strain.

CHAPTER VII

CONCLUSIONS AND FUTURE WORK

7.1 Coating Process Improvements and New Functionalities Developments

The majority of this dissertation is focused on improvements in the LbL deposition process and developments of new functionalities. These improvements make gas barrier nanocoatings applicable not only to polyester but also to polyolefin substrates. The improved barrier performance reduces the processing time through simple pH and ionic strength manipulation of clay suspensions, which ultimately makes LbL assembly more appealing to packaging and pressurized systems. The self-healing function found in PEI/PAA assemblies improves the robustness of these gas barrier coatings. Potential future work is also presented here, including a polymer-clay complex gas barrier coating that can further simplify the coating procedure, and a vapor-responsive polymer actuator that can be used for sensors, artificial muscles, etc.

7.1.1 Multilayer Gas Barrier Coating for BOPP

It was shown in Chapter III that the all-polymer (polyethylenimine/poly(acrylic acid)) and polymer-clay (polyethylenimine/vermiculite) multilayer nanocoatings are applicable to biaxially oriented polypropylene (BOPP) film, which marked the first demonstration of polyolefin barrier improvement using layer-by-layer assembly. A 30 bilayer PEI/VMT nanocoating (226 nm thick) improves the OTR of 17.8 μm thick BOPP by more than 30X, rivaling most inorganic coatings. PEI/PAA multilayers achieve

comparable barrier with only 12 bilayers due to greater thickness, but these films exhibit increased oxygen permeability at high humidity due to swelling. The PEI/VMT coatings exhibit improved oxygen barrier even at 100% RH (and also improve moisture barrier by more than 40%). This high barrier BOPP meets the criteria for sensitive food and some electronics packaging applications and this cost-effective coating technology provides an opportunity to produce high barrier polypropylene film on an industrial scale.

7.1.2 Altering Clay pH for High Gas Barrier

Chapter IV described a "pH clay" strategy, where the pH of montmorillonite (MMT) aqueous suspension was reduced in a PEI/PAA/PEI/MMT quadlayer (QL) nanocoating. The reduced pH causes the preceding PEI layer to be more charged, which leads to more clay deposition per layer. As the clay pH is altered, a balance is found between high polymer diffusion (at natural pH 10) and high clay deposition that increases with decreasing pH. Clay at pH 6 provides the best compromise of dense packing and adequate spacing between layers. At pH 6, a three QL coating (44 nm thick) exhibits an undetectable oxygen transmission rate (<0.005 $cm^3/(m^2$ day atm)) on a 179 μm thick PET substrate. The calculated oxygen permeability is orders of magnitude lower than silicon oxide (SiO_x) and metalized thin films (<5×10^{-22} cm^3 cm/(cm^2 s Pa)).

7.1.3 Altering Clay Ionic Strength for High Gas Barrier

The influence of MMT suspension ionic strength on oxygen barrier of PEI/MMT multilayer gas barrier nanocoating was studied in Chapter V. At pH 6.5 the amphoteric

edge sites of MMT have a neutral net charge, and a moderate concentration of NaCl effectively shields the charge from neighboring platelets, allowing van der Waals forces to attract the edges to one another. This edge-to-edge bonding creates a much more tortuous path for diffusing oxygen molecules. An 8 BL PEI/MMT multilayer coating (~50 nm thick), assembled with 5 mM NaCl in the aqueous clay suspension, exhibits an order of magnitude reduction in oxygen transmission rate relative to its salt-free counterpart. This "salty clay" strategy produces the best barrier among polymer-clay bilayer systems and also reduced the number of layers necessary for high gas barriers.

7.1.4 Self-Healing Super Oxygen Gas Barrier

Chapter VI demonstrated the self-healing behavior of a PEI/PAA multilayer gas barrier coating. An 8 BL PEI/PAA (~700 nm thick) exhibits an OTR undetectable to commercial instrumentation (<0.005 $cm^3/(m^2$ day atm)). The barrier property of this nanocoating was lost after tensile stretching due to its rigidity, which was then completely restored after high humidity exposure. The OTR of this multilayer nanocoating remained below detection after 10 stretching-healing cycles, which shows this healing process to be highly robust. The high oxygen barrier and self-healing behavior of this polymer multilayer nanocoating makes it ideal for packaging (food, electronics, and pharmaceutical) and gas separation applications.

7.2 Future Research Directions

7.2.1. Polyvinyl Alcohol/Montmorillonite Complex Gas Barrier Coating

Despite the improvements in the LbL coating process presented in the previous chapters, one of the biggest disadvantages of layer-by-layer assembly is the numerous steps (e.g., dipping, spraying, rinsing, etc.) required to produce films with sufficient gas barrier. PVOH/MMT assembly has been previously reported for improved mechanical strength.[130] In this potential future study, a polyvinyl alcohol/montmorillonite complex is prepared, followed by drop casting on polymer substrate. This complex coating has high transparency, mechanical properties and gas barrier.

Although PVOH is not a charged polyelectrolyte in water, two major interactions have been identified between PVOH and MMT.[130, 244] The first interaction is the hydrogen bonding between the O atoms of MMT and the H atoms of PVOH. A stable six-membered ring structure is also formed with 1 Al and 2 O atoms from MMT and 3 C atoms from PVOH. As a result, a viscous paste is formed after mixing and stirring. Figure 34 shows the thickness of these complex coatings with varying clay concentration after drop casting and drying on a piece of PET substrate. Thin film thickness decreases with clay concentration in the final dry coating, due to the increased film density. The elastic modulus increases from 0.3 GPa for neat PVOH to 20.3 GPa for a 50% clay composite (at room condition), as shown in Figure 35, which is also accompanied by a loss in extensibility.

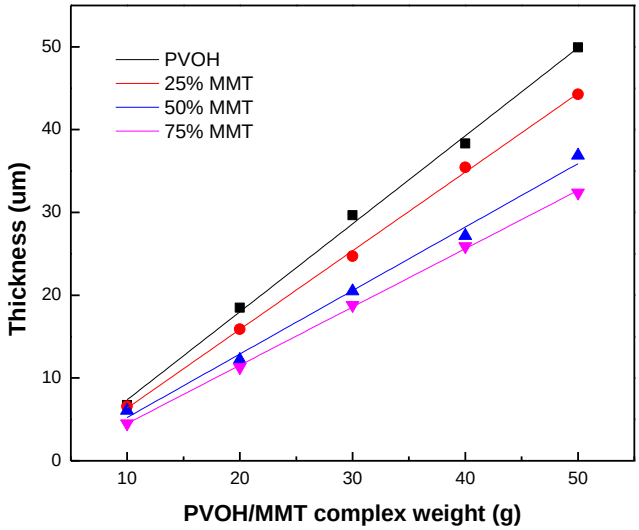

Figure 34. Thickness of PVOH/MMT complex coatings as a function of complex weight cast on PET (4×6 in.). Clay concentration in the final coating was controlled by the ratio of PVOH and MMT solutions during mixing.

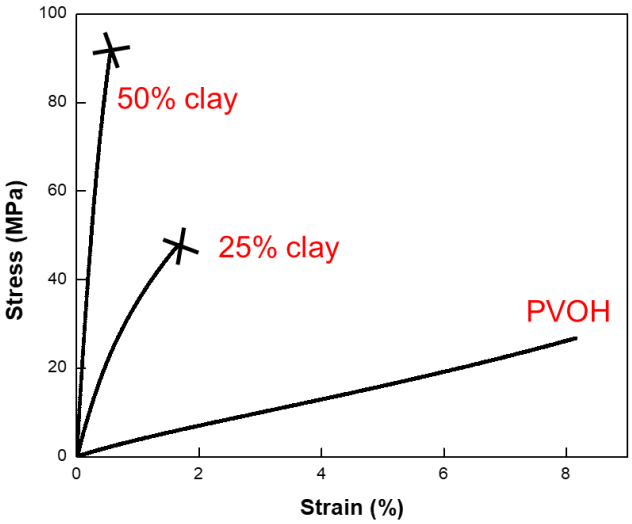

Figure 35. Stress/strain behavior of neat PVOH and PVOH/MMT complex coatings with varying clay concentration.

Oxygen barrier was also tested for neat PVOH and PVOH/MMT composites with different clay concentration, as shown in Figure 36. 7g of 2 wt% PVOH (or complex) was cast on a 4×6 in. PET substrate, which leads to dry coatings with thickness ~3 μm. The OTR for the 179 μm PET substrate is around 8.5 $cm^3/(m^2$ day atm), which is reduced below the detection limit (<0.005 $cm^3/(m^2$ day atm)) with a 50% clay coating. This high barrier and good transparency is probably related to the improved clay alignment during the curing (stirring) and drying process, which will be further supported by TEM cross-sectional images. We expect to see the barrier improve with clay concentration, due to their impermeable nature. The 75% clay thin film likely had defects that led to a higher OTR. Much more study of this system is clearly needed.

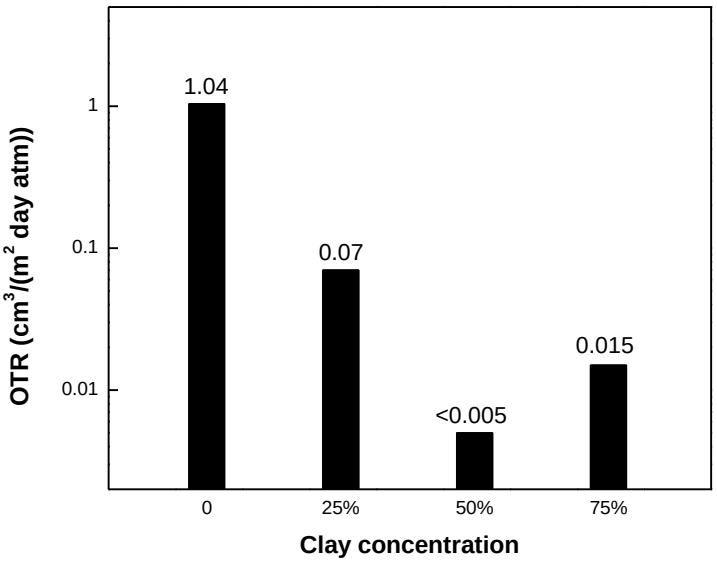

Figure 36. Oxygen transmission rate (OTR) of 7g neat PVOH and PVOH/MMT composite coatings on PET at 0% RH.

7.2.2. Vapor-Driven Multilayer Polymer Actuator

Polymer actuators can change their shape in response to external stimuli. They have attracted significant interest in sensors, biomedical applications, etc.[137, 245] Most of the polymer actuators demonstrated to-date are electroactive polymers (EPAs), which rely on the separation of positive and negative charge centers when an electric field is applied.[246] Humidity, light, and redox chemical responsive polymer actuators have also been reported.[247-249] A methanol-responsive multilayer actuator has also been demonstrated with free standing polyethylenimine (PEI)/poly(acrylic acid) (PAA) films.[228] Inspired by the structure of a bimetal stripe, which is usually comprised of two metals with different thermal expansion coefficients (e.g., brass (19×10^{-6}/°C) and steel (11×10^{-6}/°C)), a multilayer polymer actuator was prepared with a stack of PEI/PAA and polyurethane (PU)/PAA LbL films. The responsive behavior of this actuator results from the different swelling behavior of PEI/PAA (50% in water) and PU/PAA (190% in methanol) layers.

The bending (curling) degrees were measured by drawing two tangent lines on the edges of the actuator film in pictures taken with a contact angle camera, as shown in Figure 37. It was found that the bending degrees in both water vapor and methanol vapor environments can be precisely controlled by changing the thickness ratio of PEI/PAA and PU/PAA films, as shown in Figure 38. The analysis of the bimetal strip deformation has been reported previously using the Timoshenko formula.[250] The bending curvature can be expressed as $\frac{(1+\beta)^3}{1+4\alpha\beta+6\alpha\beta^2+4\alpha\beta^3+\alpha\beta^4}$, where α and β are the elastic modulus and thickness ratios of two metal layers, respectively. The two most important factors,

thickness and modulus, will be taken into account in finite element analysis (FEA) to simulate the polymer actuator film deformation. Moreover, a parallel circuit was built to demonstrate the environmental detection ability of this actuator membrane, which can detect different vapors and used as sensors.

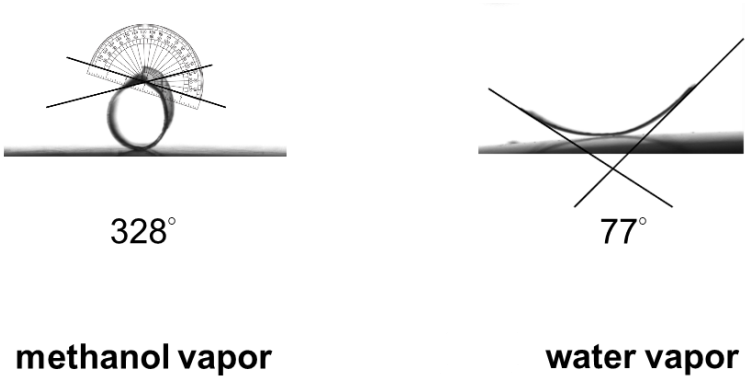

Figure 37. Schematic of bending degree measurements The pictures were taken with a contact angle camera.

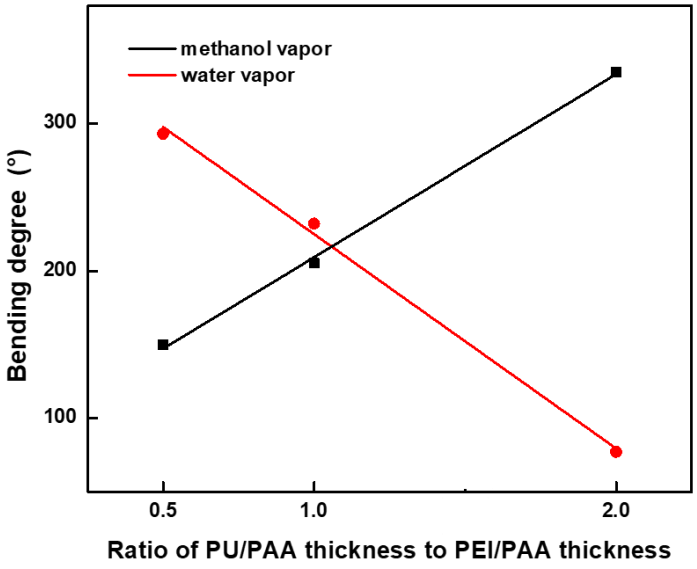

Figure 38. Bending degrees of the multilayer polymer actuator in water and methanol vapor environments as a function of thickness ratio between PEI/PAA and PU/PAA.

REFERENCES

1. Burrows, P. E.; Graff, G. L.; Gross, M. E.; Martin, P. M.; Shi, M. K.; Hall, M.; Mast, E.; Bonham, C.; Bennett, W.; Sullivan, M. B. Ultra Barrier Flexible Substrates for Flat Panel Displays. *Displays* **2001,** 22, (2), 65-69.
2. Yam, K. L.; Lee, D. S. Emerging Food Packaging Technologies: An Overview. In *Emerging Food Packaging Technologies: Principles and Practice*; Woodhead Publishing: Cambridge, United Kingdom, 2012.
3. Langowski, H. C. Permeation of Gases and Condensable Substances through Monolayer and Multilayer Structures. In *Plastic Packaging: Interactions with Food and Pharmaceuticals*; 2nd ed.; Wiley-VCH Verlag GmbH & Co. KGaA: Weinheim, Germany, 2008; Vol. 2, pp 297-347.
4. Das, S.; Yin, W. Trends in the Global Aluminum Fabrication Industry. *JOM* **2007,** 59, (2), 83-87.
5. Graff, G. L.; Burrows, P. E.; Williford, R. E.; Praino, R. F. Barrier Layer Technology for Flexible Displays. In *Flexible Flat Panel Displays*; John Wiley & Sons, Ltd: Chichester, UK, 2005; pp 57-77.
6. Lange, J.; Wyser, Y. Recent Innovations in Barrier Technologies for Plastic Packaging—a Review. *Packag. Technol. Sci.* **2003,** 16, (4), 149-158.
7. Roberts, A. P.; Henry, B. M.; Sutton, A. P.; Grovenor, C. R. M.; Briggs, G. A. D.; Miyamoto, T.; Kano, M.; Tsukahara, Y.; Yanaka, M. Gas Permeation in Silicon-Oxide/Polymer (SiO_x/PET) Barrier Films: Role of the Oxide Lattice, Nano-Defects and Macro-Defects. *J. Membr. Sci.* **2002,** 208, (1–2), 75-88.
8. Osman, M. A.; Mittal, V.; Morbidelli, M.; Suter, U. W. Polyurethane Adhesive Nanocomposites as Gas Permeation Barrier. *Macromolecules* **2003,** 36, (26), 9851-9858.
9. Choudalakis, G.; Gotsis, A. Permeability of Polymer/Clay Nanocomposites: A Review. *Eur. Polym. J.* **2009,** 45, (4), 967-984.
10. Triantafyllidis, K. S.; LeBaron, P. C.; Park, I.; Pinnavaia, T. J. Epoxy−Clay Fabric Film Composites with Unprecedented Oxygen-Barrier Properties. *Chem. Mater.* **2006,** 18, (18), 4393-4398.
11. Ebina, T.; Mizukami, F. Flexible Transparent Clay Films with Heat-Resistant and High Gas-Barrier Properties. *Adv. Mater.* **2007,** 19, (18), 2450-2453.
12. Decher, G. Layer-by-Layer Assembly (Putting Molecules to Work). In *Multilayer Thin Films*; Wiley-VCH Verlag GmbH & Co. KGaA: Weinheim, Germany, 2012; pp 1-21.

13. Borges, J.; Mano, J. F. Molecular Interactions Driving the Layer-by-Layer Assembly of Multilayers. *Chem. Rev.* **2014,** 114, (18), 8883-8942.

14. Bertrand, P.; Jonas, A.; Laschewsky, A.; Legras, R. Ultrathin Polymer Coatings by Complexation of Polyelectrolytes at Interfaces: Suitable Materials, Structure and Properties. *Macromol. Rapid Commun.* **2000,** 21, (7), 319-348.

15. Hagen, D. A.; Saucier, L.; Grunlan, J. C. Controlling Effective Aspect Ratio and Packing of Clay with pH for Improved Gas Barrier in Nanobrick Wall Thin Films. *ACS Appl. Mater. Interfaces* **2014,** 6, (24), 22914-22919.

16. Yan, N.; Capezzuto, F.; Buonocore, G. G.; Lavorgna, M.; Xia, H.; Ambrosio, L. Gas-Barrier Hybrid Coatings by the Assembly of Novel Poly(Vinyl Alcohol) and Reduced Graphene Oxide Layers through Cross-Linking with Zirconium Adducts. *ACS Appl. Mater. Interfaces* **2015,** 7, (40), 22678-22685.

17. Dou, Y.; Pan, T.; Xu, S.; Yan, H.; Han, J.; Wei, M.; Evans, D. G.; Duan, X. Transparent, Ultrahigh-Gas-Barrier Films with a Brick–Mortar–Sand Structure. *Angew. Chem. Int. Ed.* **2015,** 54, (33), 9673-9678.

18. Cho, C.; Culebras, M.; Wallace, K. L.; Song, Y.; Holder, K.; Hsu, J.-H.; Yu, C.; Grunlan, J. C. Stable N-Type Thermoelectric Multilayer Thin Films with High Power Factor from Carbonaceous Nanofillers. *Nano Energy* **2016,** 28, 426-432.

19. Tzeng, P.; Stevens, B.; Devlaming, I.; Grunlan, J. C. Polymer–Graphene Oxide Quadlayer Thin-Film Assemblies with Improved Gas Barrier. *Langmuir* **2015,** 31, (21), 5919-5927.

20. Holder, K. M.; Cain, A. A.; Plummer, M. G.; Stevens, B. E.; Odenborg, P. K.; Morgan, A. B.; Grunlan, J. C. Carbon Nanotube Multilayer Nanocoatings Prevent Flame Spread on Flexible Polyurethane Foam. *Macromol. Mater. Eng.* **2016,** 301, (6), 665-673.

21. Carosio, F.; Alongi, J. Ultra-Fast Layer-by-Layer Approach for Depositing Flame Retardant Coatings on Flexible Pu Foams within Seconds. *ACS Appl. Mater. Interfaces* **2016,** 8, (10), 6315-6319.

22. Wang, Y.; Yang, X.; Peng, H.; Wang, F.; Liu, X.; Yang, Y.; Hao, J. Layer-by-Layer Assembly of Multifunctional Flame Retardant Based on Brucite, 3-Aminopropyltriethoxysilane, and Alginate and Its Applications in Ethylene-Vinyl Acetate Resin. *ACS Appl. Mater. Interfaces* **2016,** 8, (15), 9925-9935.

23. Ariga, K.; Kawakami, K.; Ebara, M.; Kotsuchibashi, Y.; Ji, Q.; Hill, J. P. Bioinspired Nanoarchitectonics as Emerging Drug Delivery Systems. *New J. Chem.* **2014,** 38, (11), 5149-5163.

24. Shi, J.; Wang, X.; Xu, S.; Wu, Q.; Cao, S. Reversible Thermal-Tunable Drug Delivery across Nano-Membranes of Hollow PUA/PSS Multilayer Microcapsules. *J. Membr. Sci.* **2016,** 499, 307-316.

25. Podsiadlo, P.; Arruda, E. M.; Kheng, E.; Waas, A. M.; Lee, J.; Critchley, K.; Qin, M.; Chuang, E.; Kaushik, A. K.; Kim, H.-S.; Qi, Y.; Noh, S.-T.; Kotov, N. A. Lbl Assembled Laminates with Hierarchical Organization from Nano- to Microscale: High-Toughness Nanomaterials and Deformation Imaging. *ACS Nano* **2009,** 3, (6), 1564-1572.

26. Humood, M.; Chowdhury, S.; Song, Y.; Tzeng, P.; Grunlan, J. C.; Polycarpou, A. A. Nanomechanical Behavior of High Gas Barrier Multilayer Thin Films. *ACS Appl. Mater. Interfaces* **2016,** 8, (17), 11128-11138.

27. Xiao, F.-X.; Miao, J.; Liu, B. Layer-by-Layer Self-Assembly of CdS Quantum Dots/Graphene Nanosheets Hybrid Films for Photoelectrochemical and Photocatalytic Applications. *J. Am. Chem. Soc.* **2014,** 136, (4), 1559-1569.

28. Placido, T.; Fanizza, E.; Cosma, P.; Striccoli, M.; Curri, M. L.; Comparelli, R.; Agostiano, A. Electroactive Layer-by-Layer Plasmonic Architectures Based on Au Nanorods. *Langmuir* **2014,** 30, (10), 2608-2618.

29. Saetia, K.; Schnorr, J. M.; Mannarino, M. M.; Kim, S. Y.; Rutledge, G. C.; Swager, T. M.; Hammond, P. T. Spray-Layer-by-Layer Carbon Nanotube/Electrospun Fiber Electrodes for Flexible Chemiresistive Sensor Applications. *Adv. Funct. Mater.* **2014,** 24, (4), 492-502.

30. Stevens, B.; Dessiatova, E.; Hagen, D. A.; Todd, A. D.; Bielawski, C. W.; Grunlan, J. C. Low-Temperature Thermal Reduction of Graphene Oxide Nanobrick Walls: Unique Combination of High Gas Barrier and Low Resistivity in Fully Organic Polyelectrolyte Multilayer Thin Films. *ACS Appl. Mater. Interfaces* **2014,** 6, (13), 9942-9945.

31. Meaud, J.; Sain, T.; Yeom, B.; Park, S. J.; Shoultz, A. B.; Hulbert, G.; Ma, Z.-D.; Kotov, N. A.; Hart, A. J.; Arruda, E. M. Simultaneously High Stiffness and Damping in Nanoengineered Microtruss Composites. *ACS Nano* **2014,** 8, (4), 3468-3475.

32. Yanagida, S.; Kosakai, Y.; Yasumori, A. Preparation of Gold Nanoparticle Dispersed TiO_2-Polymer Composite Film by a Combined Layer-by-Layer and Photocatalytic Deposition Method. *Colloids Surf. Physicochem. Eng. Aspects* **2014,** 456, 55-61.

33. Ferreira, M.; Rubner, M. Molecular-Level Processing of Conjugated Polymers. 1. Layer-by-Layer Manipulation of Conjugated Polyions. *Macromolecules* **1995,** 28, (21), 7107-7114.

34. Priolo, M. A.; Holder, K. M.; Gamboa, D.; Grunlan, J. C. Influence of Clay Concentration on the Gas Barrier of Clay–Polymer Nanobrick Wall Thin Film Assemblies. *Langmuir* **2011,** 27, (19), 12106-12114.

35. Priolo, M. A.; Gamboa, D.; Grunlan, J. C. Transparent Clay− Polymer Nano Brick Wall Assemblies with Tailorable Oxygen Barrier. *ACS Appl. Mater. Interfaces* **2009,** 2, (1), 312-320.

36. Lu, Y.; Zhuk, A.; Xu, L.; Liang, X.; Kharlampieva, E.; Sukhishvili, S. A. Tunable Ph and Temperature Response of Weak Polyelectrolyte Brushes: Role of Hydrogen Bonding and Monomer Hydrophobicity. *Soft Matter* **2013,** 9, (22), 5464-5472.

37. Dubas, S. T.; Schlenoff, J. B. Swelling and Smoothing of Polyelectrolyte Multilayers by Salt. *Langmuir* **2001,** 17, (25), 7725-7727.

38. Porcel, C.; Lavalle, P.; Decher, G.; Senger, B.; Voegel, J.-C.; Schaaf, P. Influence of the Polyelectrolyte Molecular Weight on Exponentially Growing Multilayer Films in the Linear Regime. *Langmuir* **2007,** 23, (4), 1898-1904.

39. Yang, Y.-H.; Haile, M.; Park, Y. T.; Malek, F. A.; Grunlan, J. C. Super Gas Barrier of All-Polymer Multilayer Thin Films. *Macromolecules* **2011,** 44, (6), 1450-1459.

40. Priolo, M. A.; Gamboa, D.; Holder, K. M.; Grunlan, J. C. Super Gas Barrier of Transparent Polymer−Clay Multilayer Ultrathin Films. *Nano Lett.* **2010,** 10, (12), 4970-4974.

41. Priolo, M. A.; Holder, K. M.; Guin, T.; Grunlan, J. C. Recent Advances in Gas Barrier Thin Films Via Layer-by-Layer Assembly of Polymers and Platelets. *Macromol. Rapid Commun.* **2015,** 36, (10), 866-879.

42. Langowski, H.-C. Permeation of Gases and Condensable Substances through Monolayer and Multilayer Structures. In *Plastic Packaging*; Wiley-VCH Verlag GmbH & Co. KGaA: Weinheim, Germany, 2008; pp 297-347.

43. Leterrier, Y. Durability of Nanosized Oxygen-Barrier Coatings on Polymers. *Prog. Mater Sci.* **2003,** 48, (1), 1-55.

44. Willhite, C. C.; Karyakina, N. A.; Yokel, R. A.; Yenugadhati, N.; Wisniewski, T. M.; Arnold, I. M. F.; Momoli, F.; Krewski, D. Systematic Review of Potential Health Risks Posed by Pharmaceutical, Occupational and Consumer Exposures to Metallic and Nanoscale Aluminum, Aluminum Oxides, Aluminum Hydroxide and Its Soluble Salts. *Crit. Rev. Toxicol.* **2014,** 44, (sup4), 1-80.

45. Paula, M. M. d. S.; Rodrigues, F. B. B. M.; Bernardin, A. M.; Fiori, M. A.; Angioletto, E. Characterization of Aluminized Polyethylene Blends *via* Mechanical Recycling. *Mater. Sci. Eng. A* **2005,** 403, (1), 37-41.

46. Gall, R. L.; Anklin, R. T.; Mende, W. B.; Reclamation and Rejuvenation of Plastic and Metal from Metallized Plastic. U.S. Patent 4406411A, Sep 27, 1983.

47. Chatham, H. Oxygen Diffusion Barrier Properties of Transparent Oxide Coatings on Polymeric Substrates. *Surf. Coat. Technol.* **1996,** 78, (1), 1-9.

48. Grove, W. On the Electro-Chemical Polarity of Gases. *Trans. R. Soc.* **1852,** 142, 87.

49. Schiller, N.; Straach, S.; Fahland, M.; Charton, C. Barrier Coatings on Plastic Web, Presented at 44th Annual Technical Conference Proceedings, Society of Vacuum Coaters, Albuquerque, NM, 2001; pp 184-188.

50. Westwood, W. Physical Vapor Deposition. In *Microelectronic Materials and Processes*; Kluwer Academic Publishers: Dordrecht, The Netherlands, 1989; Vol. 164, p 133.

51. Adamov, M.; Perović, B.; Nenadović, T. Electrical and Structural Properties of Thin Gold Films Obtained by Vacuum Evaporation and Sputtering. *Thin Solid Films* **1974,** 24, (1), 89-100.

52. Mattox, D. M. Handbook of Physical Vapor Deposition (PVD) Processing 2nd ed.; Elsevier: Amsterdam, Netherlands, p 3.

53. Treutlein, R.; Bergsmann, M.; Stonley, C. J. Reel-to-Reel Vacuum Metallization. In *Organic Electronics*; Wiley-VCH Verlag GmbH & Co. KGaA: Weinheim, Germany, 2006; pp 181-202.

54. Mattox, D. M. Handbook of Physical Vapor Deposition (PVD) Processing. 2nd ed.; Elsevier: Amsterdam, Netherlands, p 215.

55. Jamieson, E.; Windle, A. Structure and Oxygen-Barrier Properties of Metallized Polymer Film. *J. Mater. Sci.* **1983,** 18, (1), 64-80.

56. Smith, A.; Copeland, N.; Gerrerd, D.; Nicholas, D. 49th Annual Technical Conference Proceedings, Presented at Society of Vacuum Coaters, Albuquerque, NM, 2002; pp 525-529.

57. Inagaki, N.; Tasaka, S.; Nakajima, T. Preparation of Oxygen Gas Barrier Polypropylene Films by Deposition of SiO_x Films Plasma-Polymerized from Mixture of Tetramethoxysilane and Oxygen. *J. Appl. Polym. Sci.* **2000,** 78, (13), 2389-2397.

58. Erlat, A. G.; Spontak, R. J.; Clarke, R. P.; Robinson, T. C.; Haaland, P. D.; Tropsha, Y.; Harvey, N. G.; Vogler, E. A. SiO_x Gas Barrier Coatings on

Polymer Substrates: Morphology and Gas Transport Considerations. *J. Phys. Chem. B* **1999,** 103, (29), 6047-6055.

59. Bichler, C.; Langowski, H.-C.; Moosheimer, U.; Seifert, B. Adhesion Mechanism of Aluminum, Aluminum Oxide, and Silicon Oxide on Biaxially Oriented Polypropylene (BOPP), Poly(Ethyleneterephthalate) (PET), and Poly(Vinyl Chloride) (PVC). *J. Adhes. Sci. Technol.* **1997,** 11, (2), 233-246.

60. da Silva Sobrinho, A.; Czeremuszkin, G.; Latreche, M.; Dennler, G.; Wertheimer, M. A Study of Defects in Ultra-Thin Transparent Coatings on Polymers. *Surf. Coat. Technol.* **1999,** 116, 1204-1210.

61. Pavlidou, S.; Papaspyrides, C. D. A Review on Polymer–Layered Silicate Nanocomposites. *Prog. Polym. Sci.* **2008,** 33, (12), 1119-1198.

62. Kango, S.; Kalia, S.; Celli, A.; Njuguna, J.; Habibi, Y.; Kumar, R. Surface Modification of Inorganic Nanoparticles for Development of Organic–Inorganic Nanocomposites—a Review. *Prog. Polym. Sci.* **2013,** 38, (8), 1232-1261.

63. Jagadale, T. C.; Takale, S. P.; Sonawane, R. S.; Joshi, H. M.; Patil, S. I.; Kale, B. B.; Ogale, S. B. N-Doped TiO_2 Nanoparticle Based Visible Light Photocatalyst by Modified Peroxide Sol− Gel Method. *J. Phys. Chem. C* **2008,** 112, (37), 14595-14602.

64. Haes, A. J.; Van Duyne, R. P. A Nanoscale Optical Biosensor: Sensitivity and Selectivity of an Approach Based on the Localized Surface Plasmon Resonance Spectroscopy of Triangular Silver Nanoparticles. *J. Am. Chem. Soc.* **2002,** 124, (35), 10596-10604.

65. Fu, X.; Qutubuddin, S. Polymer–Clay Nanocomposites: Exfoliation of Organophilic Montmorillonite Nanolayers in Polystyrene. *Polymer* **2001,** 42, (2), 807-813.

66. Song, Z.; Xu, T.; Gordin, M. L.; Jiang, Y.-B.; Bae, I.-T.; Xiao, Q.; Zhan, H.; Liu, J.; Wang, D. Polymer–Graphene Nanocomposites as Ultrafast-Charge and -Discharge Cathodes for Rechargeable Lithium Batteries. *Nano Lett.* **2012,** 12, (5), 2205-2211.

67. Bower, C. A., *Studies on the Forms and Availability of Soil Organic Phosphorus*. Agricultural Experiment Station, Iowa State College of Agriculture and Mechanic Arts: 1949; Vol. 362.

68. Okada, A.; Usuki, A. Twenty Years of Polymer-Clay Nanocomposites. *Macromol. Mater. Eng.* **2006,** 291, (12), 1449-1476.

69. Jitputti, J.; Rattanavoravipa, T.; Chuangchote, S.; Pavasupree, S.; Suzuki, Y.; Yoshikawa, S. Low Temperature Hydrothermal Synthesis of

Monodispersed Flower-Like Titanate Nanosheets. *Catal. Commun.* **2009,** 10, (4), 378-382.

70. Anglin, E. J.; Cheng, L.; Freeman, W. R.; Sailor, M. J. Porous Silicon in Drug Delivery Devices and Materials. *Adv. Drug Del. Rev.* **2008,** 60, (11), 1266-1277.

71. Feng, Q.; Wu, J.; Chen, G.; Cui, F.; Kim, T.; Kim, J. A Mechanistic Study of the Antibacterial Effect of Silver Ions on Escherichia Coli and Staphylococcus Aureus. *J. Biomed. Mater. Res.* **2000,** 52, (4), 662-668.

72. Vaia, R.; Giannelis, E. Liquid Crystal Polymer Nanocomposites: Direct Intercalation of Thermotropic Liquid Crystalline Polymers into Layered Silicates. *Polymer* **2001,** 42, (3), 1281-1285.

73. Cui, Y.; Kumar, S.; Rao Kona, B.; van Houcke, D. Gas Barrier Properties of Polymer/Clay Nanocomposites. *RSC Adv.* **2015,** 5, (78), 63669-63690.

74. Fornes, T.; Yoon, P.; Keskkula, H.; Paul, D. Nylon 6 Nanocomposites: The Effect of Matrix Molecular Weight. *Polymer* **2001,** 42, (25), 09929-09940.

75. Davis, C. H.; Mathias, L. J.; Gilman, J. W.; Schiraldi, D. A.; Shields, J. R.; Trulove, P.; Sutto, T. E.; Delong, H. C. Effects of Melt-Processing Conditions on the Quality of Poly(Ethylene Terephthalate) Montmorillonite Clay Nanocomposites. *J. Polym. Sci., Part B: Polym. Phys.* **2002,** 40, (23), 2661-2666.

76. Tang, Y.; Hu, Y.; Wang, J.; Zong, R.; Gui, Z.; Chen, Z.; Zhuang, Y.; Fan, W. Influence of Organophilic Clay and Preparation Methods on EVA/Montmorillonite Nanocomposites. *J. Appl. Polym. Sci.* **2004,** 91, (4), 2416-2421.

77. Gopakumar, T.; Lee, J.; Kontopoulou, M.; Parent, J. Influence of Clay Exfoliation on the Physical Properties of Montmorillonite/Polyethylene Composites. *Polymer* **2002,** 43, (20), 5483-5491.

78. Liu, X.; Wu, Q. Polyamide 66/Clay Nanocomposites *via* Melt Intercalation. *Macromol. Mater. Eng.* **2002,** 287, (3), 180-186.

79. Eisa, W. H.; Abdel-Moneam, Y. K.; Shabaka, A. A.; Hosam, A. E. M. *In situ* Approach Induced Growth of Highly Monodispersed Ag Nanoparticles within Free Standing PVA/PVP Films. *Spectrochim. Acta Mol. Biomol. Spectrosc.* **2012,** 95, 341-346.

80. Yano, K.; Usuki, A.; Okada, A. Synthesis and Properties of Polyimide-Clay Hybrid Films. *J. Polym. Sci., Part A: Polym. Chem.* **1997,** 35, (11), 2289-2294.

81. Xu, R.; Manias, E.; Snyder, A. J.; Runt, J. Low Permeability Biomedical Polyurethane Nanocomposites. *J. Biomed. Mater. Res. Part A* **2003,** 64A, (1), 114-119.

82. Gusev, A. A.; Lusti, H. R. Rational Design of Nanocomposites for Barrier Applications. *Adv. Mater.* **2001,** 13, (21), 1641-1643.

83. Nielsen, L. E. Models for the Permeability of Filled Polymer Systems. *J. Macromol. Sci., Chem.* **1967,** 1, (5), 929-942.

84. Messersmith, P. B.; Giannelis, E. P. Synthesis and Barrier Properties of Poly(E-Caprolactone)-Layered Silicate Nanocomposites. *J. Polym. Sci., Part A: Polym. Chem.* **1995,** 33, (7), 1047-1057.

85. Brydges, W.; Gulati, S.; Baum, G. Permeability of Glass Ribbon-Reinforced Composites. *J. Mater. Sci.* **1975,** 10, (12), 2044-2049.

86. Bharadwaj, R. K. Modeling the Barrier Properties of Polymer-Layered Silicate Nanocomposites. *Macromolecules* **2001,** 34, (26), 9189-9192.

87. Priolo, M. A.; Holder, K. M.; Greenlee, S. M.; Stevens, B. E.; Grunlan, J. C. Precisely Tuning the Clay Spacing in Nanobrick Wall Gas Barrier Thin Films. *Chem. Mater.* **2013,** 25, (9), 1649-1655.

88. Walther, A.; Bjurhager, I.; Malho, J.-M.; Pere, J.; Ruokolainen, J.; Berglund, L. A.; Ikkala, O. Large-Area, Lightweight and Thick Biomimetic Composites with Superior Material Properties *via* Fast, Economic, and Green Pathways. *Nano Lett.* **2010,** 10, (8), 2742-2748.

89. Lagaron, J.; Catalá, R.; Gavara, R. Structural Characteristics Defining High Barrier Properties in Polymeric Materials. *Mater. Sci. Technol.* **2004,** 20, (1), 1-7.

90. Morlier, A.; Cros, S.; Garandet, J.-P.; Alberola, N. Gas Barrier Properties of Solution Processed Composite Multilayer Structures for Organic Solar Cells Encapsulation. *Sol. Energy Mater. Sol. Cells* **2013,** 115, 93-99.

91. Wong, C. Recent Advances in IC Passivation and Encapsulation: Process Techniques and Materials. *Polymers for Electronic and Photonic Applications, AT&T Bell Laboratories* **1993**, 167-209.

92. Weaver, M.; Michalski, L.; Rajan, K.; Rothman, M.; Silvernail, J.; Brown, J. J.; Burrows, P. E.; Graff, G. L.; Gross, M. E.; Martin, P. M. Organic Light-Emitting Devices with Extended Operating Lifetimes on Plastic Substrates. *Appl. Phys. Lett.* **2002,** 81, (16), 2929-2931.

93. Moro, L. L.; Krajewski, T. A.; Rutherford, N. M.; Philips, O.; Visser, R. J.; Gross, M. E.; Bennett, W. D.; Graff, G. L. Process and Design of a Multilayer Thin Film Encapsulation of Passive Matrix OLED Displays, Presented at Proceedings of SPIE, 2003; pp 83-93.

94. Spee, D.; Rath, J.; Schropp, R. Using Hot Wire and Initiated Chemical Vapor Deposition for Gas Barrier Thin Film Encapsulation. *Thin Solid Films* **2015,** 575, 67-71.

95. Lee, J. G.; Kim, H. G.; Kim, S. S. Defect-Sealing of Al_2O_3/ZrO_2 Multilayer for Barrier Coating by Plasma-Enhanced Atomic Layer Deposition Process. *Thin Solid Films* **2015,** 577, 143-148.

96. Iler, R. K. Multilayers of Colloidal Particles. *J. Colloid Interface Sci.* **1966,** 21, (6), 569-594.

97. Decher, G. Fuzzy Nanoassemblies: Toward Layered Polymeric Multicomposites. *Science* **1997,** 277, (5330), 1232-1237.

98. Decher, G.; Hong, J.; Schmitt, J. Buildup of Ultrathin Multilayer Films by a Self-Assembly Process: III. Consecutively Alternating Adsorption of Anionic and Cationic Polyelectrolytes on Charged Surfaces. *Thin Solid Films* **1992,** 210, 831-835.

99. Schwarz, B.; Schönhoff, M. Surface Potential Driven Swelling of Polyelectrolyte Multilayers. *Langmuir* **2002,** 18, (8), 2964-2966.

100. Hua, F.; Cui, T.; Lvov, Y. M. Ultrathin Cantilevers Based on Polymer−Ceramic Nanocomposite Assembled through Layer-by-Layer Adsorption. *Nano Lett.* **2004,** 4, (5), 823-825.

101. Linford, M. R.; Auch, M.; Möhwald, H. Nonmonotonic Effect of Ionic Strength on Surface Dye Extraction During Dye− Polyelectrolyte Multilayer Formation. *J. Am. Chem. Soc.* **1998,** 120, (1), 178-182.

102. Kong, B.-S.; Geng, J.; Jung, H.-T. Layer-by-Layer Assembly of Graphene and Gold Nanoparticles by Vacuum Filtration and Spontaneous Reduction of Gold Ions. *Chem. Commun.* **2009**, (16), 2174-2176.

103. Chluba, J.; Voegel, J.-C.; Decher, G.; Erbacher, P.; Schaaf, P.; Ogier, J. Peptide Hormone Covalently Bound to Polyelectrolytes and Embedded into Multilayer Architectures Conserving Full Biological Activity. *Biomacromolecules* **2001,** 2, (3), 800-805.

104. Eckle, M.; Decher, G. Tuning the Performance of Layer-by-Layer Assembled Organic Light Emitting Diodes by Controlling the Position of Isolating Clay Barrier Sheets. *Nano Lett.* **2001,** 1, (1), 45-49.

105. Lee, S. W.; Kim, B.-S.; Chen, S.; Shao-Horn, Y.; Hammond, P. T. Layer-by-Layer Assembly of All Carbon Nanotube Ultrathin Films for Electrochemical Applications. *J. Am. Chem. Soc.* **2008,** 131, (2), 671-679.

106. Lvov, Y.; Ariga, K.; Ichinose, I.; Kunitake, T. Assembly of Multicomponent Protein Films by Means of Electrostatic Layer-by-Layer Adsorption. *J. Am. Chem. Soc.* **1995,** 117, (22), 6117-6123.

107. Lvov, Y.; Haas, H.; Decher, G.; Moehwald, H.; Mikhailov, A.; Mtchedlishvily, B.; Morgunova, E.; Vainshtein, B. Successive Deposition of Alternate Layers of Polyelectrolytes and a Charged Virus. *Langmuir* **1994,** 10, (11), 4232-4236.

108. Lvov, Y. M.; Lu, Z.; Schenkman, J. B.; Zu, X.; Rusling, J. F. Direct Electrochemistry of Myoglobin and Cytochrome $P450_{cam}$ in Alternate Layer-by-Layer Films with DNA and Other Polyions. *J. Am. Chem. Soc.* **1998,** 120, (17), 4073-4080.

109. Podsiadlo, P.; Michel, M.; Lee, J.; Verploegen, E.; Wong Shi Kam, N.; Ball, V.; Lee, J.; Qi, Y.; Hart, A. J.; Hammond, P. T. Exponential Growth of LbL Films with Incorporated Inorganic Sheets. *Nano Lett.* **2008,** 8, (6), 1762-1770.

110. Sukhishvili, S. A.; Granick, S. Layered, Erasable, Ultrathin Polymer Films. *J. Am. Chem. Soc.* **2000,** 122, (39), 9550-9551.

111. Serizawa, T.; Hashiguchi, S.; Akashi, M. Stepwise Assembly of Ultrathin Poly(Vinyl Alcohol) Films on a Gold Substrate by Repetitive Adsorption/Drying Processes. *Langmuir* **1999,** 15, (16), 5363-5368.

112. Zhang, Y.; Cao, W. Self-Assembly of Small Molecules: An Approach Combining Electrostatic Self-Assembly Technology with Host–Guest Chemistry. *New J. Chem.* **2001,** 25, (3), 483-486.

113. Liu, Y.; Bruening, M. L.; Bergbreiter, D. E.; Crooks, R. M. Multilayer Dendrimer–Polyanhydride Composite Films on Glass, Silicon, and Gold Wafers. *Angew. Chem. Int. Ed.* **1997,** 36, (19), 2114-2116.

114. Wang, X.; Jiang, Z.; Shi, J.; Liang, Y.; Zhang, C.; Wu, H. Metal–Organic Coordination-Enabled Layer-by-Layer Self-Assembly to Prepare Hybrid Microcapsules for Efficient Enzyme Immobilization. *ACS Appl. Mater. Interfaces* **2012,** 4, (7), 3476-3483.

115. Spaeth, K.; Brecht, A.; Gauglitz, G. Studies on the Biotin–Avidin Multilayer Adsorption by Spectroscopic Ellipsometry. *J. Colloid Interface Sci.* **1997,** 196, (2), 128-135.

116. Jiang, C.; Liu, X.; Luo, C.; Zhang, Y.; Shao, L.; Shi, F. Controlled Exponential Growth in Layer-by-Layer Multilayers Using High Gravity Fields. *J. Mater. Chem. A* **2014,** 2, (34), 14048-14053.

117. Patel, P. A.; Dobrynin, A. V.; Mather, P. T. Combined Effect of Spin Speed and Ionic Strength on Polyelectrolyte Spin Assembly. *Langmuir* **2007,** 23, (25), 12589-12597.

118. Li, M.; Zhang, J.; Nie, H.-J.; Liao, M.; Sang, L.; Qiao, W.; Wang, Z. Y.; Ma, Y.; Zhong, Y.-W.; Ariga, K. *In situ* Switching Layer-by-Layer Assembly: One-Pot Rapid Layer Assembly *via* Alternation of Reductive and Oxidative Electropolymerization. *Chem. Commun.* **2013,** 49, (61), 6879-6881.

119. Izquierdo, A.; Ono, S. S.; Voegel, J. C.; Schaaf, P.; Decher, G. Dipping Versus Spraying: Exploring the Deposition Conditions for Speeding up Layer-by-Layer Assembly. *Langmuir* **2005,** 21, (16), 7558-7567.

120. Xiang, F.; Givens, T. M.; Grunlan, J. C. Fast Spray Deposition of Super Gas Barrier Polyelectrolyte Multilayer Thin Films. *Ind. Eng. Chem. Res.* **2015,** 54, (19), 5254-5260.

121. Chang, S.; Slopek, R. P.; Condon, B.; Grunlan, J. C. Surface Coating for Flame-Retardant Behavior of Cotton Fabric Using a Continuous Layer-by-Layer Process. *Ind. Eng. Chem. Res.* **2014,** 53, (10), 3805-3812.

122. Mateos, A. J.; Cain, A. A.; Grunlan, J. C. Large-Scale Continuous Immersion System for Layer-by-Layer Deposition of Flame Retardant and Conductive Nanocoatings on Fabric. *Ind. Eng. Chem. Res.* **2014,** 53, (15), 6409-6416.

123. Nuraje, N.; Asmatulu, R.; Cohen, R. E.; Rubner, M. F. Durable Antifog Films from Layer-by-Layer Molecularly Blended Hydrophilic Polysaccharides. *Langmuir* **2011,** 27, (2), 782-791.

124. Lee, D.; Rubner, M. F.; Cohen, R. E. All-Nanoparticle Thin-Film Coatings. *Nano Lett.* **2006,** 6, (10), 2305-2312.

125. Donath, E.; Sukhorukov, G. B.; Caruso, F.; Davis, S. A.; Möhwald, H. Novel Hollow Polymer Shells by Colloid-Templated Assembly of Polyelectrolytes. *Angew. Chem. Int. Ed.* **1998,** 37, (16), 2201-2205.

126. Tang, Z.; Wang, Y.; Podsiadlo, P.; Kotov, N. A. Biomedical Applications of Layer-by-Layer Assembly: From Biomimetics to Tissue Engineering. *Adv. Mater.* **2006,** 18, (24), 3203-3224.

127. Cho, C.; Stevens, B.; Hsu, J.-H.; Bureau, R.; Hagen, D. A.; Regev, O.; Yu, C.; Grunlan, J. C. Completely Organic Multilayer Thin Film with Thermoelectric Power Factor Rivaling Inorganic Tellurides. *Adv. Mater.* **2015,** 27, (19), 2996-3001.

128. Kim, D.; Tzeng, P.; Barnett, K. J.; Yang, Y.-H.; Wilhite, B. A.; Grunlan, J. C. Highly Size-Selective Ionically Crosslinked Multilayer Polymer Films for Light Gas Separation. *Adv. Mater.* **2014,** 26, (5), 746-751.

129. Li, Y.-C.; Schulz, J.; Mannen, S.; Delhom, C.; Condon, B.; Chang, S.; Zammarano, M.; Grunlan, J. C. Flame Retardant Behavior of Polyelectrolyte−Clay Thin Film Assemblies on Cotton Fabric. *ACS Nano* **2010,** 4, (6), 3325-3337.

130. Podsiadlo, P.; Kaushik, A. K.; Arruda, E. M.; Waas, A. M.; Shim, B. S.; Xu, J.; Nandivada, H.; Pumplin, B. G.; Lahann, J.; Ramamoorthy, A.; Kotov, N. A. Ultrastrong and Stiff Layered Polymer Nanocomposites. *Science* **2007,** 318, (5847), 80-83.

131. Kotov, N. A.; Magonov, S.; Tropsha, E. Layer-by-Layer Self-Assembly of Alumosilicate−Polyelectrolyte Composites: Mechanism of Deposition, Crack Resistance, and Perspectives for Novel Membrane Materials. *Chem. Mater.* **1998,** 10, (3), 886-895.

132. Cho, C.; Xiang, F.; Wallace, K. L.; Grunlan, J. C. Combined Ionic and Hydrogen Bonding in Polymer Multilayer Thin Film for High Gas Barrier and Stretchiness. *Macromolecules* **2015,** 48, (16), 5723-5729.

133. Zhao, L.; Yuan, B.; Geng, Y.; Yu, C.; Kim, N. H.; Lee, J. H.; Li, P. Fabrication of Ultrahigh Hydrogen Barrier Polyethyleneimine/Graphene Oxide Films by LbL Assembly Fine-Tuned with Electric Field Application. *Composites Part A* **2015,** 78, 60-69.

134. Song, Y.; Tzeng, P.; Grunlan, J. C. Super Oxygen and Improved Water Vapor Barrier of Polypropylene Film with Polyelectrolyte Multilayer Nanocoatings. *Macromol. Rapid Commun.* **2016,** 37, (12), 963-968.

135. Carosio, F.; Colonna, S.; Fina, A.; Rydzek, G.; Hemmerlé, J.; Jierry, L.; Schaaf, P.; Boulmedais, F. Efficient Gas and Water Vapor Barrier Properties of Thin Poly(Lactic Acid) Packaging Films: Functionalization with Moisture Resistant Nafion and Clay Multilayers. *Chem. Mater.* **2014,** 26, (19), 5459-5466.

136. Song, E.-H.; Kang, B.-H.; Kim, T.-Y.; Lee, H.-J.; Park, Y.-W.; Kim, Y.-C.; Ju, B.-K. Highly Oriented Gold/Nanoclay–Polymer Nanocomposites for Flexible Gas Barrier Films. *ACS Appl. Mater. Interfaces* **2015,** 7, (8), 4778-4783.

137. Stuart, M. A. C.; Huck, W. T.; Genzer, J.; Müller, M.; Ober, C.; Stamm, M.; Sukhorukov, G. B.; Szleifer, I.; Tsukruk, V. V.; Urban, M. Emerging Applications of Stimuli-Responsive Polymer Materials. *Nat. Mater.* **2010,** 9, (2), 101.

138. Hashidzume, A.; Harada, A. Stimuli-Responsive Polymers. In *Encyclopedia of Polymeric Nanomaterials*; Springer-Verlag GmbH: Berlin, German, 2013; pp 1-6.

139. Meng, H.; Li, G. A Review of Stimuli-Responsive Shape Memory Polymer Composites. *Polymer* **2013,** 54, (9), 2199-2221.

140. Alarcon, C. d. l. H.; Pennadam, S.; Alexander, C. Stimuli Responsive Polymers for Biomedical Applications. *Chem. Soc. Rev.* **2005,** 34, (3), 276-285.

141. Mura, S.; Nicolas, J.; Couvreur, P. Stimuli-Responsive Nanocarriers for Drug Delivery. *Nat. Mater.* **2013,** 12, (11), 991.

142. Ng, K. K.; Shakiba, M.; Huynh, E.; Weersink, R. A.; Roxin, A.; Wilson, B. C.; Zheng, G. Stimuli-Responsive Photoacoustic Nanoswitch for *in vivo* Sensing Applications. *ACS Nano* **2014,** 8, (8), 8363-8373.

143. Borges, J.; Rodrigues, L. C.; Reis, R. L.; Mano, J. F. Layer-by-Layer Assembly of Light-Responsive Polymeric Multilayer Systems. *Adv. Funct. Mater.* **2014,** 24, (36), 5624-5648.

144. Antipina, M. N.; Kiryukhin, M. V.; Skirtach, A. G.; Sukhorukov, G. B. Micropackaging *via* Layer-by-Layer Assembly: Microcapsules and Microchamber Arrays. *Int. Mater. Rev.* **2014,** 59, (4), 224-244.

145. Deshmukh, P. K.; Ramani, K. P.; Singh, S. S.; Tekade, A. R.; Chatap, V. K.; Patil, G. B.; Bari, S. B. Stimuli-Sensitive Layer-by-Layer (LbL) Self-Assembly Systems: Targeting and Biosensory Applications. *J. Controlled Release* **2013,** 166, (3), 294-306.

146. Yu, A.; Liang, Z.; Cho, J.; Caruso, F. Nanostructured Electrochemical Sensor Based on Dense Gold Nanoparticle Films. *Nano Lett.* **2003,** 3, (9), 1203-1207.

147. Hu, S.-H.; Tsai, C.-H.; Liao, C.-F.; Liu, D.-M.; Chen, S.-Y. Controlled Rupture of Magnetic Polyelectrolyte Microcapsules for Drug Delivery. *Langmuir* **2008,** 24, (20), 11811-11818.

148. Skirtach, A. G.; De Geest, B. G.; Mamedov, A.; Antipov, A. A.; Kotov, N. A.; Sukhorukov, G. B. Ultrasound Stimulated Release and Catalysis Using Polyelectrolyte Multilayer Capsules. *J. Mater. Chem.* **2007,** 17, (11), 1050-1054.

149. Antipov, A. A.; Sukhorukov, G. B.; Leporatti, S.; Radtchenko, I. L.; Donath, E.; Möhwald, H. Polyelectrolyte Multilayer Capsule Permeability Control. *Colloids Surf. Physicochem. Eng. Aspects* **2002,** 198, (Supplement C), 535-541.

150. Antipov, A. A.; Sukhorukov, G. B.; Leporatti, S.; Radtchenko, I. L.; Donath, E.; Möhwald, H. Polyelectrolyte Multilayer Capsule Permeability Control. *Colloids Surf. Physicochem. Eng. Aspects* **2002,** 198, 535-541.

151. Ghosh, S. K. Self-Healing Materials: Fundamentals, Design Strategies, and Applications. In *Self-Healing Materials*; Wiley-VCH Verlag GmbH & Co. KGaA: Weinheim, Germany, 2009; pp 1-28.

152. Reisch, A.; Roger, E.; Phoeung, T.; Antheaume, C.; Orthlieb, C.; Boulmedais, F.; Lavalle, P.; Schlenoff, J. B.; Frisch, B.; Schaaf, P. On the Benefits of Rubbing Salt in the Cut: Self-Healing of Saloplastic PAA/PAH Compact Polyelectrolyte Complexes. *Adv. Mater.* **2014,** 26, (16), 2547-2551.

153. Skorb, E. V.; Andreeva, D. V. Layer-by-Layer Approaches for Formation of Smart Self-Healing Materials. *Polym. Chem.* **2013,** 4, (18), 4834-4845.

154. Skorb, E. V.; Andreeva, D. V. Self-Healing Properties of Layer-by-Layer Assembled Multilayers. *Polym. Int.* **2015,** 64, (6), 713-723.

155. Chen, D.; Wu, M.; Li, B.; Ren, K.; Cheng, Z.; Ji, J.; Li, Y.; Sun, J. Layer-by-Layer-Assembled Healable Antifouling Films. *Adv. Mater.* **2015,** 27, (39), 5882-5888.

156. Wang, X.; Wang, Y.; Bi, S.; Wang, Y.; Chen, X.; Qiu, L.; Sun, J. Optically Transparent Antibacterial Films Capable of Healing Multiple Scratches. *Adv. Funct. Mater.* **2014,** 24, (3), 403-411.

157. Manna, U.; Lynn, D. M. Restoration of Superhydrophobicity in Crushed Polymer Films by Treatment with Water: Self-Healing and Recovery of Damaged Topographic Features Aided by an Unlikely Source. *Adv. Mater.* **2013,** 25, (36), 5104-5108.

158. Li, Y.; Chen, S.; Wu, M.; Sun, J. Polyelectrolyte Multilayers Impart Healability to Highly Electrically Conductive Films. *Adv. Mater.* **2012,** 24, (33), 4578-4582.

159. Chen, S.; Li, X.; Li, Y.; Sun, J. Intumescent Flame-Retardant and Self-Healing Superhydrophobic Coatings on Cotton Fabric. *ACS Nano* **2015,** 9, (4), 4070-4076.

160. Vogt, C. d.; Ball, V.; Mutterer, J. r. m.; Schaaf, P.; Voegel, J.-C.; Senger, B.; Lavalle, P. Mobility of Proteins in Highly Hydrated Polyelectrolyte Multilayer Films. *J. Phys. Chem. B* **2012,** 116, (17), 5269-5278.

161. Shchukin, D.; Möhwald, H. A Coat of Many Functions. *Science* **2013,** 341, (6153), 1458-1459.

162. Gu, Y.; Huang, X.; Wiener, C. G.; Vogt, B. D.; Zacharia, N. S. Large-Scale Solvent Driven Actuation of Polyelectrolyte Multilayers Based on Modulation of Dynamic Secondary Interactions. *ACS Appl. Mater. Interfaces* **2015,** 7, (3), 1848-1858.

163. Dong, J.; Ding, J.; Weng, J.; Dai, L. Graphene Enhances the Shape Memory of Poly(Acrylamide-Co-Acrylic Acid) Grafted on Graphene. *Macromol. Rapid Commun.* **2013,** 34, (8), 659-664.

164. Mount, E. M. Oriented Films-Troubleshooting and Characterization. In *Handbook of Troubleshooting Plastics Processes*; John Wiley & Sons, Inc.: Hoboken, NJ, 2012; pp 133-165.

165. Brody, A. L. Food Packaging. In *Van Nostrand's Scientific Encyclopedia*; John Wiley & Sons, Inc.: Hoboken, NJ, 2005.

166. Charton, C.; Schiller, N.; Fahland, M.; Holländer, A.; Wedel, A.; Noller, K. Development of High Barrier Films on Flexible Polymer Substrates. *Thin Solid Films* **2006,** 502, (1–2), 99-103.

167. Jang, W.-S.; Grunlan, J. C. Robotic Dipping System for Layer-by-Layer Assembly of Multifunctional Thin Films. *Rev. Sci. Instrum.* **2005,** 76, (10), 103904.

168. Picart, C.; Mutterer, J.; Richert, L.; Luo, Y.; Prestwich, G. D.; Schaaf, P.; Voegel, J.-C.; Lavalle, P. Molecular Basis for the Explanation of the Exponential Growth of Polyelectrolyte Multilayers. *Proc. Natl. Acad. Sci.* **2002,** 99, (20), 12531-12535.

169. Hagen, D. A.; Foster, B.; Stevens, B.; Grunlan, J. C. Shift-Time Polyelectrolyte Multilayer Assembly: Fast Film Growth and High Gas Barrier with Fewer Layers by Adjusting Deposition Time. *ACS Macro Lett.* **2014,** 3, (7), 663-666.

170. Xiang, F.; Tzeng, P.; Sawyer, J. S.; Regev, O.; Grunlan, J. C. Improving the Gas Barrier Property of Clay–Polymer Multilayer Thin Films Using Shorter Deposition Times. *ACS Appl. Mater. Interfaces* **2014,** 6, (9), 6040-6048.

171. Merindol, R.; Diabang, S.; Felix, O.; Roland, T.; Gauthier, C.; Decher, G. Bio-Inspired Multiproperty Materials: Strong, Self-Healing, and Transparent Artificial Wood Nanostructures. *ACS Nano* **2015,** 9, (2), 1127-1136.

172. Cui, M.; Ng, W. S.; Wang, X.; Darmawan, P.; Lee, P. S. Enhanced Electrochromism with Rapid Growth Layer-by-Layer Assembly of Polyelectrolyte Complexes. *Adv. Funct. Mater.* **2015,** 25, (3), 401-408.

173. Salehi, A.; Desai, P. S.; Li, J.; Steele, C. A.; Larson, R. G. Relationship between Polyelectrolyte Bulk Complexation and Kinetics of Their Layer-by-Layer Assembly. *Macromolecules* **2015,** 48, (2), 400-409.

174. Priolo, M. A.; Holder, K. M.; Greenlee, S. M.; Grunlan, J. C. Transparency, Gas Barrier, and Moisture Resistance of Large-Aspect-Ratio Vermiculite Nanobrick Wall Thin Films. *ACS Appl. Mater. Interfaces* **2012,** 4, (10), 5529-5533.

175. Zhang, Z.; Britt, I. J.; Tung, M. A. Permeation of Oxygen and Water Vapor through EVOH Films as Influenced by Relative Humidity. *J. Appl. Polym. Sci.* **2001,** 82, (8), 1866-1872.

176. Muramatsu, M.; Okura, M.; Kuboyama, K.; Ougizawa, T.; Yamamoto, T.; Nishihara, Y.; Saito, Y.; Ito, K.; Hirata, K.; Kobayashi, Y. Oxygen Permeability and Free Volume Hole Size in Ethylene–Vinyl Alcohol

Copolymer Film: Temperature and Humidity Dependence. *Radiat. Phys. Chem.* **2003,** 68, (3–4), 561-564.

177. Bharadwaj, R. Effect of H_2O on the Diffusion of N_2 in PMMA: A Molecular Dynamics Simulation Study. *Macromolecules* **2002,** 35, (13), 5334-5336.

178. Grunlan, J. C.; Grigorian, A.; Hamilton, C. B.; Mehrabi, A. R. Effect of Clay Concentration on the Oxygen Permeability and Optical Properties of a Modified Poly(Vinyl Alcohol). *J. Appl. Polym. Sci.* **2004,** 93, (3), 1102-1109.

179. Leväsalmi, J.-M.; McCarthy, T. J. Poly(4-Methyl-1-Pentene)-Supported Polyelectrolyte Multilayer Films: Preparation and Gas Permeability. *Macromolecules* **1997,** 30, (6), 1752-1757.

180. Nolte, A. J.; Treat, N. D.; Cohen, R. E.; Rubner, M. F. Effect of Relative Humidity on the Young's Modulus of Polyelectrolyte Multilayer Films and Related Nonionic Polymers. *Macromolecules* **2008,** 41, (15), 5793-5798.

181. Deng, L.; Hägg, M.-B. Swelling Behavior and Gas Permeation Performance of PVAM/PVA Blend FSC Membrane. *J. Membr. Sci.* **2010,** 363, (1–2), 295-301.

182. Misiano, C.; Simonetti, E.; Cerolini, P.; Staffetti, F.; Fusi, A. Silicon Oxide Barrier Improvement on Plastic Substrate, Presented at 33rd Annual Technical Conference Proceedings, Society of Vacuum Coaters, 1991; p 105.

183. Felts, J. T.; Grubb, A. D. Commercial-Scale Application of Plasma Processing for Polymeric Substrates: From Laboratory to Production. *J. Vac. Sci. Technol.* **1992,** 10, (4), 1675-1681.

184. Agres, L.; Ségui, Y.; Delsol, R.; Raynaud, P. Oxygen Barrier Efficiency of Hexamethyldisiloxane/Oxygen Plasma-Deposited Coating. *J. Appl. Polym. Sci.* **1996,** 61, (11), 2015-2022.

185. Yang, Y.-H.; Bolling, L.; Haile, M.; Grunlan, J. C. Improving Oxygen Barrier and Reducing Moisture Sensitivity of Weak Polyelectrolyte Multilayer Thin Films with Crosslinking. *RSC Adv.* **2012,** 2, (32), 12355-12363.

186. Zhai, L.; Cebeci, F. Ç.; Cohen, R. E.; Rubner, M. F. Stable Superhydrophobic Coatings from Polyelectrolyte Multilayers. *Nano Lett.* **2004,** 4, (7), 1349-1353.

187. Seethamraju, S.; Rao, A. D.; Ramamurthy, P. C.; Madras, G. Layer-by-Layer Assembly of Nafion on Surlyn with Ultrahigh Water Vapor Barrier. *Langmuir* **2014,** 30, (48), 14606-14611.

188. Daiko, Y.; Katagiri, K.; Matsuda, A. Proton Conduction in Thickness-Controlled Ultrathin Polycation/Nafion Multilayers Prepared *via* Layer-by-Layer Assembly. *Chem. Mater.* **2008,** 20, (20), 6405-6409.

189. Ploehn, H. J.; Liu, C. Quantitative Analysis of Montmorillonite Platelet Size by Atomic Force Microscopy. *Ind. Eng. Chem. Res.* **2006,** 45, (21), 7025-7034.

190. Falla, W. R.; Mulski, M.; Cussler, E. Estimating Diffusion through Flake-Filled Membranes. *J. Membr. Sci.* **1996,** 119, (1), 129-138.

191. Arunvisut, S.; Phummanee, S.; Somwangthanaroj, A. Effect of Clay on Mechanical and Gas Barrier Properties of Blown Film LDPE/Clay Nanocomposites. *J. Appl. Polym. Sci.* **2007,** 106, (4), 2210-2217.

192. Kim, H.; Miura, Y.; Macosko, C. W. Graphene/Polyurethane Nanocomposites for Improved Gas Barrier and Electrical Conductivity. *Chem. Mater.* **2010,** 22, (11), 3441-3450.

193. Vladimirov, V.; Betchev, C.; Vassiliou, A.; Papageorgiou, G.; Bikiaris, D. Dynamic Mechanical and Morphological Studies of Isotactic Polypropylene/Fumed Silica Nanocomposites with Enhanced Gas Barrier Properties. *Compos. Sci. Technol.* **2006,** 66, (15), 2935-2944.

194. Lee, J.-H.; Jung, D.; Hong, C.-E.; Rhee, K. Y.; Advani, S. G. Properties of Polyethylene-Layered Silicate Nanocomposites Prepared by Melt Intercalation with a PP-g-MA Compatibilizer. *Compos. Sci. Technol.* **2005,** 65, (13), 1996-2002.

195. Hagen, D.; Box, C.; Greenlee, S.; Xiang, F.; Regev, O.; Grunlan, J. High Gas Barrier Imparted by Similarly Charged Multilayers in Nanobrick Wall Thin Films. *RSC Adv.* **2014,** 4, (35), 18354-18359.

196. Inagaki, N.; Tasaka, S.; Hiramatsu, H. Preparation of Oxygen Gas Barrier Poly(Ethylene Terephthalate) Films by Deposition of Silicon Oxide Films Plasma-Polymerized from a Mixture of Tetramethoxysilane and Oxygen. *J. Appl. Polym. Sci.* **1999,** 71, (12), 2091-2100.

197. Struller, C.; Kelly, P.; Copeland, N.; Tobin, V.; Assender, H.; Holliday, C.; Read, S. Aluminium Oxide Barrier Films on Polymeric Web and Their Conversion for Packaging Applications. *Thin Solid Films* **2014,** 553, 153-156.

198. Lagaly, G.; Olphen, H. v. In *An Introduction to Clay Colloid Chemistry*; 2nd ed.; Wiley-VCH Verlag GmbH & Co. KGaA: Weinheim, Germany, 1978; Vol. 82, pp 236-237.

199. Abend, S.; Lagaly, G. Sol–Gel Transitions of Sodium Montmorillonite Dispersions. *Appl. Clay Sci.* **2000,** 16, (3–4), 201-227.

200. Benna, M.; Kbir-Ariguib, N.; Magnin, A.; Bergaya, F. Effect of pH on Rheological Properties of Purified Sodium Bentonite Suspensions. *J. Colloid Interface Sci.* **1999,** 218, (2), 442-455.

201. Santiwong, S. R.; Guan, J.; Waite, T. D. Effect of Ionic Strength and pH on Hydraulic Properties and Structure of Accumulating Solid Assemblages During Microfiltration of Montmorillonite Suspensions. *J. Colloid Interface Sci.* **2008,** 317, (1), 214-227.

202. Brandenburg, U.; Lagaly, G. Rheological Properties of Sodium Montmorillonite Dispersions. *Appl. Clay Sci.* **1988,** 3, (3), 263-279.

203. Durán, J. D. G.; Ramos-Tejada, M. M.; Arroyo, F. J.; González-Caballero, F. Rheological and Electrokinetic Properties of Sodium Montmorillonite Suspensions: I. Rheological Properties and Interparticle Energy of Interaction. *J. Colloid Interface Sci.* **2000,** 229, (1), 107-117.

204. Tombácz, E.; Szekeres, M. Colloidal Behavior of Aqueous Montmorillonite Suspensions: The Specific Role of pH in the Presence of Indifferent Electrolytes. *Appl. Clay Sci.* **2004,** 27, (1–2), 75-94.

205. Tombácz, E.; Szekeres, M. Surface Charge Heterogeneity of Kaolinite in Aqueous Suspension in Comparison with Montmorillonite. *Appl. Clay Sci.* **2006,** 34, (1–4), 105-124.

206. Dubas, S. T.; Schlenoff, J. B. Polyelectrolyte Multilayers Containing a Weak Polyacid: Construction and Deconstruction. *Macromolecules* **2001,** 34, (11), 3736-3740.

207. Dubas, S. T.; Farhat, T. R.; Schlenoff, J. B. Multiple Membranes from "True" Polyelectrolyte Multilayers. *J. Am. Chem. Soc.* **2001,** 123, (22), 5368-5369.

208. Kaushik, A. K.; Podsiadlo, P.; Qin, M.; Shaw, C. M.; Waas, A. M.; Kotov, N. A.; Arruda, E. M. The Role of Nanoparticle Layer Separation in the Finite Deformation Response of Layered Polyurethane-Clay Nanocomposites. *Macromolecules* **2009,** 42, (17), 6588-6595.

209. Harris, J. J.; Bruening, M. L. Electrochemical and in Situ Ellipsometric Investigation of the Permeability and Stability of Layered Polyelectrolyte Films. *Langmuir* **2000,** 16, (4), 2006-2013.

210. Schlenoff, J. B.; Ly, H.; Li, M. Charge and Mass Balance in Polyelectrolyte Multilayers. *J. Am. Chem. Soc.* **1998,** 120, (30), 7626-7634.

211. Hager, M. D.; Greil, P.; Leyens, C.; van der Zwaag, S.; Schubert, U. S. Self-Healing Materials. *Adv. Mater.* **2010,** 22, (47), 5424-5430.

212. Thakur, V. K.; Kessler, M. R. Self-Healing Polymer Nanocomposite Materials: A Review. *Polymer* **2015,** 69, 369-383.

213. White, S. R.; Sottos, N. R.; Geubelle, P. H.; Moore, J. S.; Kessler, M. R.; Sriram, S. R.; Brown, E. N.; Viswanathan, S. Autonomic Healing of Polymer Composites. *Nature* **2001,** 409, (6822), 794-797.

214. Cho, S. H.; White, S. R.; Braun, P. V. Self-Healing Polymer Coatings. *Adv. Mater.* **2009,** 21, (6), 645-649.

215. Toohey, K. S.; Sottos, N. R.; Lewis, J. A.; Moore, J. S.; White, S. R. Self-Healing Materials with Microvascular Networks. *Nat. Mater.* **2007,** 6, (8), 581-585.

216. Yang, Y.; Urban, M. W. Self-Healing Polymeric Materials. *Chem. Soc. Rev.* **2013,** 42, (17), 7446-7467.

217. Chen, X.; Dam, M. A.; Ono, K.; Mal, A.; Shen, H.; Nutt, S. R.; Sheran, K.; Wudl, F. A Thermally Re-Mendable Cross-Linked Polymeric Material. *Science* **2002,** 295, (5560), 1698-1702.

218. Chung, C.-M.; Roh, Y.-S.; Cho, S.-Y.; Kim, J.-G. Crack Healing in Polymeric Materials *via* Photochemical [2+2] Cycloaddition. *Chem. Mater.* **2004,** 16, (21), 3982-3984.

219. Froimowicz, P.; Frey, H.; Landfester, K. Towards the Generation of Self-Healing Materials by Means of a Reversible Photo-Induced Approach. *Macromol. Rapid Commun.* **2011,** 32, (5), 468-473.

220. Chen, X.; Wudl, F.; Mal, A. K.; Shen, H.; Nutt, S. R. New Thermally Remendable Highly Cross-Linked Polymeric Materials. *Macromolecules* **2003,** 36, (6), 1802-1807.

221. Hentschel, J.; Kushner, A. M.; Ziller, J.; Guan, Z. Self-Healing Supramolecular Block Copolymers. *Angew. Chem. Int. Ed.* **2012,** 51, (42), 10561-10565.

222. Nakahata, M.; Takashima, Y.; Yamaguchi, H.; Harada, A. Redox-Responsive Self-Healing Materials Formed from Host–Guest Polymers. *Nat. Commun.* **2011,** 2, 511.

223. Wang, Z.; Urban, M. W. Facile UV-Healable Polyethylenimine-Copper (C_2H_5N-Cu) Supramolecular Polymer Networks. *Polym. Chem.* **2013,** 4, (18), 4897-4901.

224. Burattini, S.; Greenland, B. W.; Hayes, W.; Mackay, M. E.; Rowan, S. J.; Colquhoun, H. M. A Supramolecular Polymer Based on Tweezer-Type π–π Stacking Interactions: Molecular Design for Healability and Enhanced Toughness. *Chem. Mater.* **2011,** 23, (1), 6-8.

225. Yang, Y.; Ding, X.; Urban, M. W. Chemical and Physical Aspects of Self-Healing Materials. *Prog. Polym. Sci.* **2015,** 49, 34-59.

226. Liu, F.; Urban, M. W. Recent Advances and Challenges in Designing Stimuli-Responsive Polymers. *Prog. Polym. Sci.* **2010,** 35, (1–2), 3-23.

227. Yoo, P. J.; Zacharia, N. S.; Doh, J.; Nam, K. T.; Belcher, A. M.; Hammond, P. T. Controlling Surface Mobility in Interdiffusing Polyelectrolyte Multilayers. *ACS Nano* **2008,** 2, (3), 561-571.

228. Gu, Y.; Zacharia, N. S. Self-Healing Actuating Adhesive Based on Polyelectrolyte Multilayers. *Adv. Funct. Mater.* **2015,** 25, (24), 3785-3792.

229. Zhuk, A.; Xu, L.; Ankner, J. F.; Sukhishvili, S. A. Selective Water Uptake within Micelle-Containing Layer-by-Layer Films of Various Architectures: A Neutron Reflectometry Study. *Soft Matter* **2013,** 9, (2), 410-417.

230. Wong, J. E.; Rehfeldt, F.; Hänni, P.; Tanaka, M.; Klitzing, R. v. Swelling Behavior of Polyelectrolyte Multilayers in Saturated Water Vapor. *Macromolecules* **2004,** 37, (19), 7285-7289.

231. Olson, B. G.; Lin, J.; Nazarenko, S.; Jamieson, A. M. Positron Annihilation Lifetime Spectroscopy of Poly(Ethylene Terephthalate): Contributions from Rigid and Mobile Amorphous Fractions. *Macromolecules* **2003,** 36, (20), 7618-7623.

232. Kirkegaard, P.; Eldrup, M.; Mogensen, O. E.; Pedersen, N. J. Program System for Analysing Positron Lifetime Spectra and Angular Correlation Curves. *Comput. Phys. Commun.* **1981,** 23, (3), 307-335.

233. Eldrup, M.; Lightbody, D.; Sherwood, J. N. The Temperature Dependence of Positron Lifetimes in Solid Pivalic Acid. *Chem. Phys.* **1981,** 63, (1), 51-58.

234. Gu, Y.; Ma, Y.; Vogt, B. D.; Zacharia, N. S. Contraction of Weak Polyelectrolyte Multilayers in Response to Organic Solvents. *Soft Matter* **2016,** 12, (6), 1859-1867.

235. Xiang, F.; Ward, S. M.; Givens, T. M.; Grunlan, J. C. Super Stretchy Polymer Multilayer Thin Film with High Gas Barrier. *ACS Macro Lett.* **2014,** 3, (10), 1055-1058.

236. Holder, K. M.; Priolo, M. A.; Secrist, K. E.; Greenlee, S. M.; Nolte, A. J.; Grunlan, J. C. Humidity-Responsive Gas Barrier of Hydrogen-Bonded Polymer–Clay Multilayer Thin Films. *J. Phys. Chem. C* **2012,** 116, (37), 19851-19856.

237. Kim, D.; Tzeng, P.; Barnett, K. J.; Yang, Y. H.; Wilhite, B. A.; Grunlan, J. C. Highly Size-Selective Ionically Crosslinked Multilayer Polymer Films for Light Gas Separation. *Adv. Mater.* **2014,** 26, (5), 746-751.

238. Nolte, A. J.; Cohen, R. E.; Rubner, M. F. A Two-Plate Buckling Technique for Thin Film Modulus Measurements: Applications to Polyelectrolyte Multilayers. *Macromolecules* **2006,** 39, (14), 4841-4847.

239. Bauer, F.; Willert-Porada, M. Characterisation of Zirconium and Titanium Phosphates and Direct Methanol Fuel Cell (DMFC) Performance of Functionally Graded Nafion (R) Composite Membranes Prepared out of Them. *J. Power Sources* **2005,** 145, (2), 101-107.

240. Dlubek, G.; Redmann, F.; Krause-Rehberg, R. Humidity-Induced Plasticization and Antiplasticization of Polyamide 6: A Positron Lifetime Study of the Local Free Volume. *J. Appl. Polym. Sci.* **2002,** 84, (2), 244-255.

241. Mohamed, H. F. M.; Ito, K.; Kobayashi, Y.; Takimoto, N.; Takeoka, Y.; Ohira, A. Free Volume and Permeabilities of O_2 and H_2 in Nafion Membranes for Polymer Electrolyte Fuel Cells. *Polymer* **2008,** 49, (13–14), 3091-3097.

242. Choi, I.-s.; Kraft, O.; Schwaiger, R. Validity of the Reduced Modulus Concept to Describe Indentation Loading Response for Elastoplastic Materials with Sharp Indenters. *J. Mater. Res.* **2009,** 24, (3), 998-1006.

243. Oliver, W. C.; Pharr, G. M. An Improved Technique for Determining Hardness and Elastic Modulus Using Load and Displacement Sensing Indentation Experiments. *J. Mater. Res.* **1992,** 7, (6), 1564-1583.

244. Amore Bonapasta, A.; Buda, F.; Colombet, P. Cross-Linking of Poly(Vinyl Alcohol) Chains by Al Ions in Macro-Defect-Free Cements: A Theoretical Study. *Chem. Mater.* **2000,** 12, (3), 738-743.

245. Alici, G.; Huynh, N. N. Predicting Force Output of Trilayer Polymer Actuators. *Sens. Actuator A Phys.* **2006,** 132, (2), 616-625.

246. Biggs, J.; Danielmeier, K.; Hitzbleck, J.; Krause, J.; Kridl, T.; Nowak, S.; Orselli, E.; Quan, X.; Schapeler, D.; Sutherland, W. Electroactive Polymers: Developments of and Perspectives for Dielectric Elastomers. *Angew. Chem. Int. Ed.* **2013,** 52, (36), 9409-9421.

247. Nakahata, M.; Takashima, Y.; Hashidzume, A.; Harada, A. Redox-Generated Mechanical Motion of a Supramolecular Polymeric Actuator Based on Host–Guest Interactions. *Angew. Chem. Int. Ed.* **2013,** 52, (22), 5731-5735.

248. Dai, M.; Picot, O. T.; Verjans, J. M.; de Haan, L. T.; Schenning, A. P.; Peijs, T.; Bastiaansen, C. W. Humidity-Responsive Bilayer Actuators Based on a Liquid-Crystalline Polymer Network. *ACS Appl. Mater. Interfaces* **2013,** 5, (11), 4945-4950.

249. van Oosten, C. L.; Bastiaansen, C. W. M.; Broer, D. J. Printed Artificial Cilia from Liquid-Crystal Network Actuators Modularly Driven by Light. *Nat. Mater.* **2009,** 8, (8), 677-682.

250. Zang, J.; Liu, F. Modified Timoshenko Formula for Bending of Ultrathin Strained Bilayer Films. *Appl. Phys. Lett.* **2008,** 92, (2), 021905.